ISSN 1000-9620

Marine Science Bulletin

海洋通报

Volume 10 • Number 1 2008

ISSN 1000-9620
9 771000 962001 01>

NATIONAL MARINE DATA AND
INFORMATION SERVICE OF CHINA

MARINE SCIENCE BULLETIN

Vol.10 No.1 May 2008

CONTENTS

Sea Surface Temperature Simulation of Tropical and North Pacific
Basins Using a Hybrid Coordinate Ocean Model (HYCOM) ····· GAO Song et al. (1)
Analysis of the Beach Face with High - Frequency Oscillations
and Dynamic Functions in the Swash Zone in the HOUJIANG
Beach of Guangdong Province ·····FENG Yanqing et al. (15)
The Relationship of Sulfate - methane Interface,
the Methane Flux and the Underlying Gas Hydrate·····FANG Yinxia et al. (28)
Concentrations, Accumulation and Sources of PAHs
in Surface Layer Sediments of Taizhou Bay ·····JIN Binming et al. (38)
Cultural and luminescent Conditions of a Marine luminous Bacterium·····FANG Hongda et al. (46)
Effects of Heavy Metal and Pollutants on the Non - special
Immunity of the Shrimp and Crab ····· Al Chunxiang et al. (54)
Contrast of Seismic Reflection Characteristics of Gas Hydrate Distribution
between Northeast SCS Slope and Hengchun Ridge ·····SHANG Jihong et al. (64)
Analysis on the Basement Constitution of the Southern Okinawa Trough ····· LIU Jianhua et al. (75)
Seagrass Bed Ecosystem Service Valuation — A Case
Research on Hepu Seagrass Bed in Guangxi Province····· HAN Qiuying et al. (87)

U.S. NATIONAL OCEANIC AND ATMOSPHERIC ADMINISTRATION
NOAA
U.S. DEPARTMENT OF COMMERCE

LIBRARY
FEB 18 2009
National Oceanic &
Atmospheric Administration
U.S. Dept. of Commerce

Sea Surface Temperature Simulation of Tropical and North Pacific Basins Using a Hybrid Coordinate Ocean Model (HYCOM)

GAO Song[1, 2], Lü Xianqing[2], WANG Haitang[3]

1. *North Sea Marine Forecast Center of State Oceanic Administration, Qingdao* 266033, *Shandong China;*
2. *Laboratory of Physical Oceanography, Ocean University of China, Qingdao* 266003, *Shandong China;*
3. *Qingdao Huanhai Marine Engineering Prospecting Institute, Qingdao* 266033, *Shandong China*

Abstract: A Hybrid Coordinate Ocean Model (HYCOM) is used to simulate the sea surface temperature of the Tropical and North Pacific. Based on the different combinations of two air-Sea flux data sets (COADS and ECMWF) and two bulk parameter formulas (non-constant and constant), four numerical experiments are carried out. The following conclusions can be deduced from the numerical results. (1) The numerical results using non-constant bulk parameter formula are much better than those using constant one. In the Pacific area from 40°N to 20°S, the annual average SST obtained from the experiment using non-constant bulk parameter formula is 0.21 °C higher than that from the satellite-based SST climatology (the pathfinder data). However, the difference is 0.63 °C for the experiment when the using constant one. (2) HYCOM successfully simulates the monthly variation of climatological SST in tropical and north Pacific basins and monthly spatial variation of Western Pacific Warm Pool. Especially in the Pacific area from 40°N to 20°S, the difference of the seasonal averaged SST between pathfinder data and the result of experiment 2 (using COADS data set and non-constant bulk parameter formula) is only about 0.02 °C. (3)The simulation results using different Air-Sea flux data are different and the difference is very large in some regions. In the northwest of the model region, the annual average SST obtained from experiment 2 (using COADS data set) is 1°C higher than that obtained from experiment 4 (using ECMWF data set). Contrarily, the result of experiment 4 is 1 °C larger than that of experiment 2 in the southeast of the model region. The largest difference is about 4 °C occurred near the area of 58°N, 140°E and the Bohai sea.

LIBRARY
Pacific Islands Fisheries Science Cente
NOAA Fisheries
Honolulu, Hawai'i

Keywords: ocean model; air-sea flux; sea surface temperature (SST);

1 Description of HYCOM model

The Hybrid Coordinate Ocean Model (HYCOM) is a primitive equation global ocean general circulation model with hybrid vertical coordinates(isopycnic coordinate、sigma coordinate and z coordinate) that evolved from the Miami Isopycnic-Coordinate Ocean Model (MICOM) by Rainer Bleck[1-3] and his colleagues. In recent years, some scholars have carried out much research based on HYCOM model.

Received on November 6, 2007

Bleck[3] proved theoretically that HYCOM model can be used in the shallow seas and non-stratificated areas through the combination of isopycnic coordinate、z coordinate and sigma coordinate. And he also proved through the experiment that the model is capable of maintaining a physically consistent layer structure over long period (the integral time is 100 years in the experiment). Chassignet et al. [4] discussed the importance of thermobaricity and the choice of reference pressure in the simulation. Thacker [5, 6] used optimal interpolation to assimilate XBT data into HYCOM. This approach can be generalized to accommodate other types of data. Halliwell [7] evaluated the vertical coordinate and vertical mixing algorithms included in the Hybrid Coordinate Ocean Model in low-resolution climatological simulations of the Atlantic Ocean. By comparing simulations to climatology, the best model performance is realized using hybrid coordinates in conjunction with one of the three available differential vertical mixing models: the nonlocal K-Profile Parameterization, the NASA GISS level 2 turbulence closure and the Mellor–Yamada level 2.5 turbulence closure. Kara [8-13] examined the sensitivity of sea surface temperature (SST) to water turbidity, and the effects of ocean turbidity on upper-ocean circulation features including sea surface height and mixed layer depth (MLD) and on annual mean climatological time scales in the Black Sea using the eddy-resolving HYCOM, which includes a nonslab KPP mixed layer model. Lee et al. [14] designed a series of ocean general circulation (OGCM) model experiments to determine the annual cycle of the Western Hemisphere Warm Pool (WHWP) heat budget and to assess the appropriateness of commonly used surface flux data sets in driving HYCOM simulations of the WHWP in HYCOM. Chassignet et al. [15,16] assimilates the XBT, CTD and Argo data to the HYOM, which is an eddy-resolving (1/12°), configured with 22 layers, and fully global ocean prediction system.

The above research is focused on the Atlantic Ocean and the Black Sea. In this paper, we will simulate the monthly variation of climatological SST in tropical and north pacific basins based on the different combinations of two air-sea flux data sets and two bulk parameter formulas.

2 Model Configuration

2.1 Model Configuration

The computational domain spans the tropical and north Pacific basins from 20°S to 62 °N and from 100 °E to 65 °W. The standard Mercator coordinate is used and the resolution is $1° \times 1° \times \cos(\theta)$ (θ is latitude). The zonal grid resolution is $(1 \times \cos\theta) \times 111.2$ km, and the meridional grid resolution is $1 \times (\cos\theta \times 111.2)$ km, that insures the grid is a square, and the length gradually decreases from 111.2 km at the tropic to 73.86 km at 62 °N. The computational grids is 196×103 (Fig.1).

The model is configured with 22 layers. Since we are interested exclusively in upper-ocean physical processes, we use a surface reference pressure for our target potential density values of 19.50, 20.01, 20.52, 21.03, 21.54, 22.05, 22.56, 23.07, 23.58, 24.09, 24.60, 25.13, 25.27, 26.11, 26.44, 26.72, 26.95, 27.14, 27.30, 27.44, 27.56 and 27.66. The target densities of the top seven layers are chosen to be lighter than water encountered almost everywhere in the ocean so that they exits as level coordinates at

the surface and provide reasonable vertical resolution in the surface mixed layer. The bottom topography is based on ETOP05 data. The KPP vertical mixing model is used. And details regarding the implementation of KPP in HYCOM can be found in Halliwell[7].

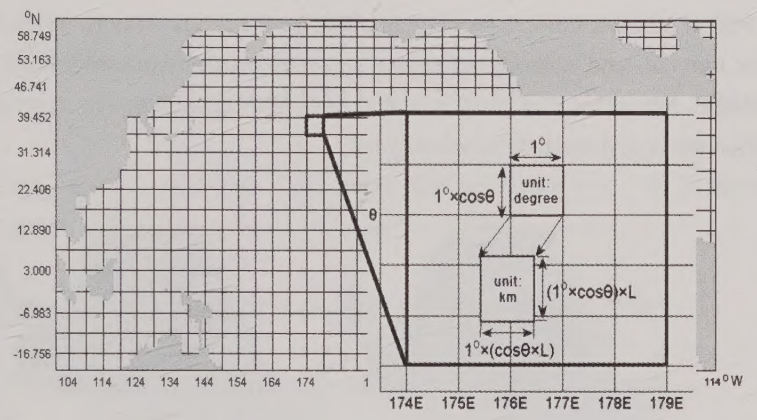

Fig.1 Grid location. As a result of graphic size limit, every 5 grids draw a line to mark in this chart, where θ is latitude, and L equals$2\pi R/360$, and R represents the earth radius.

The southern edges of the model domain are treated as opened boundary and the initial field is the Levitus climatological monthly averaged temperature and salinity in January. Boundary conditions are provided by buffer zones that are ten grid points wide within which temperature and salinity are relaxed to Levitus climatological values with the relaxation time scale increasing from 20 to 120 days. And on the sea surface, salinity relaxation is adopted. The model run for 20 years. And the results show that the upper-ocean is generally stable after ten years' integral, so we just compare the mean values of the later 5 years, that is, the mean values from the 16th year to the 20th year of the 20 years.

2.2 Sea surface force

2.2.1 Heat balance

The thermodynamics and momentum exchanges on the air-sea interface have very important effects on the SST, SSH, MLD and upper-ocean circulation. The effects mainly arise from two aspects: 1) the difference of the data sets [13]; 2) the difference of the bulk parameter formulas. In this paper, two air-sea flux data sets and two bulk parameter formulas are combined to form four numerical experiments and examine the effects of air-sea flux on the model results.

The two data sets are COADS based on the observation with the resolution of 1° × 1°and ECMWF based on the reanalysis simulations with the resolution of 1.125° × 1.125°. Through comparison we find that COADS is generally accordant with ECMWF, but there are still some differences. Especially, the spacial averaged ECMWF wind speed data (10 m, Fig. 2) are about 0.5 m/s larger than those of COADS

data. In the northwest Pacific, the maximum wind speed in August of ECMWF is 10.15 m/s, while the corresponding speed of COADS is only 8.16 m/s. In the area where wind speed is less than 1 m/s, that of ECMWF is 0.3 m/s less than that of COADS value. For example, in January, the minimum ECMWF wind speed is 0.28 m/s, while the minimum COADS wind speed is 0.88 m/s (But the difference of wind speed is less than the limit of 3.5 m/s and it does not has effect on the model results, which is determined by the bulk parameter formula, and authors will select better bulk parameter formula to decrease the limit). Moreover, ECMWF data show that there is a little area near coast with low wind speed of about 3m/s which is less than the speed around the ocean area.

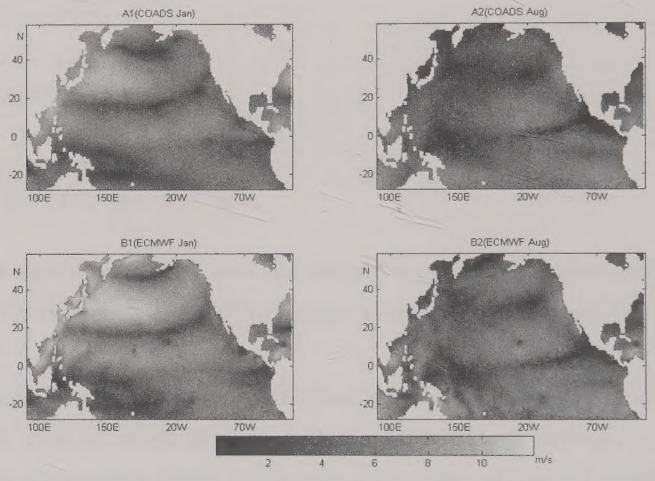

Fig. 2 Climatological monthly mean Wind speed at sea surface (10m) (ms^{-1})

A1 COADS January ; A2 COADS August ; B1 ECMWF January ; B2 ECMWF August

In HYCOM, the effect of air-sea exchanges (except the mechanical effect of the wind) on the mixed layer is summed in the calculation of thermal balance:

$$B = R + H + \varepsilon \tag{1}$$

Where R is $Q_s - Q_b$, Q_s the solar radiation by the surface, Q_b the radiation emitted by the surface, H the sensible heat, and ε the latent heat, and B the radiative exchange. A positive flux of sensible heat corresponds to a loss.

A contribution of energy by the sea following the sign of the difference between the sea and the atmospheric boundary layer:

$$H = C_{pair} E_x (T_s - T_a) \tag{2}$$

E_x is an exchange coefficient expressed as: $E_x = \rho_a C_T W$ (3)

Where ρ_α is mass/volume of the air, C_T sensible heat transfer coefficient, C_{Pair} specific heat of the air, T_s sea surface temperature, T_a temperature in the atmospheric boundary layer(10 meters above the sea surface), and W wind velocity(10 meters above the sea surface).

Responsible for important quantities of heat exchanged between the sea and atmosphere by evaporation, the latent heat flux always induces a heat loss of the ocean. To formulate this term in the balance estimation, in HYCOM, the expression is:

$$\varepsilon = E_x L\left(H_u - E_v\right) \tag{4}$$

Where E_x is an exchange coefficient expressed as:

$$E_x = \rho_a C_L W \tag{5}$$

C_L is latent heat transfer coefficient. L is latent heat of evaporation. H_u is specific humidity. E_v is evaporation.

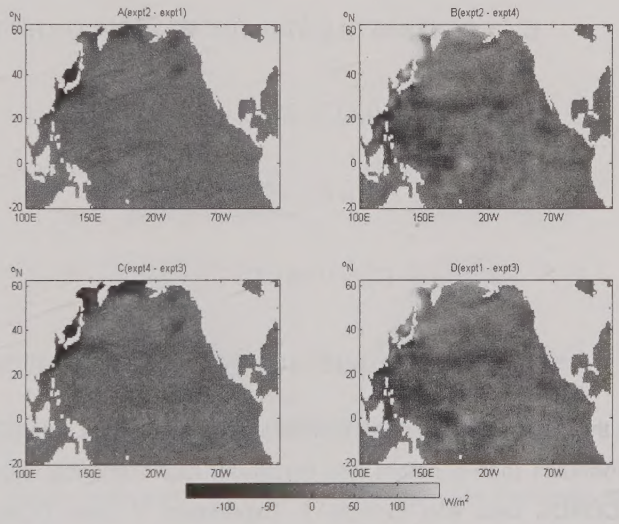

Fig. 3 Air-Sea heat flux surplus difference in January

(A) difference of expt 2 and expt 1; (B) difference of expt 4 and expt 2;

(C) difference of expt 4 and expt 3; (D) difference of expt 1 and expt 3;

2.2.2 Mechanical energy transfers

Mechanical energy transfers caused by the wind can be expressed by a wind stress $\overrightarrow{\tau_s}(t)$ induced by the wind speed $\overrightarrow{W}(t)$ as following:

$$\overrightarrow{\tau_s} = \rho_a C_D \left|\overrightarrow{W}\right| \overrightarrow{W} \tag{6}$$

C_D is a coefficient realizing sea surface drag. It is set as $C_D \approx 10^{-3}$. The expression of the drag velocity at the surface is obtained by the relation : ${u^2}_s \vec{x} = \overrightarrow{\tau_s} / \rho_o$.

At the point z, the classic parametrization of the concept of turbulent diffusion is used as:

$$\bar{\tau}(z) = \rho K_M \frac{\partial \bar{u}}{\partial z} \tag{7}$$

Where $\bar{x}$ is unit horizontal vector, and K_M is the coefficient of turbulent momentum diffusion.

2.2.3 Bulk parameter formulas

The different bulk parameter formulas (non-constant and constant) have great effect on the model results. In this paper, we compare the different bulk parameter formulas, to make sure which one is better.

Formula 1. : constant bulk parameter formula, $C_T = 0.0012$, $C_L = 0.0012$, $C_D = 0.0013$

Formula 2. : non-constant bulk parameter formula[17]

$$C_{L0} = 0.885\times10^{-3} + 0.0748\times10^{-3}W - 0.00143\times10^{-3}W^2 \tag{8}$$

$$C_{L1} = -0.113\times10^{-4} + 4.89\times10^{-4}W^{-1} \tag{9}$$

$$C_L = C_{L0} + C_{L1}\times(T_s - T_a) \tag{10}$$

$$C_T = 0.98\times C_L \tag{11}$$

$$C_D = 0.862\times10^{-3} + 0.088\times10^{-3}W - 0.00089\times10^{-3}W^2 \tag{12}$$

Thus, based on the different combinations of two air-sea flux data sets (COADS and ECMWF) and two bulk parameter formulas (non-constant and constant), four numerical experiments are carried out: experiment 1 uses COADS data and formula 1; Experiment 2 uses COADS data and formula 2; experiment 3 uses ECMWF data and formula 1. experiment 4 uses ECMWF data and formula 4.

We take January for example, whose air-sea flux difference is representational, to explain the difference of radiative exchange induced by different data sets and different bulk parameter formulas. From Fig.3 A and C, and comparing formula 2 with formula 1, the difference is within $\pm$ 10 W/m^2 in the most area. But near the boundary of northwest Pacific ocean, especially in the East China Sea and around the Japan Sea, result of formula 2 is 20 % lower than that of formula 1 (100 W/m^2). The analysis of experiment results suggests that result of formula 2 is obviously improved. From Fig. 3B, D we can find that the results of the two formulas using CODAS data set are both 15 % (20 W/m^2) larger than those using ECMWF data inside the ocean. Near the northwest coast to the north of 40°N, the value is about 150 W/m^2. While in the west of equatorial Pacific Ocean, the value using CODAS data is 75 W/m^2 lower than that using ECMWF. From below experiment result, are just the areas where model simulated results are not good. Although the result of formula 2 is improved, the simulated SST is still about 2 °C higher than Pathfinder data.

3 Result analysis

3.1 SST analysis

In this paper, climatological monthly averaged SST data of Pathfinder data set from 1985 to 1997 are used to compare with the model results. Pathfinder data set is based on the satellite data, and its resolution is 9.3 km. But the data is smoothed using 7×7 grids, so its effective resolution is about 30 km. Pathfinder climatological data is widely used to compare with simulative results [18]. The difference between simulated values (HYCOM SST) and satellite data values (Pathfinder SST) is calculated by formulas 13 and 14. For the case of comparison, the values of model are interpolated into the grid of Pathfinder data set.

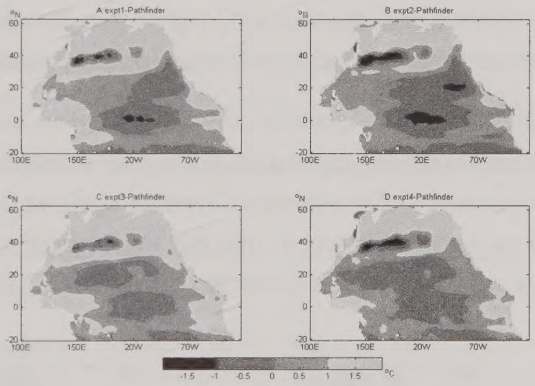

Fig. 4 Annual mean HYCOM SST and the annual mean Pathfinder SST differences

(A) annual mean SST ME difference of expt 1 and Pathfinder; (B) annual mean SST ME difference of expt 2 and Pathfinder; (C) annual mean SST ME difference of expt 3 and Pathfinder; (D) annual mean SST ME difference of expt 4 and Pathfinder;

The statistical relationship between HYCOM simulated SST (Y) and the Pathfinder SST (X) is:

$$ME = \overline{Y} - \overline{X} \tag{13}$$

$$rms = [\frac{1}{n}\sum_{i=1}^{n}(Y_i - X_i)^2]^{1/2} \tag{14}$$

where the subscript *i* represents the month, and *n* equals 12, *ME* is mean error and rms is the root mean square.

Generally speaking (Fig. 4), the annual averaged SST ME in the open ocean is much smaller than that in the coastal areas. From the experiment 2 and experiment 4 (Fig. 4B, D) one can find that the former is about 0.5 °C less than the latter. The authors believe that it may arise from the not good simulation of

the sea surface forcing data in the coastal areas.

Fig.5A shows that the changes of annual average SST arising from different bulk parameter formulas are mainly concentrated in the region north of 40°N. And its intensity is about -1.5 °C (that is to say, the result from formula 2 is 1.5 °C lower than that from formula 1, which is more close to Pathfinder data), and its spatial distribution is very similar to the spatial distribution of SST ME which is larger than 1.5 °C in Fig. 4A-D. So the authors believe that the model result may get further improvement by improving the air-sea flux parameter formulas. From Fig. 5B, we can find that the difference between CODAS and ECMWF data sets can significantly affect the model results, and the difference of annual average SST ranges from -1.5 °C to 1.5 °C, and in the north-west of the simulated area, simulated SST by using CODAS data is about 1 °C higher than that simulated SST by using ECMWF data; While in the south-east of the simulated area, simulated SST by using ECMWF data is about 1 °C higher than that using CODAS data. The maximum is in the vicinity of 58°N, 140°E and in the Bohai Sea, and the max simulated SST by using CODAS data is about 4 °C higher than that using ECMWF data. Thus, the difference between the different data sets has a great impact on the simulation results.

Despite the good simulation results of the model in the area to the south of 40°N, in the area to the north of 40°N, the simulated values are above 2 °C higher than Pathfinder values, we believe that the following factors may be relevant: 1) The selection of vertical layers of the model; 2) The model didn't consider the effect of sea ice and precipitation; 3) The quality problem of the air-sea flux data in this area. So in the following discuss, we will emphasize on the simulation results in the area south of 40°N.

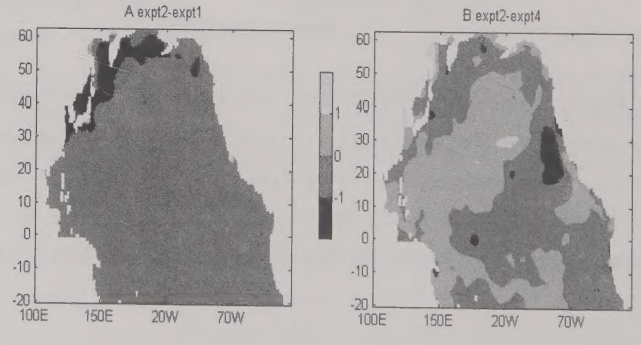

Fig. 5 simulated annual mean SST differences

(A) Annual mean SST ME difference of expt 2 and expt 1; (B) Annual mean SST ME difference of expt 2 and expt 4;

From the values of ME in Tab. 1, we can find that the results of experiment 2 and experiment 4 are obviously better than those of experiment 1 and experiment 3. The result of experiment 1 (0.58 °C) is 220 % larger than that of experiment 2 (0.18 °C), and the result of experiment 3 (0.68 °C) is 172 % larger than that of experiment 4 (0.25 °C). We can draw the similar conclusion from the rms values. It suggests that the air-sea flux bulk parameter formula 2 is obviously better than that of the formula 1. On the other hand, the ME values of experiment 3 and experiment 4 are respectively higher than the values of

experiment 1 and experiment 2 respectively. The value of experiment 3 is 17 % larger than that of experiment 1, while the value of experiment 4 is 39 % larger than that of experiment 2. And the *rms* values of experiment 1 and experiment 2 are respectively larger than that of experiment 3 and experiment 4. The value of experiment 1 is 2 % larger than that of experiment 3, while the value of experiment 2 is 9 % larger than that of experiment 4. It is suggested that in most area, the results from CODAD data are better, but in some area, the error may be larger than the results from ECMWF data. We can find this point from Fig. 4B, D. In the Japan sea, just near the Kuroshio Extension（150°E—170°E，36°N—38°N）, the range of ME which is lower than -1.5 °C in Fig. 4B is larger than that in Fig. 4D.

Through the comparison of the monthly average SST from HYCOM numerical simulation and Pathfinder data set, we also can draw a few valuable conclusions. From Fig. 6 we can find that the monthly ME curve of experiment 2 (4) is generally parallel to that of experiment 1 (3), which suggests that formula 2 has a total temperature drift of about 0.4 °C compared with formula 1, and its results are more closer to Pathfinder data. In winter and spring, simulation results of experiment 2 (CODAS data set) are closest to the Pathfinder value, the mean value of 6 months' ME is 0.02 °C. The fluctuation of ME of experiment 4 (ECMWF data set) during 12 months is 47 % smaller than that of experiment 2 (0.22 °C).

Tab.1 Annual mean SST ME and rms for four experiments. (℃) (statistic from 40°N to 20°S in Pacific)

	ME /°C	Rms /°C
Expt 1	0.58	1.05
Expt 2	0.18	0.89
Expt 3	0.68	1.03
Expt 4	0.25	0.82

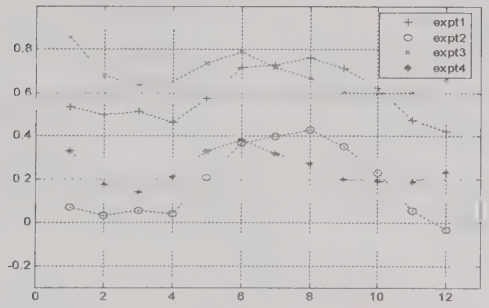

Fig.6 spatial variability monthly mean HYCOM SST ME (°C) + expt 1; ○ expt 2; × expt 3; * expt 4

The statistic results of monthly average SST prove the superiority of block parameter formulas 2 to block parameter formulas 1. Thus, the following discussion is only concentrated on experiment 2 and 4. Taking the west Pacific warm pool for example, we focus on analyzing the difference between air-sea flux data sets and its effect on the model.

3.2 The West Pacific Warm Pool analysis

Previously studies commonly select three important characteristic values of warm pool to evaluate the model results such as the warm pool center, its area and its intensity [19]. Restricted by the paper length, we only select the West Pacific Warm Pool area to analyze.

The West Pacific Warm Pool (WPWP) area is defined as the surrounded grid number of geographical longitude and latitude which is surrounded by the 28 °C isothermal. We can see from Fig.7 that experiment 2 and experiment 4 commendably simulated the monthly variation of the warm pool area and shape. The distribution range begins to enlarge from January and move norwards, and reach peak value in September, then attenuate quickly.

From Fig. 8, we can see more clearly that the WPWP area of experiment 2(4) increases from smallest one in January (February) with the value of 2084 (2197) to the largest one in September with the value of 3480 (3095), then decreases to 2179 (2281) in December. The simulated distribution range of experiment 2 in spring, autumn and winter is smaller than that of Pathfinder, and the simulated distribution range of experiment 4 in summer is larger than that of Pathfinder data set.

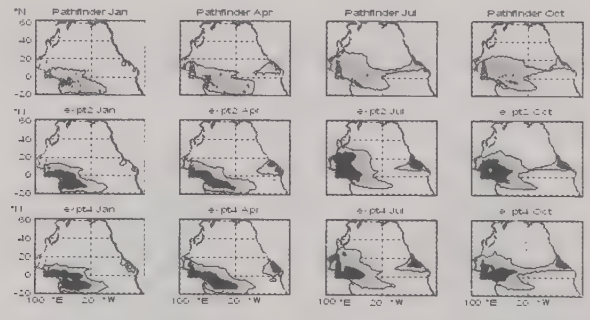

Fig. 7 Spatial monthly variability of West Pacific Warm Pool （WPWP）. X-coordinate represents longit （°E）; Y-coordinate latitude（°N）, and light color denotes 30 °C ≥SST ≥28 °C; and deep color denotes SST ≥30 °C.

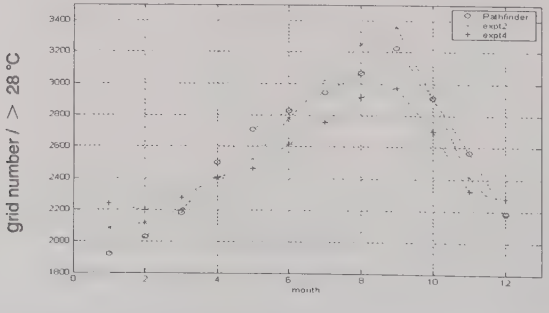

Fig. 8 Monthly averaged variability in WPWP area. X-coordinate represents month; Y-coordinate grid numbers of SST≥28 °C

○ Pathfinder ; × expt 2; + expt 4

4 Sensitive Experiment

HYCOM adopts hybrid coordinate of isopycnal coordinate, z coordinate and sigma coordinate, and this kind of coordinate is very complex. Different layer schemes affect the simulated results obviously. Thus, in order to discuss why the standard experiment cannot simulate well to the north of 40°N, the author designs a sensitive experiment to compare with the standard experiment. The sensitive experiment considers the vertical layers of the Atlantic Ocean, and the target potential density values are 19.5, 20.24, 20.98, 21.72, 22.46, 23.20, 23.94, 24.64, 25.22, 25.70, 26.11, 26.44, 26.72, 26.95, 27.14, 27.30, 27.44, 27.56, 27.66, 27.74, 27.80 and 27.84[20]. Other model configurations are the same with the standard experiment 2 (adopting CODAS data set and parameter formulas 2).

Fig.9 is the distribution of ME in January from standard experiment 2 and sensitive experiment. We can find that in the area to the south of 40°N, the results of the two experiments are generally accordant. In the area to the north of 40°N, the result of sensitive experiment is obviously better in the northeast Pacific Ocean, the SST difference in January between model result and Pathfinder data decrease to the value within 1.5 °C. But the sensitive experiment result become obviously bad in northeast Pacific Ocean, and the maximum SST difference in January between model result and Pathfinder data is 6 °C. Thus, the selection of target potential density is very important, we should select different vertical layers scheme according to different research objects.

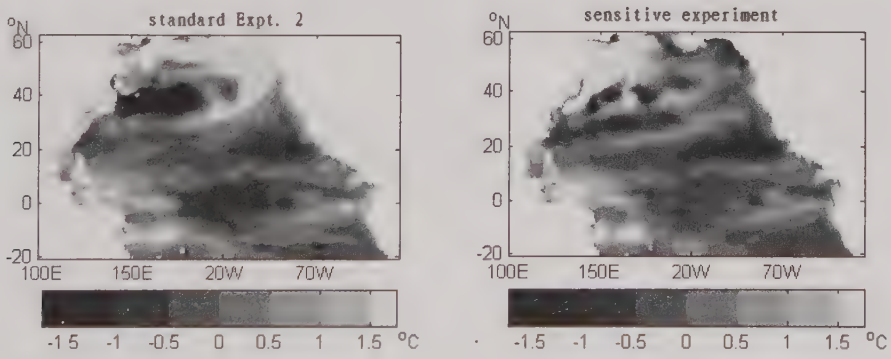

Fig. 9 SST ME of standard experiment 2 and sensitive experiment in January. (°C)

5 Conclusions and Outlook

In this paper, climatological SST variation of tropical and north pacific basins is simulated, and the effects on model results of COADS、ECMWF data sets and two kinds of bulk parameter formulas (constant bulk parameter formula and non-constant bulk parameter formula) are analyzed. The simulated annual averaged SST and monthly averaged SST results show that:

(1) The non-constant bulk parameter formula is better than the constant bulk parameter formula. In the Pacific Ocean from 40°N to 20°S, the annual averaged SST obtained from the experiment using non-constant bulk parameter formula is 0.21 °C higher than using Pathfinder data. However, the value from the experiment using constant bulk parameter formula is 0.63 °C higher than that from Pathfinder data.

(2) HYCOM successfully simulates the monthly variation of climatological SST of tropical and north pacific basins and monthly spatial variation of the West Pacific Warm Pool. Especially in the Pacific from 40°N to 20°S, the seasonal averaged SST of experiment 2 (using COADS data set and non-constant bulk parameter formula) is only about 0.02 °C higher than that from Pathfinder data.

(3) Different air-sea flux data significantly affect model results. In the northwest of model region, the annual average SST obtained from experiment 2 (COADS used) is 1 °C larger than that obtained from experiment 4 (ECMWF used). Contrarily, the result of experiment 4 is 1 °C larger than that of experiment 2 in the Southeast of model region. The largest difference is about 4 °C occurred near (58°N, 140°E) and the Bohai sea.

Although the model succeeds in simulating the monthly variation of SST of Tropical and North Pacific basins, it can not commendably simulate SST in the areas near Kuroshio Extension and north of 40^0N. The authors will farther simulate SST in Kuroshio and the upper-ocean structure in China Sea. And the experiment will be improved from the following aspects: 1) assimilate the observed data into HYCOM model via optimal interpolation; 2) select better bulk parameter formulas to overcome the limit of minimum wind speed; 3) adopt more turbulent close schemes to compare; 4) design reasonable vertical layers scheme according to the characteristic of Kuroshio.

Partial support for this research was provided by the State Ministry of Science and Technology of China through grant 2007AA09Z118, the National Basic Research Program of China through grant 2005CB422308 and the Specialized Research Fund for the Doctoral Program of Higher Education through grant 20050423007.

References

[1] Halliwell G R, Bleck R, Chassignet E P. Atlantic ocean simulations performed using a new Hybrid Coordinate Ocean Model (HYCOM) [C]. EOS, Fall AGU Meeting. 1998.

[2] Halliwell G R, Bleck R, Chassignet E P, et al. Mixed layer model validation in Atlantic ocean simulations using the Hybrid Coordinate Ocean Model (HYCOM) [C]. EOS, 80, OS304. 2000.

[3] Bleck R. An oceanic general circulation model framed in hybrid isopycnic-cartesian coordinates [J]. Ocean Modelling, 2002, 4: 55-88.

[4] Chassignet E P, L T Smith, G R Halliwell, et al. North Atlantic simulations with the Hybrid Coordinate Ocean Model (HYCOM): Impact of the vertical coordinatechoice, reference pressure, and thermobaricity [J]. Phys. Oceanogr., 2003, 33: 2504–2526

[5] Thacker W C, O E Esenkov. Assimilating XBT data into HYCOM [J]. Journal of Atmospheric and Oceanic

Technology, 2002, 19: 709-724.

[6] Thacker W C, S K Lee, G R Halliwell. Assimilating 20 years of Atlantic XBT data into HYCOM: a first look [J]. Ocean Modeling, 2004, 7: 183-210.

[7] Halliwell G R. Evaluation of vertical coordinate and vertical mixing algorithms in the HYbrid Coordinate Ocean Model (HYCOM) [J]. Ocean Modelling, 2004, 7: 285-322.

[8] Kara A B, A J Wallcraft, H E Hurlburt. How does solar attenuation depth affect the ocean mixed layer? Water turbidity and atmospheric forcing impacts on the simulation of seasonal mixed layer variability in the turbid Black Sea [J]. Climate, 2005,18: 389-409.

[9] Kara A B, A J Wallcraft, H E Hurlburt. A new solar radiation penetration scheme for use in ocean mixed layer studies: an application to the Black Sea using a fine-resolution Hybrid Coordinate Ocean Model (HYCOM) [J]. Phys. Oceanogr., 2005, 35: 13-32.

[10] Kara A B. A J Wallcraft. H E Hurlburt. Sea surface temperature sensitivity to water turbidity from simulations of the turbid Black Sea using HYCOM [J]. Phys. Oceanogr., 2005, 35: 3-54.

[11] Kara A B, H E Hurlburt, A J Wallcraft. Stability-dependent exchange coefficients for air-sea fluxes [J]. Atmos. Oceanic. Technol., 2005, 22: 1080-1094.

[12] Kara A B, H E Hurlburt, A J Wallcraft, et al. Black Sea mixed layer sensitivity to various wind and thermal forcing products on climatological time scales[J]. Climate, 2005, 18: 5266-5293.

[13] Kara A B, H E Hurlburt, A J Wallcraft, et al. Corrigendum for Black Sea mixed layer sensitivity to various wind and thermal forcing products on climatological time scales [J]. Climate, 2006, 19: 494-495.

[14] Lee S K, D B Enfield, C Wang. Ocean general circulation model sensitivity experiments on the annual cycle of Western Hemisphere Warm Pool [J]. Geophys. Res., 110, C09004, 2005,doi: 10.1029/2004JC002640.

[15] Chassignet E P, H E Hurlburt, O M Smedstad, et al. Generalized vertical coordinates for eddy-resolving global and coastal ocean forecasts [J]. Oceanography, 2006, 19: 20-31.

[16] Chassignet E P, H E Hurlburt, O M Smedstad, et al. Ocean prediction with the Hybrid Coordinate Ocean Model (HYCOM) [C]. In: Ocean Weather Forecasting: An Integrated View of Oceanography, Chassignet E P. J Verron (Eds.). Springer, 2006: 413-426.

[17] Kara A B, Pochford P A, Hurlburt H E. Efficient and accurate bulk parameterizations of air-sea fluxes for use in general circulation models [J]. Atmos. Ocean Tech., 2000, 17: 1421-1438.

[18] Casey K S, P Cornillon. A comparison of satellite and in situ–based sea surface temperature climatologies [J]. Climate, 1999, 12, 1848–1863.

[19] FANG Lixin, CHEN Ge, FANG Chaoyang, et al. An Investigation of Recent Western Pacific Warm Pool Variabilities Based on AVHRR / SST [J]. Journal of Ocean University of China. 2004, 34(1):103-108

[20] Shaji C, C Wang, G R Halliwell, et al. Simulation of tropical Pacific and Atlantic Oceans using a hybrid coordinate ocean model [J]. Ocean Modelling, 2005, 9: 253-282.

HYCOM 模式对赤道及北太平洋海表温度的模拟

高松[1,2]，吕咸青[2]，王海棠[3]

（1. 国家海洋局北海预报中心，山东 青岛，266033；2. 中国海洋大学物理海洋实验室，山东 青岛，266003；
3. 青岛环海海洋工程勘察研究院，山东 青岛，266033）

摘 要：本文使用 HYCOM 数值模式，根据两种海气通量数据集（COADS、ECMWF）和两种海气通量块体参数化方案（常数块体参数化方案和非常数块体参数化方案）的不同结合，构成 4 组数值实验，分别模拟了赤道及北太平洋的气候态海表温度。实验结果表明：1）在本文的实验中，非常数块体参数化方案优于常数块体参数化方案；在太平洋 40°N-20°S 区域内，采用前者得到的年平均海表温度比 Pathfinder 卫星资料高约 0.21 °C，而采用后者得到的年平均海表温度比 Pathfinder 卫星资料高约 0.63 °C。2）HYCOM 数值模式很好的模拟了赤道及北太平洋的气候态海表温度变化及西太平洋暖池空间分布的月变化。特别是实验 2（采用 COADS 数据集和非常数块体参数化方案），在太平洋 40°N - 20°S 区域内，冬春两季平均 SST 仅比 Pathfinder 卫星数据集高 0.02 °C。3）不同的海气通量数据会对模式结果产生明显的影响。对比采用 COADS 数据集的实验 2 结果与采用 ECMWF 数据集的实验 4 结果可以发现，在模拟区域的西北部，实验 2 比实验 4 的年平均 SST 高约 1 °C；在模拟区域的东南部，实验 4 比实验 2 的年平均 SST 高约 1 °C。两者差的最大值出现在 58°N、140°E 附近及中国渤海，约为 4 °C（实验 2 比实验 4 的年平均 SST 高约 4 °C）。

关键词：海洋模式；海气通量；海表温度；

Analysis of the Beach Face with High-Frequency Oscillations and Dynamic Functions in the Swash Zone in the Houjiang Beach of Guangdong Province

FENG Yanqing [1, 2], CHEN Zishen [2], LI Zhilong [2], LI Zhiqiang [2]

1. South China Sea marine engineering surveying center, state oceanic administration, Guangzhou 510300, *Guangdong, China;*

2. Department of water resources and environment, Sun Yat-sen University, Guangzhou 510275, *Guangdong, China*

Abstract: Using the data of beach face high oscillations and waves and flows of the surf zones influenced by the swells, the characteristics including beach face variation trends, trend shapes, oscillation periods, oscillation intensions of different profile shapes, and the characteristic relations between different stake points on the same profile were analyzed comparatively. The relations between the beach face with high oscillations erosion and sediment and the surf zone infragravity waves were also analyzed based on the cross spectrum analysis. The results showed that the swash diffluences caused by the beach cusp rhythm topography hasten the sediment transport from the beach ridge to beach paddy, and the beach face of the swash zones has the infragravity periodic oscillations, and the oscillation intensions descend from the bottom to the top of the beach face, and the infragravity waves of the surf zones have significant effect on the high-frequency variations of erosion and sediment of the beach face.

Keywords: swash zone; SSA; infragravity waves; cross spectrum

Introduction

In the narrow sense, the beach swash zone is the area of the beach face mutually influenced by the uprush and backwash, namely, this part of the beach zone would emerge in the air for a few minutes or a few seconds, and the center position of the zone changes frequently because of the effect of the tide, tide current, coastal current and swash. Therefore, the swash zone has some spatio-temporal characteristics. Besides, the beach swash zone is one of the areas with the most direct reciprocity between the land and the sea, and it is also the sensitive and concentrative zone of the nearshore processes. The hydrodynamic condition and sediment movement of this zone have great effect on the intension of the action between the land and sea, the changes on the beach profiles, the evolvement of the coast, the stability of the coastal building, and the biology growth of the swash zone.

However, the research achievements on swash zone are less than those on near shore and surf zones. One reason for this question is the difficulty of collecting high quality data of the swash zones,

Received on September 11, 2007

another reason is the complexity of the hydrodynamics and sediment movement of this zone. These years, whereas the significance and challenge of the swash zones studies have attracted the scholars' attention and the researches on swash zone have made great progress. There is a long way to go to roundly predominate the characteristics of hydrodynamics and sediment movement in different conditions of the swash zone. Therefore, using different ideas and methods to study the swash zone has great practical and research meaning.

Based on the studies by Waddell(1973), Waddell(1976) and Sallenger(1984), et al., the author adopted the method of SSA to analyze the altitude transformation of the stake points on the beach swash zone in a period of water level changing, probed into the trends and the periodic oscillations of the beach changing, and contrastively analyzed the oscillation intensions on different points of the beach face. We combined the studies about the relations between the beach face oscillations and the swash movement, water level and hydrodynamic changes of the surf zone by Berry, Elfrink , Baldock, Holmes, Horn, Butt, Russell etc. Author also probed into the relations between the beach face changing and swash movement, and analyzed the relations between the infragravity waves of the surf zones and the high-frequency variations of erosion and sediment of the beach face.

1 The coastal background of the studying area and the environmental characteristics of the observing time

The studying area is located in the HOUJIANG beach which is in the west of JIESHI bay in the east coast of Guangdong province (Fig.1), the west-south of the study area is ZHELANG town the east-north of which is SHIGONGLIAO headland, and the two cusps are composed of granite with wide grains. The length of the bowstring of the cusp beach is about 7Km and the longest concave length is about 3 Km. By the long-term compacting of the wave, the shape of the beach is basely adapted to the long-effect of the prevailing waves to the coast line, and forms the relatively steady-going arc coast. JINYU Island is far away from the coast and can shelter the waves of the middle of the HOUJIANG beach.

In the open sea out of the beach, the average wave heights of many years is about 1.3 m, and average wave periods is 4.6 second, and the maximal wave height is 2.2 m. Wind speed, wind direction and wave direction all have great changes in a year. The tide in the sea area is irregular diurnal mixed tide, and average tide range is only 0.84 m, and the beach of this area belongs to weak tide coast controlled by waves.

The observing area lies in the middle coast of the HOUJIANG beach (Fig.1), and during the observing time, the beach face was about 40 m wide. The beach face was composed of moderate wide and fine sands, and the separation of the sands was high. There were many beach corners developing on the beach face. Lofty beach berm, steep beach face, steep ridge and deep longshore trough at the bottom of the beach face were the main forms of the beach profile. The gradient of the beach face was about 0.09 - 0.10. Under the water the slope of the beach face was much steeper, but the surf zone was narrow.

Waves at the deep water began to break up at the area about 30 m away from the coastal lines. There were active sand longshore bar and longshore trough morphology. In the deep trough the breaker waves form the big waves again and flapped the beach face to break. During the observing time, the wind direction was NNE, and waves were mainly swells, and the significant wave height was about 0.34 m in the deep trough under the beach face, and the wave period corresponding to the highest waves is about 10 seconds, and water level changed about 0.15 m.

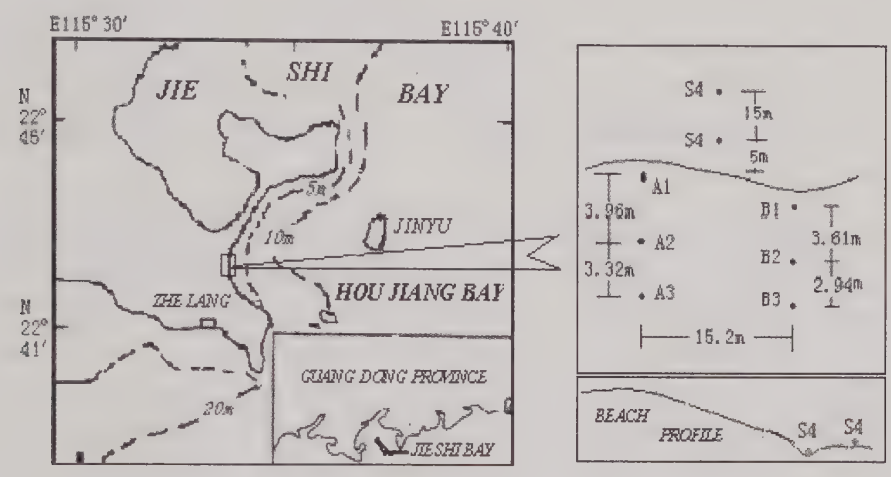

Fig.1 Sketch map of the study area showing measurement positions

2 Data and Method

2.1 Data collection and disposal

The observing time was from 9:10 to 11:25 on Oct.13, 2003.On the swash zone below the beach face put six stakes forming two observing profiles to inspect the beach face oscillations (Fig.1). One observing profile lies in the beach face ridge (A profile, gradient is 0.090), another observing profile lies in the beach face trough (B profile, gradient is 0.092). The lowest stake was about 1.5 m away from the coastal lines, and the distribution of the stakes can be found in the Fig.1. During the observing time, all the stakes lie in the swash zones basically. When observing, two people measured the height of the stakes exposed to the air every one minute, and two people recorded the data. The observer should be away from the stake as far as it can be, and measured after swashing going off so as to enhance the measuring precision.

Two S4ADW instruments were set at the longshore bar and longshore trough in the surf zone along the upright direction to the coastal line. The distance of the two instruments was about 15 m, and the S4ADW instrument near the coastal line was about 5 m away from the coastal line. During the observing time, the sampling frequency was 2 Hz.

Using each measuring stake height data subtracting the first-measuring data, we can get the time

sequence of every stake height changes to the first-measuring time. Besides, after eliminating the trends of the pressure data by S4ADW measured, then subtracting the averaging data, wave face oscillations data was get.

2.2 Method

Singular Spectrum Analysis is an effective statistic analyzing tool, whose main function is extorting as much information as possible from the limited study sequence including noise, analyzing the sequence variation trends and variation periods, filtering the noise, distinguishing and strengthening valid signals. And the SSA methods can effectively rebuild the periodical parts of different periods, and know the long-term changing ratio characteristics of the different period's parts. Simply describing its computing method as follows [9-12]:

Singular Spectrum Analysis is a transformative EOF analyzing method. A steady time sequence was shown as $\{X_t\}$, t =1... $N + m$ -1, Its time lagged matrix was made lag time experience intersecting expandedness, we can get the former

$$X^T = \begin{bmatrix} x_1 & x_2 & x_3 & \cdots & xn \\ x_2 & x_3 & x_4 & \cdots & x_{n+1} \\ x_3 & x_4 & x_5 & \cdots & x_{n+2} \\ \vdots & \vdots & \vdots & \vdots & \vdots \\ x_m & x_{m+1} & x_{m+2} & \cdots & x_{n+m-1} \end{bmatrix} \tag{1}$$

Character vectors (T—EOF), which can express the main periodic mode of the sequence, which can be used to distinguish and describe all kinds of linear and nonlinear signals included in the studying sequence. Relative to the corresponding time coefficient (T—PC), it expressed the long term changing characteristics of the corresponding periodic parts. After decomposed by SSA, the frequency signal is decomposed to the time sequence signal with the single circle periods, so we can rebuild the studying periodic part series according to the formulas as follows:

$$x_i^k = \frac{1}{i}\sum_{j=1}^{i} a_{i-j}^k E_j^k \qquad 1 \leqslant i \leqslant m\text{-}1 \tag{2}$$

$$x_i^k = \frac{1}{m}\sum_{j=1}^{m} a_{i-j}^k E_j^k \qquad m \leqslant i \leqslant n\text{-}\ m{+}1 \tag{3}$$

$$x_i^k = \frac{1}{n\text{-}i+1}\sum_{j=i-n+m}^{i} a_{i-j}^k E_j^k \qquad n - m + 2 \leqslant \mathrm{i} \leqslant \mathrm{n} \tag{4}$$

Where the formulas, a is the time coefficient, E is the eigenvector。

SSA can excellently get the signals that the periods are less than the dimensions m and spectrum width is less than 1/m from the studying time sequence. According to SSA methods, when there is one periodic signal in the studying sequence, it needs a pair of T-EOF and T-Pc and must satisfy three conditions as follows:

(1) The two linked Eigen values are nearly equal;

(2) The corresponding T-EOF are just intersecting and have the same periods with the time sequence they described.

(3) The pair of T-PC is just intersecting.

3 Analysis of the beach face variation trends and the periodic oscillation

3.1 Erosion and trends of the beach face variations

The studying object is the changing data (9：11—11：18) of the stake on the beach face. According to the SSA methods, using the studying data makes the best experiment of dimension m firstly, and chooses the best recognizing results to make the SSA analysis. The analyzed results showed that the T-EOF1 and T-EOF2 eigenvectors mainly reflected the changing trends of the beach face. The trend changing parts in terms of the formula 1-3 were rebuilt and the changing trends of the beach face were simulated (the oscillation and changing trends of the beach face shown as Fig.2). Using multinomial simulating method, we simulated the changes of actual water depth in the groove under the shorelines at the corresponding time, and these data represent the variations of surf zones water levels in the studying time (Fig.3).

As we can see from the changing line of the beach face(Fig. 2), the positions of A2、A3 on the beach face A basically kept on the eroding state with negative increase relative to the initial observing beach face, but the position of A1 experienced the circle of eroding–depositing–re-eroding processes; while we see the positions of the stakes on the beach face profile B at the bottom of the rhythm topography, they basically kept on the depositing states with positive increase. All In all, the rhythm topography of the beach corner in the studying time is in the dying phase, which is consistent with the result by eyeballing.

The studying results by Strahler, Berry, Elfrink, Baldock, Holmes, Horn et al. showed that the wave and current state of surf zones, the shape of the beach face, the constitution matter of the beach face, the changing of the underground water-level and the swash are the main factors influencing the locomotion of sediment movement [2,7,8,13]. Contacting the scene background, the actually observing record and the data analyzing, we found that the shape of surf zone and the state of the wave and current corresponding to the beach face profiles were basically same, and waves were normal incidence to the coast and had little influence on the different trends changing; water level of the surf zone changes little, and little difference on gradient and altitude between the near beach faces, but one beach profile was depositing and another was eroding. Therefore the changing of water level should not be the main reason for trends changing of the beach face. Combining the discussion of Masselink about the effect of swash to beach corner, the

author considered that owing to the difference between the beach face, the swash distributed at the ridge of the beach and converged at the concave of the beach, the sediment moved from the ridge to the concave and the ridge eroded and the concave deposited. That is to say, the difference of the swash out of the rhythm topography is the main reason for the ridge depositing and concave eroding, and it has retroaction on the existing and developing of the rhythm topography and accelerates the dying of beach corner rhythm topography.

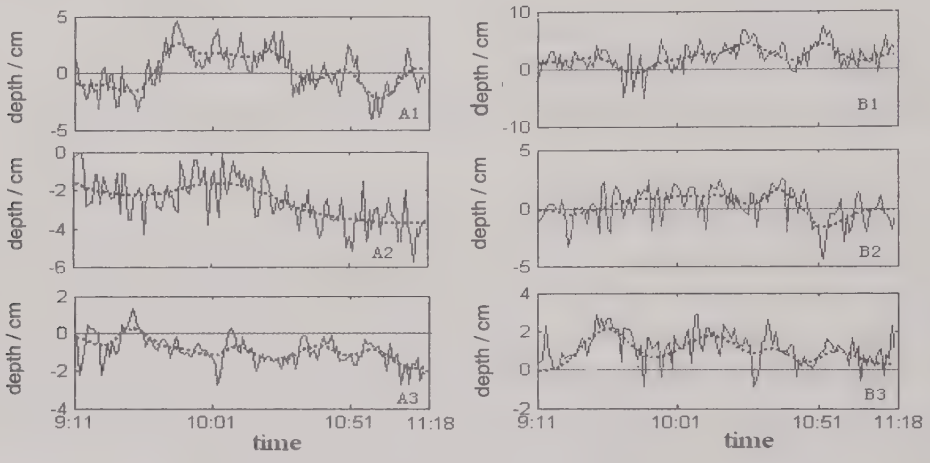

Fig.2 Sketch map of the oscillation and trend variety of the beach face

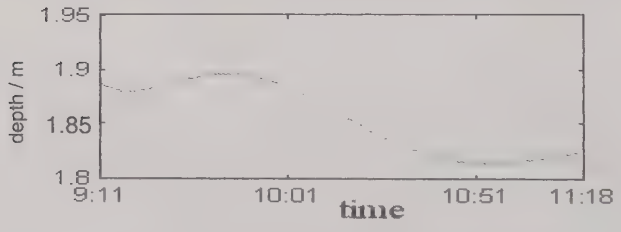

Fig.3 Sketch map of the tide level variety

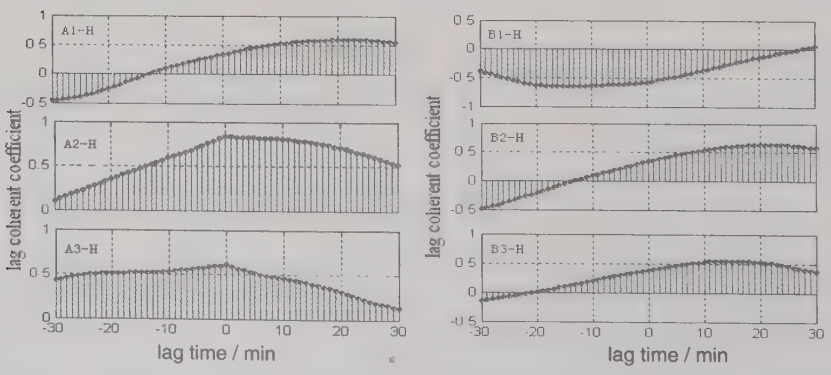

Fig.4. Cross correlation analysis between the beach face trend and tide level

The author made the analysis using the correlative function for the trends changing data of the beach face and the water level changing data at the corresponding time, and found an interesting result. From the formula:

$$r_{xy}(\tau) = \frac{1}{n-\tau}\sum_{t=1}^{n-t}\left(\frac{x_t - \bar{x}}{s_x}\right)\left(\frac{y_t - \bar{y}}{s_y}\right) \tag{5}$$

we can see that the correlation coefficient is mainly related to the distributing shape and scattering level of the time sequence *x* and *y*, but has no relation with the distributing numerical value no matter it is positive nor negative. As we can see from Fig.4, the beach face of A1,B2,B3 had obvious relativity at the time lagging water level changing about 10-20 minutes ,then we can deduce that water level changing has great lagging influence on the distributing shape of the A1,B2,B3 on the beach face. The A2 also has obvious lagging relativity with the water level changing of the surf zones, and the moment with most obvious relativity appears when the lag time is o, the author consider that the water level changing is still the main influencing factor for the trends changing shape., in despite of the strong disturbing from the influence of the slipstream converging at A2.With regard to the changing relation among A3, B1 and water level, the reason perhaps is that the position of A3 beach face is higher than that of B3,and the changing of water level hadn't directly influenced the change of A3;the position of B1was nearer to the coastal lines and lower than A1,so the direct and strong influence from the sharp broken waves and the swash reduced the influences from the changing of the water level. In a word, although there was some exhibition that changing of water level on the broken wave zone may influence the trends changing shape of beach face in the experiment, the result maybe just an accidence and need more scene observing date to analyze and validate.

3.2 Analysis of the periodic erosion and sediment oscillation of the beach face

Analyzing the eigenvectors from SSA, we find that the former ten eigenvectors include above 70% accumulative contribution(Tab.1),and the changing trends and periods of beach face are basically included in the former ten eigenvectors(the beach corner mainly included in the former eight eigenvectors). The changing curve of the rest eigenvectors are mainly turbulence and no obvious periods. So the former ten eigenvectors basically embodied the changing trends and periods of beach face, and the period part is mainly embodied in T-EOF3 —T-EOF10 eigenvectors (the ridge in T-EOF3 —T-EOF8). The trend changing is mainly embodied in T-EOF1—T-EOF2 eigenvectors. SSA inspection shows that periodic oscillation lies in the original sequence.

Analyzing the figure of the periodic erosion and sediment oscillation on the ridge of the beach face, we found that the forms of periodic erosion and sediment oscillation are basically the same either on the bottom or on the top of the swash influenced. They both had the periodic oscillation of 15 - 20 min and 8 - 9 min. Just on the hand of short periodic oscillation swash arousing, the bottom is mainly the 4minutes and 6minutes oscillation that are shorter about 2 min than the top. In the middle of the ridge where the swash influenced, the forms of the periodic oscillations were different to the bottom and top, and the periodic

oscillation was about 4-6minutes period.

Analyzing the figure of the periodic erosion and sediment oscillation on the beach face trough, we found that the oscillating periods changed little in the whole and centralized in the 2 to 6 min, and oscillating periods get longer from the bottom to the top, which was consistent with the studying results of Sallenger (1984) et al. Although the periodic changing trends on the ridge is different from Salinger's studying results, the main oscillating periods were in the range of their studying results [6].

According to the study of Baldock, Holmes, Guza, Thornton, Shen, Meyer ect, the swash on the steep beach face was mainly the infragravity frequency movement [1,2,7,8]. The periodic erosion and sediment oscillation on the swash zone mainly existed in the infragravity frequency according to the studies of the author and Sallenger. Based on these results, the author considered that there were important relations between the periodic erosion and sediment oscillations and the infragravity movements of the swash. Different profiles had different periods owing to the different shapes of the beach face. The moving forms of the infragravity were different in different beach face and the coupling processes of the beach oscillation and swash were not the same. In the whole, the characteristics of the infragravity parts in the swash and the shape of the beach face dominated the periodic erosion and sediment oscillation forms of the beach face.

In this study, the position of the concave is lower than that of the ridge, and the gradient is bigger than the later, and the infragravity oscillation of the later is more obvious than that of the former; the position of the former is higher relatively, corresponding that the observing position is ascended, presenting longer periodic oscillation. These results further confirmed the conclusion.

Tab.1 Cumulated contributing variance for the first eight eigenvectors of the beach face oscillation

	Dimension / m	T-EOF1	T-EOF2	T-EOF3	T-EOF4	T-EOF5	T-EOF6	T-EOF7	T-EOF8
A1	20	0.4178	0.5999	0.7066	0.7568	0.7894	0.8163	0.8367	0.8557
A2	24	0.4089	0.4716	0.5263	0.5796	0.6120	0.6442	0.6748	0.7040
A3	20	0.2906	0.4547	0.5998	0.6929	0.7402	0.7818	0.8129	0.8357
B1	20	0.2261	0.3829	0.4942	0.5675	0.6213	0.6638	0.7063	0.7422
B2	20	0.2130	0.3304	0.4015	0.4646	0.5271	0.5864	0.6449	0.6974
B3	20	0.2176	0.3984	0.4786	0.5293	0.5772	0.6224	0.6661	0.7088

3.3 Analysis of the oscillation intensions

Based on the studying methods of Sallenger, the original beach face oscillation data and the beach face oscillation data wiping off the means and trends factor of the each face oscillation height were through the analysis of standard deviation and let the doubled standard deviation express the total erosion and sediment oscillation intensions and periodic oscillation intensions of the corresponding time [6](Fig.7).

As we can see from the figure, the total erosion and sediment oscillation intensions and the periodic oscillation intensions at ridge and concave both had the stronger trends from land to sea, and the oscillation intensions at the concave were stronger than that at the ridge. This showed that the sediment moved more actively at the concave and at the beach position near sea at the same profile, and these parts of the beach changed more actively.

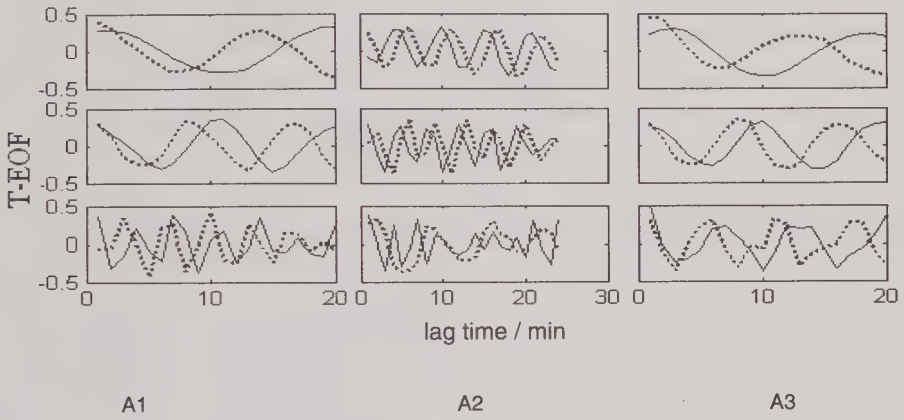

Fig.5 Distribution of the T-EOF3—T-EOF8 for the ridge oscillations (real line: odd vector; broken line: even vector

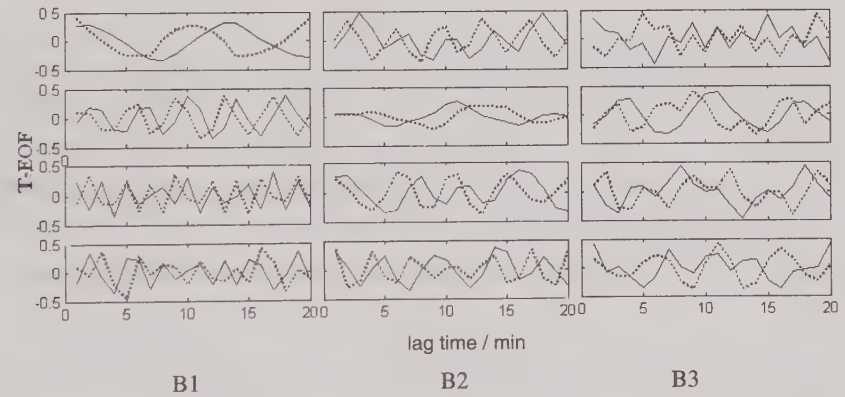

Fig.6 Distribution of the T-EOF3—T-EOF10 for the trough oscillations (real line: odd vector; broken line: even vector

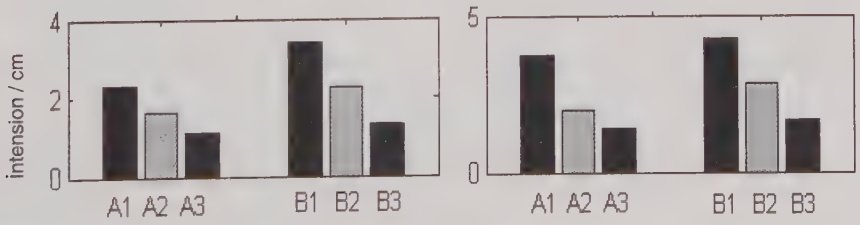

Fig.7 Histograms showing beach face oscillation (left: overall oscillation intension; right: periodic oscillation intension

Author considered that the dynamic difference induced the high coherence of the oscillation intensions on the same beach face profile. The swash intension to the beach face descended from the sea to the land, and the broken waves directly stroke the beach face near the coastal line, and the changing of water level influenced the beach face more directly and obviously. These factors induced the dynamic intension descending from the sea to the land on the beach face, and affected the disciplinary changing of the oscillation intensions. The difference of the profile shape is the ultimate reason for the difference of the oscillation intensions at the different profiles, because of the difference of the profile, on one hand, shape induced the dynamic difference on the beach in the vertical direction of the coastal lines, and on the other hand induced the diffluence and the circumfluence of swash along the coast, which induced the sediment transferring on different beach face profiles.

4 Analysis of the dynamical effect of the wave on broken wave zone

The character and the movement of the wave on the surf zones had great effect on the moving of sediment of the surf zones, the shape of the profile and the changing of the coast. The studies of Horn, Baldcock, Holmes et al. showed that the surf waves had decisive effect on the movement and the character of the swash on the beach face. Under the condition with steep beach profile, the movement of the swash mainly behaved the infragravity movement and the character of which was nearly correlated with the wave groups and the long waves of the surf zones[7]. Based on the above theories, filtering the pressure data collected by S4ADW at the 2Hz sampling frequency in the groove near the coast in the surf zones, get the wave surface bag data, and the infragravity waves data from 20 seconds to 250 seconds periods, and wave data at all frequency. Then resample the above data corresponding to the observing time of the stake at one minute sampling interval, at the same time get the height variations of each stake by the latter height subtracted the former, using the height variations reflecting the erosion and sediment of the beach face. By the cross spectrum analysis among the wave surface bag data, the infragravity waves data, the waves data, and the height variations of each stake, the relations among them were explored.

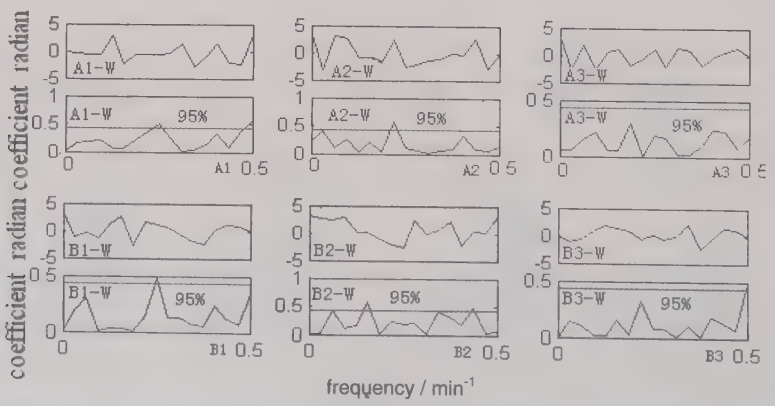

Fig.8 Cross spectrum analysis of the infragravity waves and the variation of beach face high frequency erosion and sediment

The results of the cross spectrum analyzing showed that the effect between the infragravity waves and the high frequency erosion and sediment variation of the beach face is more obvious than the other factors at the ridge of profile A and the concave of profile B (Fig.8).As seen from the figure, the correlation coefficient of the infragravity waves data and the high frequency erosion and sediment variation at the A1, A2, B, B2 beach face points reached 95 % believing level in some periods (generally from 4 min to 6 min). The phases corresponding to the periods with high believing level are positive, which showed that in this period the high frequency erosion and sediment variation lagged to the infragravity waves function, and the relation between them was obvious.

The relations between the high frequency erosion and sediment variations at the A3, B3 stake points of the beach face and the infragravity waves was less obvious than the bottom points, the author considered the reasons centralizing the following factors: (1) the character of the infragravity waves at A3, B3 beach face changed a lot when the infragravity waves in the surf zone moved to the swash zone. (2) the A3, B3 beach face points lie in the upper limit of the swash effected. Only the stronger swash can reach A3, B3 points. Therefore the A3, B3 points may not occur the erosion and sediment variation at every interval. But author considered that the high frequency erosion and sediment variation at A3, B3 are still affected and controlled by the infragravity.

5 Conclusion

Using the data of the high frequency variation in a short time and the data of waves in the surf zone influenced by swell, based on the analyzing methods of SSA and cross spectrum, the study get following conclusions:

a) The diffluence induced by the beach face rhythm topography had great effect on the movement of the sediment from ridge to the concave and accelerated the dying of the rhythm topography, and the trends changing shape of beach face is obviously influenced by the changing of water level on the broken wave zone.

b) The beach face influenced by the swash had obvious periodic erosion and sediment oscillations in the infragravity frequency, oscillating periods of the beach face augments from the beach bottom to the top. The kind of the periodic oscillation is relating to the movement of the infragravity waves in the swash and the shapes of the beach face.

c) The intension of the erosion and sediment oscillation descended from the beach bottom to the top.

d) The infragravity waves in the surf zones had great influence on the high frequency erosion and sediment variations of the beach face.

Acknowledgements

This study was supported by the National Natural Science Foundation of China under contract No. 40576041.

References:

[1] Marco Petti, Sandro Longo. Turbulence experiments in the swash zone [J]. Coastal Engineering, 2001, (43):1-24.

[2] Berry Elfrink, Tom Baldock. Hydrodynamics and sediment transport in the swash zone:a review and perspectives [J]. Coastal Engineering, 2002, (45):149-167.

[3] Archetti R, M Brocchini. An integral swash zone model with friction: an experimental and numerical investigation [J]. Coastal Engineering, 2002, (45):89-110.

[4] Gerhard Masselink, Michael Hughes. Field investigation of the sediment transport in the swash zone [J]. Continental Shelf Research, 1998, (18): 1179-1199.

[5] Marco Petti, Sandro Longo. Turbulence experiments in the swash zone [J]. Coastal Engineering, 2001, (43):1-24.

[6] Sallenger Jr A H, Richmond B M. High-freqency sediment-level oscillation in the swash zone [J]. Marine Geology, 1984, (60):155-164.

[7] Baldock T E, Holmes P, Horn D P. Low frequency swash motion induced by wave grouping [J]. Coastal Engineering, 1997, (32):197-222.

[8] Tony Butt, Paul Russell. Suspended sediment transport mechanisms in high-energy swash [J], Marine Geology, 1999, (161):361-375.

[9] Dong Anxiang, Juzhang, Yin Xianzhi. The singular spectrum analysis of snow damage in eastern Qinghai Xizang Plateau [J]. Plateau weather, 2001, 20(1):214-219.

[10] Xu Jialiang. The singular spectrum analysis for precipitation of year and seasons in Shanghai [J]. Weather Science, 1999,19(2):129-135.

[11] JiangZhihong, DingYuguo.Generality and applied features for singular spectrum analysis [J]. Acta Scientiarum of Weather,1998,56(6):737-746.

[12] Kuang Xueyuan, Zhong Lihua. Singular spectrum analysis of summer precipitation in the recent one hundred years in Nanning [J]. Guang Xi weather, 2000, 20(supplememt):26-29.

[13] Komalor P D, Qiu Jianli et al. translation. Beach process and sedimention [M]. Beijing: ocean publishing company, 1985,220-314.

[14] Masselink G. Pattiaratchi C B. Morphological evolution of beach cusps and associated swash circulation patterns [J]. Marine Geology, 1998, (146):93-113.

粤东后江湾冲流带滩面高频振动及动力作用分析

冯砚青[1,2]，陈子燊[2]，李志龙[2]，李志强[2]

（1. 国家海洋局南海工程勘察中心，广东 广州 510300；2. 中山大学水资源与环境系， 广东 广州 510275）

摘　要：利用涌浪影响下短时段内的冲流带滩面高频高程数据和碎波带波流资料，在奇异谱分析（SSA）的基础上，以比研究了不同形态滩面的冲淤变化趋势、趋势分布形状、冲淤变化周期和冲淤变化强度，以及同一条剖面不同桩点间各因素间的变化关系；用交叉谱方法探索了每分钟滩面高频冲淤变化与碎波带长重力波间的作用关系。分析结果表明，滩角韵律地形引起的冲流分流作用促进了滩脊向滩谷的泥沙转运，冲流带滩面存在明显的长重力波频段的周期性冲淤振动，滩面冲淤振动强度由滩面下部向上部递减，碎波带长重力波对滩面高频冲淤变化起重要作用。

关键词：冲流带；奇异谱分析；长重力波；交叉谱

The Relationship of Sulfate-methane Interface, the Methane Flux and the Underlying Gas Hydrate

FANG Yinxia, CHU Fengyou

The Second Institute of Oceanography & Key Lab of Submarine Geosciences, SOA, Hangzhou 310012, *China*

Abstract: The sulfate-methane interface is an important biogeochemical identification interface for the areas with high methane flux and containing gas hydrate. Above the sulfate-methane interface, the sulfate concentration in the sediment is consumed progressively for the decomposition of the organic matter and anaerobic methane oxidation. Below the sulfate-methane interface, the methane concentration increases continuously with the depth. Based on the variation characters of the sulfate and methane concentration around the sulfate-methane interface, it is feasible to estimate the intensity of the methane flux, and thereafter to infer the possible occurrence of gas hydrate. The geochemical data of the pore water taken from the northern slope of the South China Sea show the sulfate-methane interface is relatively shallow, which indicates that this area has the high methane flux. It is considered that the high methane flux is most probably caused by the occurrence of underlying gas hydrate in the northern slope of the South China Sea.

Keywords: gas hydrate; methane flux; sulfate-methane interface

Introduction

The occurrence of gas hydrate causes the concentration of the hydrocarbon gas in the sediment higher, and the decomposition of gas hydrate causes the concentration of chlorine in the pore water lower. But there is not any geochemical abnormity in the shallow sediment layer. The methane concentration of the sediment above the sulfate-methane interface (SMI) is usually very low, furthermore the most hydrocarbon gas in the sediment will be lost during the traditional core recovery from deep-water environments. So it is difficult to estimate whether the underlying gas hydrate is existence only based on the hydrocarbon gas concentration and the geochemical characters of the pore water in the shallow sediment layer. If there is no deep drilling and coring sample, how to identify the underlying gas hydrate through the geochemistry analysis of the shallow sediment and its pore water is a difficult problem. Borowski W S et al. [1,2] carried out the roundly geochemistry analysis of the drilled sediment sample obtained from Black Ridge which had drilled gas hydrate in ODP Leg 164. Through detailed study, they thought the SMI depth that determined by the sulfate and methane concentrations in the pore water and the concentration variation characters of the sulfate and methane above/below SMI could estimate the methane flux in the sediment below SMI, and thereafter to infer the possible occurrence of gas hydrate.

Received on November 8, 2007

After the past decade's explorations and researches of gas hydrate over the northern slope of the South China Sea, many kinds of evidences to infer the occurrence of gas hydrate are obtained. The northern slope of the South China Sea is a potential occurrence area of gas hydrate. But no gas hydrate sample is collected yet for the absence of the drilling exploration. So it is necessary to strengthen the research of the distributing characters of SMI in the pore water and the concentration variation characters of the sulfate and methane above/below SMI, which may provide the scientific reference for the next drilling exploration of gas hydrate in the northern slope of the South China Sea.

1 Geochemistry characters of sulfate-methane interface

Within anoxic marine sediments, the sulfate (SO_4^{2-}) is involved in two chemical reactions induced by the microbial activity that deplete the sulfate within the pore water of the sulfate reduction zone. In the first process, a vast amount of dissolved sulfate contained in the pore water is used as an oxidant by a consortium of microbes to breakdown sedimentary organic matter. This is the sulfate reduction function that induces the sulfate depletion of the pore water, and the sulfate concentration decreases continuously with the sediment depth. The second reaction involving the sulfate is anaerobic methane oxidation(AMO) occurring within the sulfate – methane interface, where the sulfate and methane are consumed at the base of the sulfate reduction zone shown by the reaction as follows [3,4]:

$$CH_4 + SO_4^{2-} \rightarrow 2HCO_3^- + HS^- + H_2O \quad (1)$$

In general, the function of sedimentary organic matter oxidized by microbe controls the sulfate concentration in the pore water and its variation gradient. But anaerobic methane oxidation may also become an important process to influence the sulfate concentration and its variation when a vast amount of methane is contained in the sediment.

The methanogenic zone is located below the sulfate reduction zone and SMI. Within marine sediment, there are two independent chemical reactions induced by microbial activity that produce methane within the methanogenic zone. One process is carbon dioxide deoxidized to methane (Reaction 2), and another is the acetate be fermented to methane (Reaction 3). The concentration of the produced methane is increasing with the depth at first.

$$CO_2 + 4H_2 \rightarrow CH_4 + 2H_2O \quad (2)$$

$$CH_3COOH \rightarrow CH_4 + CO_2 \quad (3)$$

The penetrated depth of the sulfate is nearly related with the concentration gradient of the sulfate, the sulfate flux and the oxidation velocity of methane within the zone from seafloor to SMI [5]. Fig.1 is the schematic diagram showing the chemical reactions thereabout the sulfate-methane interface in the shallow sediment. It shows the concentration variation characters of the sulfate, methane and the dissolved carbon dioxide. That is, the continuous sulfate depletion by the sulfate reduction and the anaerobic methane oxidation. The sulfate concentration decreases rapidly, and the methane

concentration increases gradually in the methanogenic zone. The concentration of the dissolved carbon dioxide represents the trend of gradually increasing thereabout the sulfate-methane interface, which suggests its continual production.

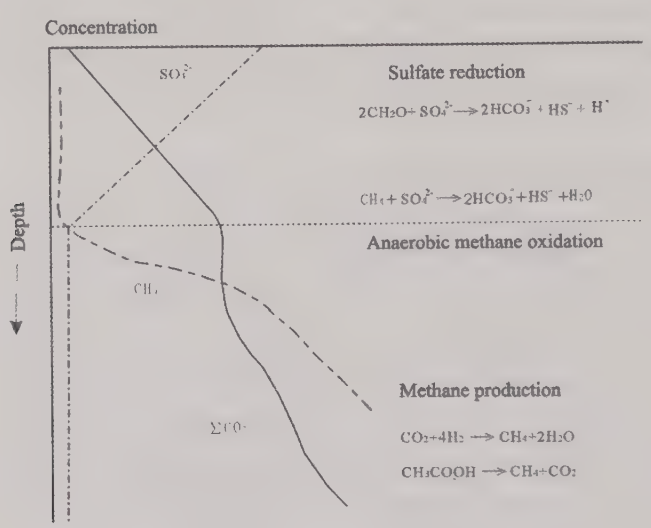

Fig.1 Schematic diagram showing the chemical reactions thereabout the sulfate-methane interface in the sediment (after Borowski W S et al., 1999) [2]

2 Relationship of SMI with methane flux and underlying gas hydrate

Borowski W S et al. [2, 6] carried out the detailed geochemistry analysis of the drilled sediment sample obtained from Black Ridge where had cored gas hydrate in ODP Leg 164. And they plotted the depth distribution chart of SMI over Black Ridge gas hydrate area. The methane and sulfate concentration variations of the shallow sediment pore water cored from ODP 164 site 994 and 995 showed in Fig.2. The figure shows that the methane concentration in the sulfate reduction zone is very low, but it increases rapidly below SMI. The vast methane consumption is resulted from anaerobic methane oxidation at the base of the sulfate reduction zone. The methane concentration is increasing rapidly below SMI because of the methane production. The sulfate concentration is mostly controlled by the amount of sedimentary organic matter. The studies of Borrows W S et al. in Black Ridge [1,2] show that the sedimentary velocity varies a little in this area, and the variation of sedimentary organic matter content is also small, but the concentration gradient of the sulfate in the pore water is big, and the most difference could be 16 times. It infers that the sulfate concentration should also be affected by other process (such as anaerobic methane oxidation) besides the reduction process. Above SMI of the sediment in Black Ridge gas hydrate area, the sulfate concentration in the pore water presents sharp linear decreasing trend. It suggests the sulfate concentration is possibly affected by the methane oxidation too.

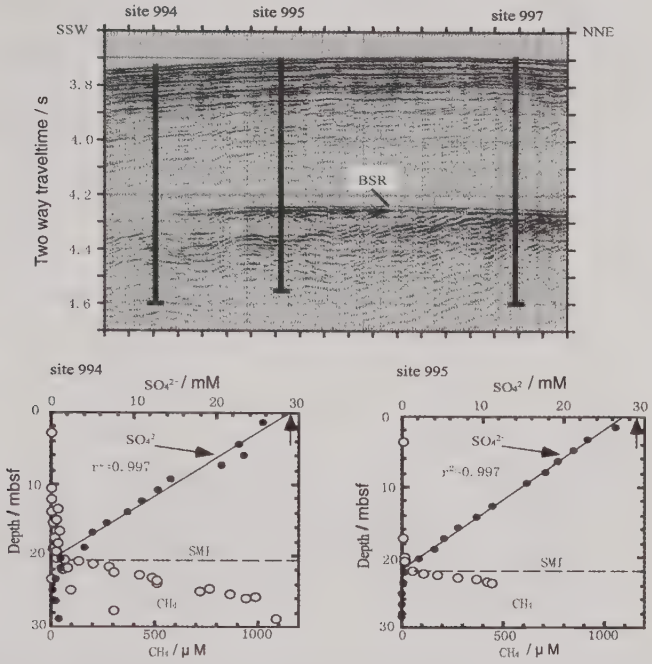

Fig.2 The distributions of BSR and SMI at ODP164 994 and 995 stations in gas hydrate area of Black Ridge (after Borowski W S et al., 2000)[6]

The study on the sulfate concentration variation also indicates the SMI depth in the deepwater sediment is generally more than 50 mbsf (meter below seafloor) [2]. However in gas hydrate area, due to the intensively influence of the methane oxidation, the sulfate concentration in the pore water would be decreasing rapidly, resulting in the SMI depth shallower. So the methane oxidation causes the SMI depth in the sediment shallower and the sulfate concentration decreasing rapidly. The methane flux affects the SMI depth and the variation gradient of the sulfate concentration directly. The methane oxidation will be enhanced by the vast upward methane, and result in the shallower SMI depth and the sharp linear decreasing of the sulfate concentration in the pore water. Consequently, the sharp linear decreasing of the sulfate concentration and the shallow SMI depth may infer the possible occurrence of the underlying gas hydrate. The statistics results of the ODP Hole data in the world also indicate that more than 95% of drilled hole in gas hydrate area have the characters of the shallow SMI depth (<50 mbsf) and the sharp linear decreasing of the sulfate concentration [7].

The relationships of SMI, the upward methane flux and the depth of gas hydrate zone are showed in Fig.3. Two cases are shown in the same gas hydrate setting (A and B) with the similar concentration ($\triangle C_A=\triangle C_B$), over a different gradient distance ($\triangle Z_A<\triangle Z_B$). Because of the shortened gradient distance in A, the magnitude of its methane concentration gradient is higher than that in B, which means the methane flux in A is bigger than that in B. The higher methane gradients near SMI, the higher the methane solubility around the base of gas hydrate stability (BGHS). The higher methane gradient is likely to result in the increasing methane production induced by the microbial activity with the depth, also is likely to relate

with the underlying gas hydrate. But the linear decreasing of the sulfate concentration showed in Fig.3 indicates that the sedimentary organic matter was consumed by the sulfate before the methane production. Furthermore, the total organic carbon (TOC) is varying little with depth in this area. So the phenomena of the high methane concentration gradient are not possibly result in the increasing methane by the strengthened methane production with the depth, and should be related with the underlying methane gas hydrates.

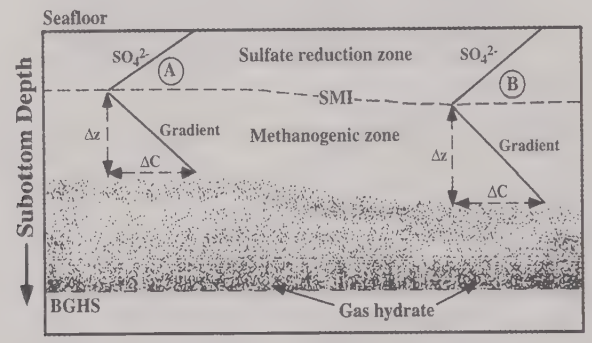

Fig.3 Cartoon showing the relationships of SMI, the upward methane flux and the depth of gas hydrate zone (after Borowski W S et al., 1999) [2]

The sulfate consumption in the pore water is controlled mostly by the quality and quantity of the sedimentary organic matter. Generally, the more sedimentary velocity, the more amount of organic matter accumulated in the sediment, and the quicker the oxidation process of the sedimentary organic matter by the sulfate reduction induced by the microbial activity. Consequently, in the area containing the vast amount of input organic matter, the sulfate is consumed by the microbial metabolize quickly. This quickens up the methane production in the marine anoxic condition, and produce the vast amount of methane. At present, it is found that the organic hydrocarbon source of marine gas hydrate is mainly microbiogenic methane. It is corresponding with the fact that the marine gas hydrate is distributing in the area of the organic-matter rich sediment in the world.

In the eastern margin of Japan Sea, detailed bathymetric and seismic profiles have revealed 36 large mud volcanoes. Each one has 20 - 40 m high and 300 - 500 m across. Onboard geochemical analysis of the pore water has shown the SMI are at around 1.5 mbsf to 3.0 mbsf. These findings strongly suggest the shallow depth of SMI is resulted from the high methane flux over that area [8].

The comparison of the bottom simulating reflector (BSR) with the sulfate-methane interface (SMI) over gas hydrate area also can obtain the relationship of the base of gas hydrate stability (BGHS) and SMI. Black Ridge is the typical gas hydrate area in the passive margin setting, and Hydrate Ridge is the typical gas hydrate area in the active margin setting. ODP 164 and 204 have verified the existence of gas hydrate over these two areas respectively (Fig.2, Fig.4). In Black Ridge gas hydrate area, BSR on the seismic profile at ODP164 site 994 and 995 are both located at 0.53 s (two way traveltime). On the assumption

that the velocity around BSR is 1600 m/s, the depth of BSR is about 424 mbsf. And the depth of SMI here is about 22 mbsf. In Hydrate Ridge gas hydrate area, the BSR on the seismic profile at ODP204 site 1244 and 1245 are respectively located at 0.22 s and 1.17 s (two way traveltime). If the velocity around BSR is also 1600 m/s, their depth of BSR are about 176 mbsf and 136 mbsf respectively. The depth of SMI is 8.5 mbsf and 7 mbsf correspondingly. These data suggest that the shallower the BSR, the symbol of BGHS, is,the shallower the depth of SMI is, moreover the ratio of the two depth is close to a constant (about 19 - 20). That is to say the BSR depth is 19 - 20 times of the SMI depth. Maybe this result is an occasional instance, and it needs to be verified by the plentiful measured data yet. But over gas hydrate area, there is assuredly an intimately relationship between the BSR depth and SMI depth.

The headspace gas analysis result of site 1244 (Fig.4) shows the SMI is located about 8.5 mbsf. At this interface the sulfate concentration is decreasing to the lowest, and the methane concentration begins to increase [9]. The highest concentration of the sulfate (29.7mM) locates at the interface of the sediment and the bottom water, but the concentration is decreasing to less than 1mM at 9.15 mbsf. The sulfate concentration doesn't decrease to zero below 9.15 mbsf, and keep it in less than 1 mM. The phenomena are possibly resulted from the water pollution during the core sampling. The variation curve of the sulfate concentration presents the linearity in the range of 4 - 7.5mbsf, and curves at the top and bottom. These are possibly related to the sulfate depletion induced by the oxidation of the sedimentary organic matter and the fluid flow of the horizontal convection.

At the condition of high methane concentration and high upward methane flux (such as in gas hydrate area), Borowski W S et al. [1] thought that the downward sulfate flux and upward methane flux would be kept in dynamic balance and they would be kept in a low reduction rate in the sulfate reduction zone. At this condition, the sulfate and methane form a pair of geochemistry combination because the sulfate and methane are both consumed by the anaerobic methane oxidation at SMI. The chemic ratio of the sulfate and methane consumed by AMO is about 1:1, so their flux at this interface is approximately equivalent. On the assumption that the sulfate depletion in the sulfate reduction zone is mainly controlled by AMO, then the upward methane flux may be calculated on the variation gradient of the sulfate concentration. We know the actual methane concentration is difficult to measure for the methane emanation during sampling. So the variation gradient of the sulfate concentration is an important parameter to calculate the methane flux.

Based on Fick's First Law, the sulfate flux from seafloor to SMI may be calculated by the follow equation:

$$J = D_0 \varphi^3 \delta C/\delta_x$$

In this equation, J expresses flux, D_0 the diffuse coefficient of the sulfate, φ the sedimentary porosity, $\delta C/\delta_x$ the variation gradient of the sulfate concentration with the depth.

The sulfate concentration variation of the pore water of ODP 164 site 994 and 995 in Black Ridge presents the linearity relation, but the relationship is not obvious in the shallow part of ODP 204 site 1244

and 1245 (Fig.2 and Fig.4). This suggests the sulfate concentration variation in the pore water is not controlled by AMO completely, and possibly effected by the underlying methane flux in the sediment too. The methane flux of site 1244 was calculated as 2.7×10^{-3} mM/(cm^2·a) based on the 5.5 mM/m of the sulfate concentration gradient between 4 mbsf and 8 mbsf. While in Black Ridge, the methane flux only has 1.8×10^{-3} mM/(cm^2·a) even though the maximal sulfate concentration gradient was selected [1,6]. Therefore the methane flux of ODP 204 site 1244 is higher by 33 % than the gas hydrate area in the passive margin setting and Hydrate ridge is a high methane flux area. So the high methane flux is a significant feature of gas hydrate area in the active margin setting.

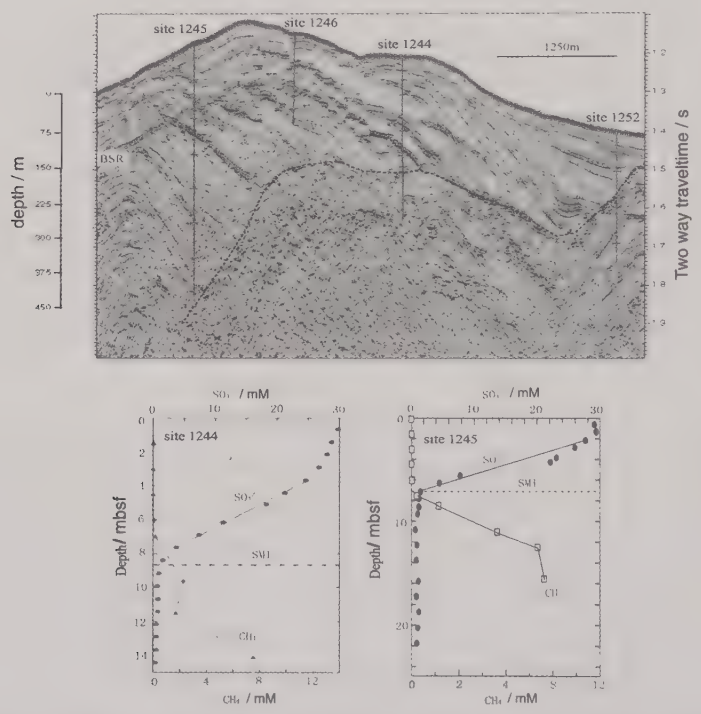

Fig.4 The distributions of BSR and SMI at ODP204 1244 and 1245 stations in gas hydrate area of Hydrate Ridge (after Gerhard Bohrmann et al., 2002) [9]

3 Concentration variations of methane and sulfate in the pore water over the northern slope of the South China Sea

After the decade explorations and researches of the natural gas hydrate resources, many kinds of evidences are obtained for the existence of gas hydrate in the northern slope of the South China Sea. This region has the relatively big sedimentary velocity. The drilling results of ODP 184 site 1144 which located in the southeast of Dongsha islands reveal the sedimentary velocity is about 400 - 1200m/Ma since 1Ma BP. This rapid sedimentary process benefits the formation of the sediment body for the occurrence of gas hydrate. Furthermore there are three tectonic movements over this region at the end of early Cretaceous,

the end of Eocene and the end of middle Miocene, which induced the fracture-rich sediment under the middle Miocene layer over the northern slope region, and some fractures even penetrate to the seafloor from basement. The development of fracture benefits the transportation of the upward hydrocarbon gas for long distance. And the tectonic activity character of long-term calmness since later Miocene is in favor of the preservation of gas hydrate. Consequently the northern slope of the South China Sea is a potential gas hydrate area. Song Haibin et al. distinguished BSR from the seismic profile SO95-10 across ODP 184 site 1144[10]. Before long, Zhang Guangxue et al. also identified BSR at 0.7s (two way traveltime) below seafloor from the seismic profile across ODP 184 site 1144, via the re-process of the plentiful multichannel seismic profiles over the northern slope region of the South China Sea [10]. The depth of the identified BSR is about 650 mbsf. Guangzhou Marine Geological Survey has carried out a mass of geophysical and multi-subject explorations over the northern slope of South China Sea since 1999, and mapped the BSR distribution area. In BSR distribution area, some characteristic physiognomy landscapes can be distinguished on the seafloor such as scar, fault-block that is the remains of the fault activity. Furthermore the seafloor has also developed the large-scale gravity-flow sediment and contourite sediment, and the authigenic carbonates are sampled in some sites. Moreover the methane abnormity and other geochemical abnormity induced by the decomposition of gas hydrate are found in this area too. For instance, there are headspace gas abnormity in site 1144, and the methane concentration in the headspace gas increases obviously between 300 mbsf and 600 mbsf. Other characteristic geochemical abnormities are found such as the low chlorine concentration of the pore water, the formation of the ^{18}O-rich authigenic siderite nodule, the shallow sulfate reduction zone and the abnormal oxygen and carbon isotopes compositional characteristics of the methane [12-14]. All of these abnormities are possibly resulted from the decomposition of gas hydrate, the dilution of the pore water and the increasing concentration of the methane. More fortunately, the distributions of these abnormities are consistent with the distribution of BSR approximately, which suggests these region is the favorable gas hydrate area.

Otherwise, the sulfate mass concentrations of the sedimentary pore water from the Area E (118°40′ - 119°40′E, 21°20′ - 22°10′N) over the northern part of the South China Sea also present the variation trend of decreasing with the depth obviously [7]. The SMI depth of five sites in this area are respectively listed as follows: site E-01 is 10.0 mbsf, site E-02 is 7.5 mbsf, site E-03 is 14.2 mbsf, site E-04 is 9.6 mbsf, and site E-05 is 8.2 mbsf. The SMI depth of the site of W-05 and W-03 located in the Area W are respectively 17.2 mbsf and 16.8 mbsf. The characteristics of rapid decreasing of the sulfate mass concentrations completely accord with the generalized result supported by the main gas hydrate area in the world, that the SMI depth in the pore water over gas hydrate area is less than 50 mbsf. But the analysis data of the drilling sites located at the northern part in ODP 184 have not the same characteristics. Besides the SMI depths of the northernmost site 1144 which is relatively shallow (about 11 mbsf), the depths of other site increase gradually from north to south. The SMI depth of site 1145, 1146, 1147 are respectively 185 mbsf, 65 mbsf and 76 mbsf [15]. The SMI depths of these sites are all bigger than the depth of the typical gas hydrate area. Besides site 1144, the methane flux of other site is relatively low, so that the occurrence possibility of in situ gas hydrate is also small. Obviously the distribution of the methane flux is not uniform

over the northern slope of the South China Sea. It is obviously higher in Dongsha islands region that is possibly related with the occurrence of the underlying gas hydrate. However the shelf of the South China Sea is rich in petroleum and nature gas, and distributes many oil gas seepages over the offshore, and the methane flux in the sediment will relatively high, and the SMI depth is shallow too. So it's necessary to conduct analysis combining with other data to estimate the occurrence of gas hydrate.

4 Conclusions

The best effective method to explore the marine gas hydrate is deep drilling, but it is not fit to utilize widely for its high cost. If no deep drilling and coring sample, how to identify the underlying gas hydrate only based the geochemistry analysis of the shallow sediment and its pore water is an attended problem. The geochemistry analysis data of the pore water over the typical gas hydrate area indicate that SMI and the concentration variation characters of sulfate and methane above/below SMI could estimate the methane flux in the sediment below the SMI, and thereafter to infer the possible occurrence of gas hydrate. The upward methane flux may control the concentration gradient of the sulfate in the pore water and the depth of SMI. So the SMI depth of the shallow sediment pore water can estimate the amount of the upward methane flux. Though some other causes (such as the existence of marine oil gas seepages) also result in the high methane flux and the shallow SMI, SMI is still an effective identification interface for the areas containing gas hydrate. The pore water analysis data taken from the potential gas hydrate area in northern slope of South China Sea show the depth of SMI is shallow, that suggest the methane flux is high in these area. This high methane flux is most probably resulted in the underlying gas hydrate, and infers the occurrence of gas hydrate deposit below the seafloor in some depth range is this area.

Acknowledgments

The project is funded by the National Basic Research Program of China (No. 2007CB411703).

Reference

[1] Borowski W S, Paull C K, Ussler III W. Marine pore water sulfate profiles indicate in situ methane flux from underlying gas hydrate [J]. Geology,1996,24,655-658.

[2] Borowski W S, Paull C K, Ussler III W. Global and local variations of interstitial sulfate gradients in deep-water, continental margin sediments: sensitivity to underlying methane and gas hydrates [J]. Mar. Geol., 1999,159,131-154.

[3] Reeburgh W S. Methane consumption in Cariaco trench waters and sediments. Earth Planet [J]. Sci. Lett., 1976, 28, 337-344.

[4] Hoehler T M, Alperin M J, Albert D B, et al. Field and laboratory studies of methane oxidation in anoxic marine sediment: evidence for a methanogen-sulfate reducer consortium [J]. Global Biogeochem,1994,8（4）: 451-463.

[5] Jørgenson B B, Weber A, Zophi J. Sulfate reductuion and anaerobic methane oxidation in Black Sea

sediments[J]. Deep-Sea Res.I, 2001,48: 2097-2120.

[6] Borowski W S, Hoehler T M, Alperin M J, et al. Significance of anaerobic methane oxidation in methane-rich sediments overlying the Blake Ridge gas hydrates [A], in: Paull C K, Matsumoto R, Wallace PJ, et al(Eds.), Proc. ODP Sci. Res. 164,2000:87-99.

[7] Jiang Shaoyong, Yang Tao, Xue Zicheng et al. Chlorine and Sulfate Concentrations in Pore Waters from Marine Sediments in the North Margin of the South China Sea and Their Implications for Gas Hydrate Exploration [J].Geoscience, 2005,19(1)：45-54.

[8] Matsumoto R, Okuda Y, Aoyama C, et al. Methane Plumes over a Marine Gas Hydrate System in the Eastern Margin of the Sea of Japan: a Proposed Mechanism for the Transport of Significant Subsurface Methane to Shallow Waters [A]. 2004, AGU Fall Meeting Abstracts, 575. San Francisco, United States.

[9] Gerhard Bohrmann, Anne M. Tréhu, Jack Baldauf, et al. Ocean Drilling Program Leg 204 Scientific Prospectus Drilling: Gas Hydrates On Hydrate Ridge,Cascadia Continental Margin[A], 2002,College Station, Taxes, 50.

[10] Song Haibin, Geng Jianhua, WANG How-king, et al. A Preliminary Study of Gas Hydrates in Dongsha Region North of South China Sea [J].Chinese Journal of Geophysics, 2001，44(5)：668-694.

[11] Zhang Guangxue, Huang Yongyang, Zhu Youhai, et al., Prospect of Gas Hydrate Resources in the South China Sea [J]. Marine Geollgy& Quaternary Geology, 2002，22(1)：75-87.

[12] Wu Bihao, ZHU Youhai, WANG Jianqiao, et a1. Gas hydrate in the South China Sea: Review and prospect [J]. EOS Trans，2000，81(22):66.

[13] Zhu Youhai, Wu Bihao, Lu Zhenquan. The prospecting for gas hydrate offshore China [J]. Mineral Deposits，2001，20(2)：174-180.

[14] Tianmin Guo, Bihao Wu, Youhai Zhu, et al. A review on the gas hydrate research in China. Journal of Petroleum Science and Engineering [J]. 2004, 41:11-20.

[15] Wang P, Prell W L, Blum P, et al. Proceeding of the Ocean Drilling Program, Initial Reports 184 [A] Taxes：College Station. 2002,623.

硫酸盐-甲烷界面与甲烷通量及下伏水合物赋存的关系

方银霞，初凤友

（国家海洋局 第二海洋研究所，国家海洋局 海底科学重点实验室，浙江 杭州 310012）

摘 要：硫酸盐-甲烷界面在富甲烷和含天然气水合物的海洋沉积区已经成为一个重要的生物地球化学识别边界。在硫酸盐-甲烷界面之上，沉积物中的硫酸盐因参与分解有机质和甲烷厌氧氧化反应而被消耗，而界面之下沉积物中的甲烷则不断生成，含量逐渐增加。根据该界面附近硫酸盐浓度和甲烷浓度的变化特征，可以判断该区甲烷流体通量的大小，从而指示下伏天然气水合物的可能赋存状况。南海北部陆坡的柱状沉积物孔隙水数据的分析显示，其硫酸盐-甲烷界面埋深比较浅，表明该海域的甲烷通量较高。这种高甲烷通量很可能是由下伏的天然气水合物所引起的，并暗示着该区下伏海底可能有天然气水合物沉积层赋存。

关键词：天然气水合物；甲烷通量；硫酸盐-甲烷界面

Concentrations, Accumulation and Sources of PAHs in Surface Layer Sediments of Taizhou Bay

JIN Binming[1], JIANG Jinhua[2]

1. *School of Life Science, Wenzhou Medical College, Wenzhou* 325035, *Zhejiang, China;*

2. *Environmental Engineering Department, Taizhou College, Linhai* 317000, *Zhejiang, China*

Abstract: The concentrations, accumulation and sources of 15 polycyclic aromatic hydrocarbons (PAHs) had been studied or evaluated in the surface layer sediments of Taizhou Bay, China. It showed that the concentrations of PAHs ranged from 85.4 to 167.6 ng/g (averaged 138.62 ng/g), and the highest level was found in Jiao Jiang Dock. Percentages of 2-, 3-, 4-, 5- and 6-cyclic aromatic hydrocarbons were 7.8 %, 42.1 %, 33.3 %, 9.6 % and 7.2 % respectively. The accumulation indices of PAHs ranged from 532.7 to 1068.9 (averaged 807.5), and the index of Phenanthrene was the highest (122.7), while that of Benzo (a) Pyrene was the lowest (2.7) among them. In Taizhou Bay, PAHs in surface layer sediments came mainly from coal burning, partly from direct pollution of petroleum hydrocarbons.

Keywords: Taizhou Bay; Surface layer sediment; PAHs; Concentration

Introduction

PAHs, as persistent organic contaminants, widely existing in the environment, mainly come from forest fires, volcanic activitives, automobile gases and oil leaking, et al. In marine environment, they threaten marine eco-environment and harm human's health through food chain as well. They were commonly carried by suspended substance in waters and atmospheric aerosol. When combined with sediments in seawater, it is very difficult for them to be degraded photochemically, or oxidated by microorganisms, and thus accumulated in sediments eventually [1]. The Study on concentrations of PAHs in marine sediments could help to understand the transmutation of contaminants reversely and reveal their pollution history [2]. Much attentions had been paid on them since 1970s worldwidely, and Chinese scholars began to study pollution charecteristics of PAHs in inshore areas since 1980s and it was shown that pollution situations were clearly positively correlative with industry development in coastal area. In recent years, environmental researchers in China had made a massive investigation on the pollution situation of PAHs in the East China Sea [3], South China Sea [4], Bohai Sea [5] and Yellow Sea [6], and found that there existed great differences in PAHs concentration among different periods and areas. So it was very necessary to make a deep research on pollution degrees, sources and concentration causes of PAHs in marine environments.

Many factors could cause the difference in concentration levels of PAHs in marine sediments, such

Received on January 4, 2008

as organic carbon content in marine sediment [7], particle diameter of sediment, the discharge amount of oily wastewater from ships, the scale of marine aquaculture, and the development of coastal industry and urbanization, etc. Many Industries such as aquaculture, chemical industry, electric power industry, terminal operation and dismantlement works of used electric appliance had been growing rapidly in the areas around Taizhou Bay ,and Taizhou Power Plant, a station consuming 10,000 tons of coal per day, might be the main source of PAHs in the marine environment of Taizhou Bay. In this paper, the concentration, accumulation and possible sources of PAHs in surface layer sediment in Taizhou Bay were studied to provide some scientific references for the sustainable development of coastwise marine industries in Taizhou.

1 Material and menthod

1.1 Sampling

Sediments and seawater were sampled in April 2006. 7 sites in inshore area (shown in Fig.1) were selected according to the current course of water system in Taizhou Bay. Station 1 was located in the entrance of Taizhou Bay (with a boatyard nearby.); Station 2 was situated near Jiaojiang Dock.; Station 3 was near the coal transportation dock used by Taizhou Power Plant; Station 4 was next to the sewage outlets of Taizhou Power Plant; Station 5 was just around the sewage outlets of Jiaojiang chemical industry area.; Station 6 was near the sewage outlets of Linhai chemical industry area and Station 7 was around the marine aquaculture area of Taizhou Bay. Collected by grab bucket sampler, surface layer sediment samples were placed in glass jars and then carried to laboratory, air-dried naturally, grinded, put in glass jars, sealed and stored for further use; Water samples from surface, middle and bottom layer of seawater were also collected in the same station simultaneously.

Fig.1 Sampling sites

1.2 Instruments and reagents

An Agilent 1100 series high-efficiency liquid chromatography (HELC) (fluorescence detector); chromatographic column specially for PAHs (3 × 250 mm, Agilent);

15 PAHs standard substances: Naphthalene, Cenaphthene, Fluorene, Phenanthrene, Anthracene, Fluoranthene, Pyrene, Benzo (a) anthracene, Chrysene, Benzo (b) fluoranthene, Benzo (k) fluoranthene, Benzo (a) pyrene, Dibenzo (a, h) anthracene, Benzo (g, hi) perylene, Indeno (1, 2, 3-cd) pyrene (purchased from Acros Organics, America); ultra-pure water ,chromatographically or analytically pure reagents for experimental use.

1.3 Pretreatment of samples

1.3.1 Pretreatment of water samples

60 mL water sample and 60 mL redistilled methylene dichloride were added into the iodine flask, ultrasonic extracted for 60 mins at 30 °C, and kept static state for 20 mins; 50 mL organic extract was moved to a rotary evaporator, condensed to 0.5 mL, then dried with nitrogen; dissolved with 2 mL HPLC pure methyl alcohol, PAHs were filtrated into the flask with 0.22 μm filter paper, and then analyzed with HPLC/FLD; Each sample was analyzed repeatedly for three times and control experiments were done at the same time. The concentration unit of PAHs in seawater was ng/g.

1.3.2 Pretreatment of sediment samples

2 g sediment was intermixed with anhydrous sodium sulfate, added 10 mL methylene dichloride, ultrasonic extracted for 60 mins, and kept static state for 20 mins, centrifuged for 10 mins with 3000 r/min; 3 mL supernatant fluid was filtered through 2 g silica gel column and eluted with 11 mL methylene dichloride plus n-hexane (1:1); Eluted fluid was condensed to 0.5 mL with a rotary evaporator , dried with nitrogen, 2 mL HPLC pure methanol added to dissolve PAHs, and then filtered into flask with 0.22 μm filter paper and finally analyzed with HPLC/FLD; each sample was analyzed repeatedly for three times and control experiments were done at the same time. The concentration unit of PAHs in surface layer sediments was ng/g.

1.4 Condition and quality control for HPLC/FLD analysis of samples PAHs

All samples were analyzed by an Agilent 1100 series high-efficiency liquid chromatography coupled with fluorescence detector. 15 μl sample was added, and methyl cyanide-water acted as carrier liquid at a constant flow rate of 0.5 mL/min, and the column temperature was 30 °C. The revised collection rate of PAHs in this analysis method was from 72 % to 115 %. The detectabilities were 0.09 $ng \cdot L^{-1}$ for Naphthalene, 0.08 for Cenaphthene, 0.05 for Fluorene, 0.04 for Phenanthrene, 0.02 for Anthracene, 0.1 for Fluoranthene, 0.05 for Pyrene, 0.2 for Benzo (a) anthracene, 0.06 for Chrysene, 0.08 for Benzo (b) fluoranthene, 0.04 for Benzo (k) fluoranthene, 0.06 for Benzo (a) pyrene, 0.1 for Dibenzo (a, h) anthracene, 0.2 for Benzo (g, hi) perylene and Indeno (1, 2, 3 - cd) pyrene respectively.

2 Results and discussion

Concentrations, accumulation indices of PAHs in samples of surface layer sediment and those of surface, middle and bottom layer water were showed in Tab.1.

Tab.1 Concentration and accumulation of PAHs in water (ng/L) and sediment

	site	Naph	Ace	Fluor	Phen	An	FlA	Pyr	BaA	Chry	BbF	BkF	BaP	DA	BP	In	∑PAHs
seawater	1	384.3	226.2	179.9	294.4	68.7	262.1	855.3	293.1	197.6	103.9	58.0	104.6	56.6	117	40.8	3242.5
	2	746.2	287.5	401.5	381.7	78.8	209.1	907.9	332.2	178.3	85.4	37.5	86.8	19.3	78	20.4	3850.6
	3	413.1	101.3	337.1	333.7	74.6	211.5	938	314.9	192.6	99.9	40.0	93.9	17.2	93.2	22.5	3283.5
	4	359.8	96.5	133.8	411.7	81.1	209.4	1126	495.2	191.5	90.3	39.7	92.3	19.3	82.1	20.7	3449.4
	5	693.8	124	465.1	435.9	82.6	246.7	853.1	308.6	187.5	93.1	39.4	88.4	23.6	85.7	28.2	3755.7
	6	370.6	61.6	489.2	337.5	78.5	221	782.6	279.6	169.1	101.8	38.9	86.2	20.8	81.1	14.1	3132.6
	7	212	56.6	277.5	280.5	74.2	216.7	819.6	310.2	193	99.1	40.6	93.2	35.6	82.6	20.8	2812.2
surface layer sediment	1	9.47	1.79	3.51	29.82	3.1	25.72	10.81	8.78	2.25	18.5	6.12	0.55	0.12	19.86	8.25	148.6
	2	24.05	2.34	14.6	59.15	3.6	15.68	2.14	8	15.84	13.26	2.34	0.21	0.24	3.63	2.51	167.6
	3	9.82	1.89	5.63	28.85	1.19	10.87	1.69	4.76	56	19.18	1.41	0.12	0.09	5.19	1.29	148.0
	4	1.04	nd	7.29	47.77	2.15	30.94	3.48	12.15	8.91	7.02	3.62	0.48	0.10	14.75	5.88	145.6
	5	11.98	1.58	10.7	65.39	6.24	12.06	1.46	8.51	14.83	5.48	0.85	0.05	0.01	1.8	0.54	141.5
	6	8.6	1.48	8.12	36.91	2.03	8.53	2.13	20.27	33.38	6.18	2.37	0.26	0.11	2.5	0.82	133.7
	7	9.38	1.39	6.83	39.54	4.64	5.43	0.99	2.99	3.06	6.25	0.81	0.07	0.01	2.75	1.24	85.4
	$\overline{X}$	10.62	1.5	8.1	43.92	3.28	15.6	3.24	9.35	19.18	10.84	2.5	0.25	0.1	7.21	2.93	138.6
accumulation indices	1	24.6	7.9	19.5	101.3	45.1	98.1	12.6	30.0	11.4	178.1	105.5	5.3	2.1	169.7	202.2	1013.4
	2	32.2	8.1	36.4	155.0	45.7	75.0	2.4	24.1	88.8	155.3	62.4	2.4	12.4	46.5	123.0	869.7
	3	23.8	18.7	16.7	86.5	15.9	51.4	1.8	15.11	290.8	192.1	35.2	1.3	5.2	55.7	57.3	867.5
	4	2.9	0	54.5	116.0	26.5	147.8	3.1	24.51	46.5	77.7	91.2	5.2	5.2	179.7	284.1	1064.9
	5	17.3	12.7	23.0	150.0	75.5	46.9	1.7	27.6	79.1	58.9	21.6	0.6	0.4	21.0	19.1	557.4
	6	23.2	24.0	16.6	109.4	25.9	38.6	2.7	72.5	197.4	60.7	60.9	3.0	5.3	30.8	58.2	729.2
	7	44.3	24.6	24.6	140.9	62.5	25.1	1.2	9.6	15.8	63.1	20.0	0.8	0.3	33.3	59.6	525.7
	$\overline{X}$	24.0	13.7	27.3	122.7	42.4	69.3	3.6	29.1	104.3	112.3	56.7	2.7	4.4	76.7	114.8	804.0

Note: 1. dry weight for contents in sediment; 2. nd : no necessity to be detected

2.1 Concentration of PAHs in surface layer sediments of Taizhou Bay

Tab.1 indicated that the concentrations of PAHs in surface layer sediments ranged from 85.4 to 167.6 ng/g, and the average value was 138.62 ng/g. In the light of 15 PAHs concentration sequence from high to low, stations in turn were 2, 1, 3, 4, 6, 5 and 7. Station 2 had the highest level (167.6 ng/g), while station 7 the lowest (85.4 ng/g), and there were little difference among station 1 - 6. PAHs pollution

situation was relatively lower compared with some reported cases both home and abroad. It was reported that there were cases where the concentration of PAHs in surface layer sediments was above 100μg/g (dry weight, the same as follows) in some countries, such as that in Narragansett Bay were 0.569 - 216 μg/g [8]; concentration of PAHs in Izmit in the Marmara, which is one of the reported highest level of PAHs ,was unexpectedly up to 30.0 - 1670.0 μg/g [9]; other cases listed were, for example, Ulsan Port of Korea (0.017 - 3.1 μg/g) [10], Aegean Sea of Greece (45 - 148 ng/g) [11], and Adriatic Waters of Italia (24.1 - 501.1 ng/g) [12], et al. In China, the concentrations of total PAHs in the East China Sea, South China Sea, Bohai Sea and Yellow Sea were 105.3 - 60000 ng/g [13,14], 82 - 49066 ng/g [15,16], 32.70 - 3558.88 ng/g [5,17] and 222.1 - 776.3 ng/g [6] respectively.

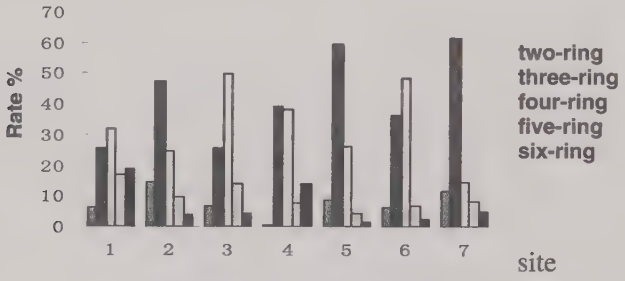

Fig.2 The rate of simple PAHs

Considering the individual ingredient, the concentration of Phenanthrene was relatively higher and averaged 43.92 ng/g, followed by Chrysene of 19.19, Benzo (b) fluoranthene of 15.60 ng/g and Naphthalene of 10.84 ng/g , whereas Dibenzo (a, h), anthracene and Benzo (a) pyrene were relatively lower than others. Some scholars considered that all carcinogenic PAHs have Phenanthrene cycle, and they could be regarded as derivatives of Phenanthren with the outstanding feature of 9 and 10 bonds of Phenanthren, because of their high electron density, and are prone to combine with DNA and RNA in cells to cause Carcinogenesis [18]. In surface layer sediments in Taizhou Bay, PAHs with HMW had been picked out in every station in some way, and maybe have potential toxic and side effect on marine organism. It is very important to carry out the further investigation and steps should be taken to insure the security of aquatic product, because Taizhou Bay had been developed to be an important aquaculture base.

2.2 Composition characteristics of PAHs in surface layer sediments

Fig.2 showed percentages of PAHs with 2 - 6 benzene ring in total PAHs concentration. Arene with 2 ring made up 0.71 % - 14.4 % of total PAHs (averaged 7.8 %), and highest level was found in station 2. Arene with 3 ring made up 25.38 % - 61.37 % of total PAHs (averaged 42.1%), and relatively high levels was found in station 2, 4, 5 and 7. Arene with 4 ring made up 14.6 % - 49.55 % of total PAHs (averaged 33.3 %), and relatively high levels in station 1, 3, 4 and 6. Arene with 5 ring made up 4.51 % - 16.9 % of total PAHs (averaged 9.6 %), and was found relatively high levels in station 1 and 3. Arene with 6 ring made up 1.66 - 19.0% of total PAHs (averaged 7.2 %), and relatively high levels in station 1 and 4. The

rates of arene with 3 ring and 4 ring were relatively high in surface layer sediments. Compared with other arene, arene with 4 ring had a uniform distribution in all stations. Another characteristic was that PAHs with more than 4 ring had a high percentage in total PAHs. In this sea area, highly toxic PAHs with more than 4 rings in this area should be paid more attention to, though total concentration of PAHs in surface layer sediments was not so high. PAHs with more than 4 rings, such as Pyrene, Fluoranthene and Benzo (a) pyrene had features with high boiling points, solvable in oil and relatively high Genotoxicity, Benzo (a) pyrene, Indeno (1, 2, 3-cd) pyrene and Dibenzo (a, h) anthracene were especially extreme carcinogens.

2.3 PAHs accumulation rules in surface layer sediments

PAHs accumulation indices in all stations were defined as the ratios of PAHs concentration in surface layer sediments to that in seawater at the same station, as showed in Tab.1. 15 PAHs accumulation index in the surface layer sediments ranged from 525.7 to 1064.9 (averaged 804.0); Phenanthrene accumulation index ranged from 86.5 to 155.0 (with the highest average value 122.7 compared with others); Indeno (1, 2, 3-cd) pyrene accumulation index ranged from 11.1 to 202.2 (averaged 114.8); Benzo (b) fluoranthene accumulation index was from 58.9 to 192.1 (averaged 112.3); Chrysene accumulation index was 104.3; and all four above were in excess of 100. Benzo (a) pyrene (2.7), Pyrene (3.6) and Dibenzo (a, h) anthracene (4.4) had low accumulation indices.

2.4 Sources analysis of PAHs in surface layer sediments

The sources of PAHs in surface layer sediments of Taizhou Bay were identified by the ratio method. If the ratio of FluA/ (FluA+ Pyr) was smaller than 0.4, it meant that the PAHs was from oil pollution. If the ratio of FluA/(FluA+ Pyr) was larger than 0.5, it meant that PAHs was from burning of firewood and coal. And if the ration was from 0.4 to 0.5, that was from burning of oil or its refined products. If the ratio of In /(In + B[gih]P) was smaller than 0.2, it meant that PAHs was from oil discharge, and from burning of fossil fuel if the rations between them. According to parameters of every station shown in Fig. 3, we could conclude that sources of PAHs in surface layer sediments in Taizhou Bay were mainly from burning of coal and fossil fuel.

Fig.3 Diagnostic ration for source identification

3 Conclusion

a) PAHs concentration in surface layer sediments ranged from 85.4 to 167.6 ng/g (averaged

138.6 ng/g). In the ordination of total PAHs concentration from high to low, station order were in turn Jiaojiang Dock, the entrance of Taizhou Bay, Taizhou Power Plant's coal dock, Taizhou Power Plant's sewage outlets, Jiaojiang Chemical Industry Park's sewage outlets, Linhai Chemical Industry Park's sewage outlets, and Taizhou Bay marine aquaculture area. Concentration of PAHs in surface layer sediment in Jiaojiang dock was the highest one of 167.6 ng/g and 2.5 times higher than that at marine aquaculture area with the lowest value of 85.4 ng/g. Compared with other marine areas home and abroad, PAHs pollution was relatively low in surface layer sediments in Taizhou Bay.

b) 15 PAHs accumulation indices in surface layer sediments ranged from 525.7 to 1064.9 (averaged 804.0). Phenanthrene accumulation index has the largest(averaged 122.7), Indeno (1, 2, 3-cd) pyrene in the next place (averaged 114.8), Benzo (b) fluoranthene was the third (averaged 112.3) ,and Benzo (a) pyrene was the least (averaged 2.7).

c) Sources of PAHs in surface layer sediments of Taizhou Bay were mainly from burning of coal and fossil fuel.

References

[1] Sicre M A, Marty J C, Saliot A, et al. Aliphatic and aromatic hydrocarbons in the Mediterranean aerosol [J]. Inter national J.of Environ.Anal.Chem, 1987, 29:73-94.

[2] Hites RA, Laflame RE, Farrington JW. Sedimenta polycyclic aromatic hydrocarbons: The historical record [J]. Science, 1977, 198:829-831.

[3] Wang X H, Xu L,Chen W Q, et al. The vertical distributions of polycyclic aromatic hydrocarbons and the tracing of pollutants in sediments of Xiamen Bay [J]. China Environmental Science. 1997, 17(1): 19-22.

[4] Luo X J, Chen S J, Mai B X, et al. Distribution and Sources of Polycyclic Aromatic Hydrocarbons in Sediments from Rivers of Pearl River Delta and Its Nearby South China Sea [J]. Environmental Science, 2005, 26(4): 129-134.

[5] Lin X M, Liu W X, Chen J L, et al. Distribution and ecological risk assessment of polycyclic aromatic hydrocarbons in surface sediments from Bohai Sea,China [J]. Acta Scientiae Circumstantiae,2005,25(1):70-75.

[6] LI B, Wu Y, Zhang J. Distribution and source of polycyclic aromatic hydrocarbons(PAHs)in surface sediment of the northern Yellow Sea [J]. China Environmental Science ,2002,22(5): 429-432.

[7] Webster L, Fryer RJ, Megginson C, et al. The polycyclic aromatic hydrocarbon and geochemical biomarker composition of sediments from sea lochs on the west coast of Scotland [J]. J Environ Monit.2004 , 6(3):219-228.

[8] Paul C. Hartmann, James G, et al. The distribution and sources of polycyclic aromatic hydrocarbons in Narragansett Bay surface sediments [J]. Marine Pollution Bulletin. 2004, 48: 351-358.

[9] Telli-Karakoc F, Tolun L, Henkelmann B, et al. Polycyclic aromatic hydrocarbons (PAHs) and polychlorinated biphenyls (PCBs) distributions in the Bay of Marmara sea: Izmit Bay [J]. Environ Pollut. 2002, 119(3): 383-397.

[10] Khim .S, Lee, K. T. Kannan K, et al. Trace Organic Contaminants in Sediment and Water from Ulsan Bay and Its Vicinity [J]. Environ. Contam. Toxicol., 2001, 40:141-150.

[11] Papadopoulou D, Samara C. Polycyclic aromatic hydrocarbon contamination and LUMIStox solvent extract toxicity of marine sediments in the North Aegean Sea, Greece [J]. Environ Toxicol. 2002, 17(6): 556-566.

[12] Magi E R, Bianco C, Ianni M, et al. Distribution of polycyclic aromatic hydrocarbons in the sediments of the Adriatic Sea [J]. Environmental Pollution, 2002, 119: 91-98.

[13] Tian Y, Zheng T L, Wang X H. Concentration, distribution and source of polucuclic aromatic hydrocarbons in surface sediments of Xiamen wastern harbor [J]. Oceanologia Etlimnologia Sinica, 2004, 35(1): 15-20.

[14] Qiu Y W, Zhou J L, K Maskaoui, et al. Distribution of polycyclic aromatic hydrocarbons in water and sediments from daya bay and their ecological hazard assessment [J]. Journal of tropical oceanography,2004, 23(4): 72-80.

[15] Wu Q H, Mai B X, Peng P A, et al. The study of grain-size distribution of PAHs and organochlorine in sedimen [J]. Environmental Monitoring in China.2004, 20(5): 1-6.

[16] Yang Y L, Mai B X, Pan J, et al. Distribution and sources of polycyclic aromatic hydrocarbon in sediments of Jiaozhou Bay [J]. Marine Environmental Science, 2003, 22(4): 38-43.

[17] Liu X M, Xu X R, Zhang X T, et al. A preliminary study on PAHs in the surface sediment samples from Dalian Bay [J]. Acta Scientiae Circumstantiae, 2001,21(4): 507-509.

[18] Xiao Y. Studies on microbial ecology toxicity of phenanthrene and isolation, characterization of phenanthrenedegrader as well as cloning and expression of degrading genes [C]. Zhejiang University. 2004.

[19] Yu X L, Zhang J. Pollution by multiring aromatic hydrocarbons and its preventive treatment strategy [J]. Environmental protection of Oil & Gas Fields,1996,6(4):53-56

[20] Yunker M B, Macdo N A, Vingarzan R,et al. PAHs in the Fraser River basin: acritical appraisal of PAH ratios as in dicators of PAH source and composition [J].Organic Geochemistry,2002,33:489-515.

台州湾海域表层沉积物中多环芳烃的浓度水平、富集规律及来源

金彬明[1]，江锦花[2]

（1. 温州医学院生命科学学院，浙江 温州，325035；2. 台州学院环境工程系，浙江 临海，317000）

摘 要：研究了台州湾海域海水和表层沉积物中 15 种多环芳烃（PAHs）的浓度水平，评价了表层沉积物对多环芳烃的富集规律，探讨其可能来源。结果表明，表层沉积物中 PAHs 的浓度范围为 85.4 ～ 167.6 ng/g，平均值为 138.62 ng/g，总多环芳烃的最大值是椒江码头。表层沉积物中二环、三环、四环、五环和六环多环芳烃占总多环芳烃的百分含量平均值分别为 7.8 %，42.1 %，33.3 %，9.6 %和 7.2 %，三环多环芳烃的含量最高；表层沉积物对多环芳烃的富集系数为 532.7 ～ 1068.9，平均值为 807.5，单组分菲的富集系数最高为 122.7，最小的是苯并（a）芘为 2.7；台州湾表层沉积物中的多环芳烃主要来源于燃煤污染，部分来源于石油烃类物质的直接污染。

关键词：台州湾；表层沉积物；多环芳烃（PAHs）；浓度水平

Cultural and luminescent Conditions of a Marine luminous Bacterium

FANG Hongda[1], DONG Yanhong[1], XU Zhanzhou[1], YUAN Yin[2], LI Xiuqin[1], YI Bin[1]

1. *South China Sea Environmental Monitoring Center, State Oceanic Administration, Guangzhou* 510300, *China*;

2. *College of Life Science and Biological Pharmacy, Guangdong Pharmaceutical University, Guangzhou* 510006, *China*

Abstract: Study of marine noctilucence in marine is important to fishery, environmental monitoring and military affairs. A luminous bacterial strain D2 was isolated from the marine sediment samples collected near Donghai Island in Zhanjiang, China. The primary cultural and luminescent conditions of luminous bacterium D2 which was identified as *Vibrio* sp. were determined in liquid culture. The results showed that pH 7.0, 35 °C, with 2.0 % NaCl, were the best growth conditions, and pH5 - 6, 20 °C, OD_{600} 0.08, with 3.0 % NaCl, were the optimal luminescent conditions.

Keywords: Luminous bacterium; growth conditions; luminescent conditions; quorum sensing system

Introduction

Luminous bacteria can emit light under normal metabolic state. Changes in environmental conditions affect the intensity of bioluminescent emission which can be detected by using toxicity induced bioluminescence sensing systems. In recent years, the luminosity of the bacteria has been discovered to show special responses to the toxicity of environmental pollutants and therefore could be used as bacterial biosensors. It has the advantages of sensitivity, accuracy and easy operation.

In 1960s, the bioluminescence of a marine bacterium *Vibrio fischeri* was reported in many researches. For the first time, Nealson et al. (1970) discovered that the intensity of bioluminescent emission was positive correlated to the density of *Vibrio fischeri* individuals. And the bioluminescent emission was controlled by the quorum sensing system (QS).

The bacteria sense cell density within groups by detecting the amount of the signal molecules in order to act as multi-cellular organisms. So they have the functions which can not be obtained by single cell. The density-dependent intercellular communication was defined as bacteria quorum sensing system (Fuqua et al. 1994). Beside bioluminescence, many physiological functions and phenotype characteristics were controlled by the signal transduction induced by quorum sensing system. They include synthesis of antibiotics, regulation of nitrogen fixation gene expression, conjugative transfer of Ti plasmid, swarming, biofilm formation and pathogenic gene expression. N-acyl-homoserine lactones（AHLs）, which was defined as autoinducers (AIs), acts as signal molecules in QS of most gram-negative bacteria. The gene

Received on November 20, 2007

expression of bacteria was triggered as soon as the concentration of AHLs molecules exceeded the critical value with the increase of cell density within groups (Fuqua 1996).

Luminous bacteria are generally assigned to four generas, that is, *Vibrio*, *Photobacterium*, *Shewanella* and *Xenorhabdus*. Classification of luminous bacteria that can emit light continuously and effectively is one of the keys to develop bacterial biosensors. A marine luminous bacterium strain was isolated from the sediment near Donghai Island, Zhan-jiang City of China. The purpose of this research was to optimize the growth and bioluminescent emission conditions.

1 Materials and methods

1.1 Materials

1.1.1 Bacterium

Based on morphological and biochemical characteristic analysis, the marine luminous bacterium D2 was identified as *Vibrio* sp. according to Bergets's Manual of determinative bacteriology.

1.1.2 Reagents and instruments

The peptone and yeast extract were produced by OXOID Company. The natural seawater was treated in darkness for weeks before it was used to preparation for culture medium. Other reagents were analytically pure. The organism density of D2 was measured by a Model 722 spectrophotometer. The intensity of bioluminescent emission was detected using a bioluminescence sensing system made in Institute of Soil Science, Chinese Academy of Science.

1.2 Methods

1.2.1 Growth curve of marine luminous bacterium D2

Cultivation of pure bacterial colonies of D2 was conducted in 3 mL 2216E medium (5.0 g peptone, 1.0g yeast powder, 1000 mL treated seawater, pH 7.0). The liquid culture was shaken well in temperature 30 °C for 15 hours. A volume of 100μL culture was combined with 200 mL LB liquid medium. The treatments were incubated at 30 °C reelingly. OD_{600} of the treatments were measured at 2 h, 4 h, 5 h, 6 h, 7 h, 8 h, 9 h, 10 h, 11 h, 12 h and 13 h, respectively.

1.2.2 Effects of the PH on the growth and luminescence of D2

Combination of pure bacterial colonies with 3 mL 2216E liquid medium was incubated at 30 °C and shaken for 15 hours overnight. A volume of 100μL culture was mixed with 25 mL 2216E medium in which pH varied from 5.0 to 8.0 in 1.0 steps. The treatments were vortexed and incubated at 30 °C. OD_{600} of the treatments were measured after 12 h cultivation. The luminous intensity of the combination of 100μL culture with 0.9 mL NaCl buffer (w/v 3 %) was also measured in which pH ranged from 4.0 to 8.0 in 1.0

steps.

1.2.3 Effects of culture temperature on the growth and luminescence of D2

A volume of 100 μL culture was combined with 25 mL 2216E liquid medium. The treatments were shaken and incubated at the temperature ranging from 20 °C to 35 °C in 5.0 °C steps. OD_{600} of the cultures were measured after 12 h cultivation. The luminous intensity of the combination of 100 μL culture with 0.9 mL NaCl buffer (w/v =3 %) was also measured at 4 °C, 20 °C, 30 °C, 35 °C and 40 °C.

1.2.4 Effects of the concentration of sodium chloride on the growth and luminescence of D2

NaCl solutions, whose concentrations ranged from 0 to 4 % (w/v) in 1.0 % steps, were used to prepare for 2216E liquid medium instead of seawater. A volume of 100 μL culture was combined with 25 mL 2216E medium mentioned above. OD_{600} of the treatments were measured after being incubated at 30 °C for 12 h. The luminous intensity of the combination of 100μL culture with 0.9 mL NaCl buffer, whose concentrations ranged from 0 to 6 %, was also measured.

1.2.5 Effect of bacteria density on the luminescence of D2

A volume of 5 mL 3 % (w/v) NaCl buffer was combined with cultures whose volumes were 5 μL, 10 μL, 20 μL, 50 μL, 100 μL and 200 μL. The luminous intensity of the treatments was measured.

2 Results

2.1 Growth curve

An exponential growth type of D2 was observed with time increased (Fig. 1). The stationary phase occurred after 11 h to 13 h incubation.

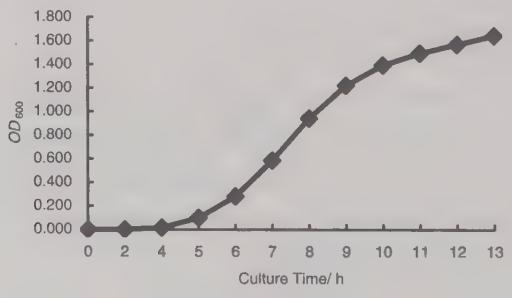

Fig. 1 Growth curve of marine luminous bacterium D2

2.2 Effects of the pH on the growth and luminescence of D2

The pH at 7.0 was optimum for growth of D2 (Fig. 2A). Bioluminescence caused by D2 occurred at

pH varying from 4 to 8. The greatest intensity of bioluminescent emission was detected at pH from 5 to 6 (Fig.2B).

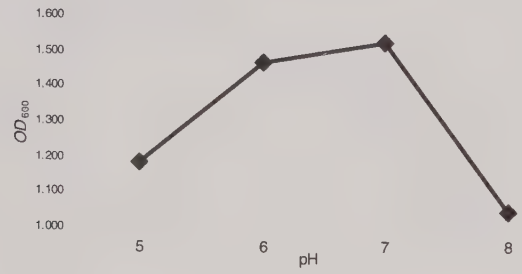

(A)

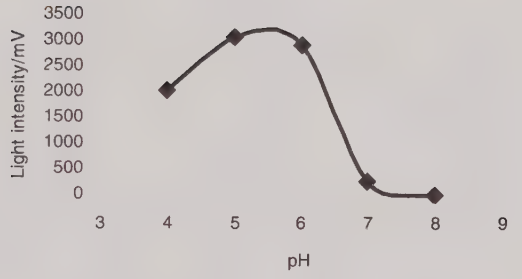

(B)

Fig. 2 Effects of the pHon the growth and luminescence of D2

2.3 Effects of culture temperature on the growth and luminescence of D2

The growth of D2 was optimum at about 35 °C (Fig.3A), while the greatest intensity of bioluminescent emission was detected at about 20 °C (Fig.3B). An inhibition on the growth of D2 by temperature was observed when it exceeded 35 °C.

2.3 Effects of the concentration of sodium chloride on the growth and luminescence of D2

The growth of D2 was optimum at 2 % (w/v) NaCl (Fig. 4A). The significant effects on luminosity of D2 by the concentration of sodium chloride have been observed in the experiment. The greatest emitted light intensity was detected at 2 % (w/v) NaCl (Fig.4B).

2.5 Effects of bacteria density on the luminescence of D2

The intensity of bioluminescent emission was significantly correlated to bacteria density. Little light was emitted when the cells were under the critical density. A burst-mode of luminosity emitted by D2 was observed as soon as the OD_{600} of the treatments reached 0.08 with a density of about 10^5 / mL.

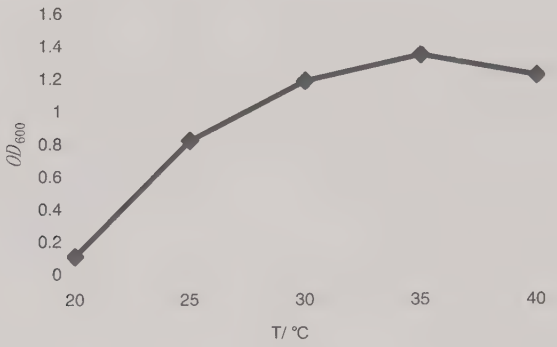

(A)

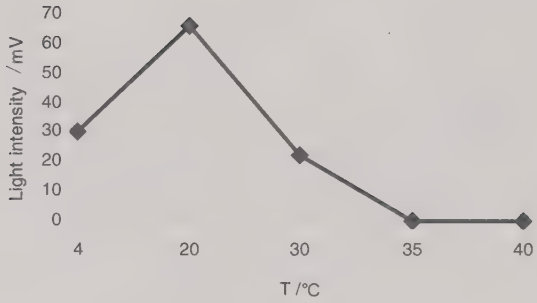

(B)

Fig. 3 Effects of culture temperature on the (A) growth and (B) luminescence of D2

3 Discussion

Marine bacteria, which were rich in environment, have great value in medicine development, ecological research and environmental protection. Marine luminous bacteria are so common that they are isolated from environment for toxicity assessment.

The marine luminous bacteria strain D2, identified as *Vibrio* genus, were isolated from the sediment near Donghai Island at Zhanjiang City. An experiment was conducted to optimize the growth and bioluminescence conditions for D2. The results showed that the optimum conditions for growing D2 were at pH 7.0, 35 °C and 2.0 % (w/v) NaCl, while the optimum conditions for bioluminescence were at pH 5 to 6, 20 °C and 3.0 % (w/v) NaCl.

A density-dependent reaction was discovered in the bioluminescence of D2. The light emission increased significantly as soon as the cell density exceeded the critical density. In contrast, none of light

emission was detected because the cell density was under the critical density. The results indicated that the critical density of D2 was OD_{600}=0.08. This suggested that the bioluminescence of D2 was also regulated by the quorum sensing system (QS).

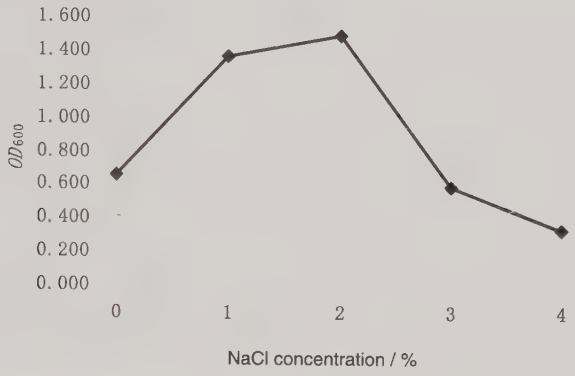

(A)

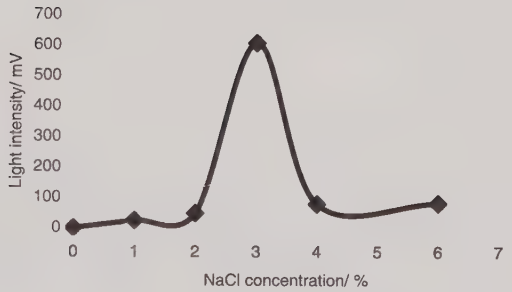

(B)

Fig. 4 Effects of the concentration of sodium chloride on the (A) growth and (B) luminescence of D2

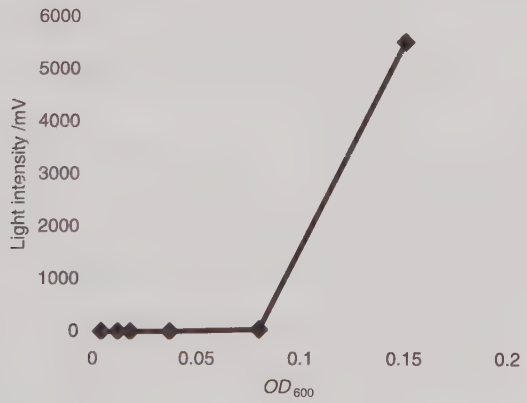

Fig. 5 Effect of bacteria density on the luminescence of D2

In the natural environment, the external cellular signal molecules were often degraded biologically or physically. Factors affecting the light emission of luminous bacteria become more complex. The external cellular signal molecules seldom reached the critical density in marine environment. In contrast, it was more practicable for the bacteria to exceed the critical density as they inhabited in the organs. For example, *Vibrio fischeri* inhabited in the organs could not compose a fluorescein enzyme to emit light until the cells reach the critical density to release enough AHLs signal molecules. Such course was not observed when *Vibrio fischeri* was free in the seawater (Engebrecht et al. 1983, 1984, 1987). Some of luminous bacteria quit light emission as soon as they left the surface of animal skins. It suggested that the bioluminescence was not only controlled by the cells density but also environmental factors such as pH which made it quite different from the niches on the surface of animal skins.

The effects on the growth and bioluminescence of D2 by environmental factors were demonstrated by the experiments. The optimal conditions for growth were different from those for bioluminescence which needs further research on whether it was specie-specific.

In summary, the researches on marine bioluminescence were of great potential for practice. The results on specie-specific spectrum are very important for developing in situ sensing systems and fast indentification kits for luminous bacteria.

Reference

[1] John G Holt, Noel R Krieg, Peter H A Sneath, et al. Bergey's Manual of Determinative Bacteriology (Ninth Edition) [M]. Williams &Wilkins, Baltimore, USA , 1994: 71-377.

[2] Nealson K H, Platt T, Hastings J W. Cellular control of the synthesis and activity of the bacterial luminescent system [J]. J Bacteriol, 1970, 104:313-322.

[3] Fuqua W C, Winans S C, Greenberg E P. Quorum sensing in bacteria: the LuxR-LuxI family of cell density-responsive transcriptional regulators [J]. J Bacteriol, 1994, 176:269-275.

[4] Fuqua W C, Winans S C. Conserved cis-acting promoter elements are required for density-dependent transcription of Agrobacterium tumefaciens conjugal transfer genes [J]. J. Bacteriol, 1996,178:435-440

[5] Engebrecht J, Nealson K, Silverman M. Bacterial bioluminescence: Isolation and genetic analysis of functions from *Vibrio fischer* [J]. Cell, 1983, 32:773-781.

[6] Engedrecht J, Silverman M. Identification of genes and gene products necessary for bacterial bioluminescence [J]. Proc Natl Acad Sci, 1984, 81: 4154-4158.

[7] Engebrecht J, Silverman M. Nucleotide sequence of the regulatory locus controlling expression of bacterial genes for bioluminescence [J]. Nucleic Acids Res, 1987, 15:10 455-10 467.

海洋发光弧菌的生长和发光条件的研究

方宏达[1]，董燕红[1]，袁茵[2]，李秀芹[1]，易斌[1]

（1. 国家海洋局南海环境监测中心，广东 广州 510300；2. 广东药学院生命科学与生物制药学院，广东 广州 510224）

摘 要：海洋生物发光研究对渔业、环境监测等有着举足轻重的意义。本文从湛江东海岛海域沉积物样品中分离出一株海洋发光弧菌（*Vibrio* sp.），本研究中编号为 D2，对这株菌的生长和发光条件进行了初步研究。实验结果表明，海洋发光弧菌 D2 在 pH 7.0、温度 35 °C、NaCl 浓度为 2.0 %时，生长状态最好；在 pH5 - 6、温度 20 °C、NaCl 浓度为 3.0 %、细菌密度 OD_{600} 达 0.08 时，发光强度最高。

关键词：发光细菌；生长条件；发光强度；细菌群体感应系统

Effects of Heavy Metal and Pollutants on the Non-special Immunity of the Shrimp and Crab

AI Chunxiang, WANG Xiaojuan, LI Shaojing, WANG Guizhong, LIN Qiongwu

College of Oceanography & Environmental Science, Xiamen University, Xiamen 361005, *Fujian, China*

Abstract: This paper attempted to review and evaluate existing information about the effects of heavy metal, ammonia-N, nitrite and the organic pollutants on the non-special immune response of the shrimp and crab, which providing theory for improving the self-immunity of shrimp and crab by meliorating cultural environment. In addition, it could provide information for further study on this field.

Keywords: Shrimp and crab, non-special immune, heavy metal, pollutants

Introduction

Recently, shrimp and crab culture is currently suffering serious losses due to infectious diseases all over the world. Disease outbreak in aquatic animals can be caused by many reasons, like wastewater from processes of industrial and agricultural production, feed and feces from aquaculture, remains of dead shrimp and crab or offing beach pollutions. All that made aquaculture environment more and more deteriorated yearly. Ecologically integrated-control on diseases of the shrimp and crab, analyzing disease resistibility of shrimp and crab, infection of pathogens and environmental physiology mechanism of immune regulation affected by environmental factors are concerned as strategies to prevent and cure diseases. Environmental stress from heavy metal and pollutants seems to be important factor for determining reduction of immunocompetence and is signalled by the appearance or the increased prevalence of diseases in shrimp and crab [1]. Environment quality of waters and influences of environmental factors on non-special immune of the shrimp and crab have become new research hotspots. This paper summarized researches of effects of environmental factors (heavy mental, ammonia-N, nitrite, pollutants) on the non-special immune of shrimp and crab at home and abroad, in order to accumulate research information of non-special immune of the shrimp and crab for further research.

1 Influence of several environmental factors on the non-special immune of the shrimp and crab

1.1 Effects of heavy metal on the non-special immune of the shrimp and crab

Heavy metal is not only poisonous to the shrimp and crab, affects the development or even results in

Received on November 30, 2007

mortality, but also is harmful to human health through biologic enrichment and food chain transfer. The effect mechanisms of heavy metal for shrimp and crab growth, development and survival are complicated, and few studies on effects of heavy metal on shrimp and crab immunity are known. If *Carcinus maenas* exposed to 500μg·L^{-1} Cd^{2+} for 30d, heamocyte phagocytic ability to bacteria will decrease [2]. *Macrobrachium rosenbergii* exposed to 1μg·L^{-1} mercuric chloride over a 30-day period, and exhibited hyperplastic gill lamellae engorged with haemocytes. And then, haemocytes were released into the interlamellar spaces through necrotic regions and they covered the entire gill lamellae, and total haemocyte counts(THC) were reduced during exposing to Hg^{2+}[3]. *Palaemon elegans* was exposed to 0.1 mg·$L^{-1}Cu^{2+}$, 0.05 mg·$L^{-1}Hg^{2+}$, 0.1 mg·$L^{-1}Cd^{2+}$, 0.5 mg·$L^{-1}Cr^{2+}$, 1.0 mg·$L^{-1}Zn^{2+}$ or 10.0 mg·$L^{-1}Pb^{2+}$, respectively, and after the initial 8 h, THC of *Palaemon elegans* in each group decreased, while after 16 h, it recovered to the original level[4]. This study showed that host itself had certain adaptability to heavy mental, and low heavy metal ion concentration was less poisonous to the host.

As a common disinfectant and remedial medicine of shrimp and crab culture, although $CuSO_4$ is effective to diseases of shrimp and crab, at the same time, long-term usage of $CuSO_4$ could affect their immunity. Low concentration (0.1 mg·L^{-1}) of $CuSO_4$ could decrease the sensitivity to *Lactococcus garvieae*, and the sensitivity increased with $CuSO_4$ concentration elevating, but when $CuSO_4$ concentration was higher than 0.2 mg·L^{-1}, superoxide anion increased in *Macrobrachium rosenbergii* [5]. Heavy mentals of different concentrations have special effects on shrimp and crab. 9.6 μg·l^{-1} Hg^{2+} and 60.5 μg·$l^{-1}Cu^{2+}$ could enhance the heamocyte phogocytic ability of *Macrobrachium malcolmsonii*, however, the THC was reduced in 90.8 μg·L^{-1} Cu^{2+}, and the heamocyte phogocytic ability was lower in 21.4 μg·L^{-1} Hg^{2+} [6]. Concentrations of Cu^{2+}, Co^{2+}, Mn^{2+} in seawater were 40, 40, 20 μg·L^{-1},respectively, AKP could be obviously activated during Mysis period, but decreased in higher concentrations; low levels of Cu^{2+} made the activities of AKP and ATPase increase. AKP activity peaked at 40 μg·L^{-1}. ATPase activity was obviously higher in the condition of Cu^{2+} (ranging from 40 to 80 μg·L^{-1}) than that in the control, but higher concentration could restrain AKP and ATPase activity. 20 μg·L^{-1} Co^{2+} could enhance the activities of AKP and ATPase, but Ni^{2+} could reduce the activity of them. Because of direct relationship between the activities of AKP, ATP and growth, effects of heavy mental on shrimp larvae development are nearly accordant with the activities of AKP and ATPase, so the activities of AKP and ATPase could be regarded as an index whether the environmental factors were suitable to survival of shrimp larvae or not [7-9]. Therefore, although high level of heavy metal is harmful to shrimp and crab, minimum or infinitesimal heavy metal ions are good for increasing hosts immune, and further study on the mechanisms are necessary

Litopenacus vannamei were exposed to 0, 1, 5, 10 or 20 mg·L^{-1} Cu^{2+} for 24, 48 and 96 h, respectively, to determine THC, PO activity, respiratory burst, phagocytic activity and clearance efficiency to *Vibrio alginolyticus*. The results showed that *Litopenacus vannamei* exposed to 1 mg·L^{-1} Cu^{2+} or higher for 24 h, and exhibited a decrease in all the above four indices, while the groups exposed to 20 mg·$L^{-1}Cu^{2+}$, had an obviously increase in respiratory burst, and the immunity of *Litopenacus vannamei* could be restrained by 1 mg·L^{-1} or higher concentration of Cu^{2+}, furthermore, sensitivity of *Litopenacus vannamei* to

V. alginolyticus has been enhanced [10].

Cu^{2+} and Zn^{2+} levels in seawater significantly affected the humoral immune factors of *Scylla serrata*. At low concentration of no-Waterborne Cu^{2+} (≤60μg·L^{-1}) and Zn^{2+} (≤100μg·L^{-1}), ceruloplasmin (CP) , PO activity both in heanolymph, the activities of superoxide dismutase (SOD), Antibacterial (U_a), Lysozyme(U_L) in hepatopancreas, heanolymph and muscle of *Scylla serrata* were enhanced with Cu^{2+} and Zn^{2+} levels' increasing. Whereas when Cu^{2+} Zn^{2+}levels increased to 75 μg·L^{-1} and 125 μg·L^{-1}, respectively, the activities of PO, SOD, U_L and U_a all declined. Activities of ACP and AKP were not affected obviously except those in hepatopancreas were restrained significantly; while in different Zn^{2+} levels, activities of ACP and AKP decreased significantly. Thus it could be seen that , Cu^{2+} and Zn^{2+} in water has significant effects on humoral immune factors of *Scylla serrata*, and good immunity could be maintained by effective controlling of Cu^{2+} and Zn^{2+} concentration（ranging from 15 - 60 μg·L^{-1} and 25 - 100 μg·L^{-1}), respectively [11].

Wu et al.(2005) reported that study on the effects of 3 kinds of heavy metal (Cu^{2+}, Zn^{2+}, Cd^{2+}) on SOD activities in hepatopancreas, gill, and haemolymph of *Litopenacus vannamei*, showed that SOD activities changed significantly with prolonged exposure of these ion (P<0105) . The SOD activities of all test objectives changed with a single peak under the exposure of Cu^{2+} (0.1 - 1 mg.L^{-1}), and the activities of hepatopancreas, gills and blood of SOD changed with the extension of time, the activities of the hepatopancreas of SOD was inhibited obviously by the Zn^{2+} under 10 mg.L^{-1}, and the activities of the hepatopancreas and gill of SOD was also inhibited obviously by the Cd^{2+} under 0.5 $mg^{+}.L^{-1}$, respectively, while 0.125 mg.L^{-1} had no-significant effect on that of gill. The SOD activities of hepatopancreas, gill and blood all increased first and then decreased under the prolonged exposure of Zn^{2+} (<10 mg.L^{-1}) and Cd^{2+} (<0.25 mg.L^{-1}).There was an obvious dose-time response relationship between test metal ions and SOD activity. The SOD activities decreased in order of hepatopancreas>gill> haemolymph, while the toxicity of test metal ions was in order of Cd^{2+}>Cu^{2+}>Zn^{2+} [12].

1.2 Effects of ammonia-N on non-special immunity of shrimp and crab

Ammonia-N is the most common pollutants in aquaculture ponds, which refers to summation of ammonia and ionic ammonia, and the ratio of ammonia and ionic ammonia is related to pH, temperature and salinity [13]. Ammonia-N dominatingly comes from extraction by cultured shrimp and crab, amination of nitric organism (remains of feedstuff and feces). 40% - 90% of nitric waste of shrimp and crab is excreted out of the epithelial cells in the terms of ammonia-N, which in water affects the development, moulting, oxygen-consumption, excretion of ammonia-N, hemocyanin level and total protein in haemolymph, osmosis regulation, ion concentration and Na^{+},K^{+}- ATPase activities of shrimp and crab [14,15]. When NH_4-N level was 1.01 mg·L^{-1} or higher, *Macrobrachium rosenbergii* hypoxia caused the susceptibility to *V. alginolyticus* increasing [16]. the susceptibility to *V. alginolyticus* of *Litopenaeus vannamei* had a direct correlation with NH_4-N level, and increased under NH_4-N concentration ranges from 0 to 20.00 mg·L^{-1}[17]. When environmental NH_4-N was 2.5 mg·L^{-1}, after 20d, *Fenneropenaeus chinensis* THC decreased, while activities of PO, SOD, peroxidase, Lysozyme and antibacterial were decreased[14]. *Macrobrachium*

rosenbergii exposure to the concentration of NH_4-N 0.55, 1.68 and 3.18 mg·L^{-1}, respectively. After 7d , PO activity was significantly reduced and generation of reactive oxygen decreased too, while changes of THC was no-significant, and phagocytic activity and clearance efficiency decreased, and susceptibility to *Lactococcus garvieae* increased [18,19] . Under *Litopenacus vannamei* exposure to the concentration of NH_4-N 0, 1.10, 5.24, 11.10 and 21.60 mg·L^{-1}, respectively, THC, hyalinocytes and granulocytes had no significant changes; while that in concentration of NH_4-N was 5.24 mg·L^{-1}, PO activity dropped significantly, but after 7d it increased again. The PO activity decreasing was not because of THC or granulocytes decreasing; in *Litopenacus vannamei*, concentration of superoxide anion was affected by that of NH_4-N in water. Exposing to the concentration of NH_4-N 21.6 mg·L^{-1}, 11.2 mg·$L^{-1}$and 21.22 mg·L^{-1}, respectively, for 7 d, SOD activity lowered obviously, and phagocytic activity and clearance efficiency of phagocyte decreased too [17] .

Under *L. stylirostris* exposure to 1.5 mg·$L^{-1}$and 3.0mg·L^{-1} NH_4-N, respectively, both PO activity and THC (mainly the hyaline cell) decreased. It was found that the amount of the transcript encoding ProPo and peroxinectin decreased by 60.5 %, which explained why haemocytes PO activity was reduced under ammonia-N stress in molecular level [20]. Ammonia-N affects the THC, activities of PO, AKP and ACP in *Fenneropenaeus chinensis* [21]. *Macrobrachium rosenbergi* exposure to 1 mg·L^{-1} ammonia-N for 1 d, 4d, 7d and 10d , respectively , PO activities both in haemolymph and muscle decreased, while that in hepatopancreas increased slightly; SOD activities in different tissues and organs increased first, and then decreased; phosphatase activity in different tissues and organs increased [22]. *L. stylirostris* exposure to the concentration of NH_4-N 21.6mg·L^{-1}、 11.2 mg·$L^{-1}$and 21.22 mg·L^{-1}, respectively, THC, PO activity in haemocytes, Lysozyme and antibacterial activity changed significantly($p<0.05$).With ammonia-N concentration increasing, THC, Lysozyme activity and antibacterial activity decreased significantly, while PO activity and susceptibility to pathogenic bacteria increased, so it was suggested that changed range of NH_4-N should be better not exceed 0.5 mg·L^{-1} or NH_4-N should not be maintained at a high level (>0.5 mg·L^{-1}) for a long time [23]. NH^+_4-N stress could result in declining haemocyte counts and phagocytic percentage, decreasing the activities of phagocytic, lysozyme, phenoloxidase, Superoxide dismutase, damaging no-specific immune system of *Eriocheir sinensis*, The reaction degree is positively related to the stress of NH^+_4-N concentration and time length treated [24].Total haemocyte count decreased while ambient ammonia increased, Superoxide dismutase (SOD) activity in haemolymph was stimulated by lower ambient ammonia concentration after short time exposure and depressed by higher ammonia concentration. Therefore, a depression in immunity [25].

Shrimp and crab immunity could be reduced under ammonia-N stress, and concurrently, susceptibility to pathogenic bacteria was increased accordingly, and it was much easier to cause diseases, so effective methods should be taken during water management in shrimp and crab culture to control the NH_4-N concentration in ponds, which could avoid shrimp and crab diseases outbreak .

1.3 Effects of nitrite on non-special immunity of shrimp and crab

After NO_2^- in water gets into the haemolymph of shrimp and crab, oxyhemocyanin can be turned into

deoxyhemocyanin, and haemocytes oxygen affinity could be reduced , then the ability of carrying oxygen decreased ,which is toxic to the aquatic organism [23]. In addition, NO_2^- also affects the excretion of nitric waste, protein level, osmosis regulation and ion concentration in Haemolymphe [26,27]. Higher NO_2^- concentration in water could result in decreasing the activities of PO, SOD, and lysozyme in *Fenneropenaeus chinensis* [28]. When NO_2^- concentration was 1.68 $mg \cdot L^{-1}$, *Macrobrachium rosenbergii* disease resistibility will be reduced significantly, and phagocytic activity and clearance efficiency to bacteria decreased, whereas more reactive oxygen produced. Higher level of reactive oxygen in body is obviously toxic to the organism, while the body disease resistibility decreased, and susceptibility to *Lactococcus garvieae* increased, and total mortality caused by infection had a positive relation to NO_2^- level [16].

Reactive oxygen generated by *Macrobrachium nipponense* increased with levels of Nacl and Sodium polyphosphate increasing, while SOD activity increased slightly at first, and then decreased. This results indicated that immune system of shrimp has certain resistibility to low concentration of poison , but will be restrained with the concentration of the poison increasing , and shrimp immunity decreased , even death was caused by diseases [30] .

The studies of effects of nitrite-N (NO_2^-N) on *Litopenacus vannamei* immune indices showed that after exposure to 0, 0.98, 4.94, 9.87and 19.99 $mg \cdot L^{-1}$ NO_2^-N for 96h , respectively, THC and PO activities in different groups decreased , while respiratory burst ((release of superoxide anion), exposure to 9.87 and 19.99 $mg \cdot L^{-1}$ NO_2^-N significantly increased ($P<0.05$). The results showed that higher level of NO_2^-N in water inhibited the immunity of *Litopenacus vannamei* and enhanced susceptibility to pathogeny, reactive oxygen level and maybe cytotoxic levels [31].

Exposure to each NO_2^-N level, reactive oxygen intermediates (ROIs) of *Macrobrachium nipponense* was obviously increased, which has a positive correlation with NO_2^-N level. Sublethal exposure to NO_2^-N for 24 h, ROIs increased by 97 % than the control, while activities of SOD, CAT and glutathione peroxidase(GPX) were 67 %, 80.6 % and 82.7 % lower than those of the control, respectively. The results showed that unbalance of peroxidative ability and antioxidative ability is one toxic mechanism of NO_2^-N to shrimp. After exposure to 1 mg L^{-1} NO_2^-N for 1 d, 4 d, 7 d and 10 d, respectively, PO activity in both haemolymph and muscle of *Macrobrachium rosenbergii* decreased ,while that in hepatopancreas increased slightly; SOD activities in different tissues and organs increased first and then decreased, however, phosphatase activity increased [22].

NO_2^-N stress could be toxic to shrimp and crab, also could decrease immunity of shrimp and crab, and increase susceptibility to pathogens, so it was much easier to cause shrimp and crab diseases, and hence, effective methods should be taken to control the NO_2^-N concentration in water management of shrimp and crab culture.

1.4 Effects of pollutants in water on shrimp and crab non-special immunity

Pollutants is a primary pollutant which affects the growth, development and survival of shrimp and

crab, resulting in reducing shrimp and crab immunity, both in natural and culture water. Pollutants not only cause the immunity of shrimp and crab reduced, but also have seriously toxic effects in cell and molecule level, causing pathological changes and numerous death. Up to the present, studies on effects of pollutants on shrimp and crab immune system are very few, and toxic mechanism is not clear yet. At present, dominant effects of pollutants on enzymes related to non-special immunity, small molecule active material and changes of qualities, kinds, ratio and function of haemocytes have been studied, in order to find the alterative regulation of these indices, and to regard those much more related to pollutant levels as indicators of shrimp and crab immunity during culture.

Formulated feed was used for pollutant source to study effects of organic pollution on *Fenneropenaeus chinensis* body's intraenvironment and extraenvironment, and susceptibility to pathogens, respectively. The results showed that DO level apparently decreased, while COD, NH; -N and NO_2-N rapidly increased in experimental pools; susceptibility to pathogens was elevated by 1 - 3 times; activities of SOD, PO and Lysozyme deceased by 22 %, 50 % and 28 % - 86 % , respectively . THC increased about 50 %, which was related to some toxicant produced by decomposing formulated feed in the aquatic environment, made water worse, reduced activities of enzyme which was related to disease resistibility and promoted outbreaks of diseases, and especially decrease of generation of ammonia-N and DO activity was significant [31,32]. Propiconazole affecting the non-activated haemocytes will stimulate *Litopenacus vannamei* haemocytes to generate superoxide anion; if it affected activated haemocytes by yeast polysaccharide, levels of superoxide anion could be reduced [33]. *Crangon crangon* living in harbour dredge spoils and polluted by PCBs, PAHs and heavy metal, both THC and PO activity in haemocytes was lower than those living in clean sand [34]. *Crangon* exposed to sublethal concentration (0.05-500μg· L^{-1}) of PCB_{15} and PCB_{17}, respectively, and THC and PO activities in haemocytes decreased , while PCB_{17} has no great effects on disease resistibility [35].

Studies indicated that Monocrotophos stress could reduce activities of PO and SOD in *Fenneropenaeus chinensis*, and this change could be enhanced with Monocrotophos concentration increasing and time prolonging, and the main reason was that the structures of tissue and cell were damaged by Monocrotophos, resulting in capability of synthesizing enzyme decreased. Further study will be conducted to determine whether there was direct effects on the activities of SOD and PO under Monocrotophos stress. Monocrotophos stress may inhibit the recognition abilities and eliminate pathogens. In addition, Lysozyme activity can be reduced under Monocrotophos stress[38,39] .

Shrimp and crab culture has been puzzled by pollutants, and to eliminate pollutants is very important way to avoid shrimp and crab diseases outbreaks, therefore, studies on rapidly decomposing and transforming of pollutants in shrimp and crab culture is essential and practical meanings for promoting safe and healthy culture of shrimp and crab.

2 Several suggestions about studies on effects of environmental factors on the non-special immunity of shrimp and crab

Up to the present, knowledge about immunology of shrimp and crab is not very systemic, composition and character of shrimp and crab immune system, generating regulation and character of immune factors , and the mechanisms of cell immunity and humoral immunity all have not been studied clearly yet; evaluating system of effects of environmental factors on non-special immunity of shrimp and crab has not been set up ,which badly affected the implementation of preventing methods which were used to increase the resistibility. Accordingly, to focus studies on effects of environmental factors on non-special immunity of cultured shrimp and crab, has crucial academic meanings and practical values.

Further studies on effects of environmental factors on non-special immunity include the followings:

1) To study composition and character of immune system of shrimp and crab, generating regulation and character of immune factors, and the mechanisms of cell immunity and humoral immunity further and systemically, to set up immune parameter data-base of healthy shrimp and crab, for example, THC, phagocytic activity, respiratory burst, PO activity, SOD activity, antibacterial peptide, agglutinin, bacteriolysis activity and antibacterial activity and so on. In order to evaluate exactly health of cultured shrimp and crab, and improve the culture environment, prevent and control the disease outbreaks in time .

2) To study effects of interaction of environmental factors on immunity of shrimp and crab, and to set up general-technic system which is to be used for water regulation in safe and healthy culture of shrimp and crab.

3) To study mechanism of effects of environmental factors on immunity of shrimp and crab, and study further effects of changes of environmental factors on expression of immune genes, especially, by modern molecular biology technique.

4) To really do well in environmental factors monitoring and diseases detecting in safe and healthy culture , to discuss relation between environmental factors and immune parameters; to set up methods and indices system to evaluate health of shrimp and crab rapidly and exactly.

In addition, shrimp and crab disease outbreak is nearly related to environmental quality, and after hosts getting in touch with pollutants, non-special immunity in shrimp and crab will incisively change. Therefore, if changes of non-special immune indices in shrimp and crab can be used to monitor degree of environment pollution, there will be certain developing and practical foreground in environmental monitoring practice.

Acknowledgements

This work was funded in part by a grant from the National High Technology Research and

Development Program of China (863 Program)(2007AA091406), a grant from the Jiangsu Provincial Key Laboratory of Coastal Wetland Bioresources and Environmental Protection(JLCBE05007), and a grant from NingBo Natural Science Foundation (2006A610086).

References

[1] Moullac G L, Philippe H. Environmental factors affecting immune responses in Crustacea.Aquaculture, 2000, 191:121-131

[2] Truscott R, White K N. The influence of metal and temperature stress on the immune system of crabs [J]. Functional Ecology, 1990, 4: 455-461.

[3] Victor B, Narayanan M, JonesNelson D,et al. Gill pathology and hemocyte response in mercury exposed *Macrobrachium rosenbergii* Heller [J].Environmental Biology,1990,11:61-65.

[4] Lorenzon S, Francese M, Smith V J. et al. Heavy metals affect the circulating haemocyte number in the shrimp *Palaemon elegans* [J]. Fish & Shellfish Immunology, 2001, 11 (6): 459-472.

[5] Cheng W, Wang C H. The susceptibility of the giant freshwater prawn *Macrobrachium rosenbergii* to *Lactococcus garvieae* and its resistance under copper sulfate stress [J]. Dis Aquat Organ, 2001, 47:137-144.

[6] Yamuna A, Saravana Bhavan P, Geraldine P. Effects of Hg and Cu on hemocytes-mediated functions in the prawn, *Macrobrachium malcolmsonii* [J]. J Environ Biol. 2002, 23(1):7-13.

[7] Liu C Q, Wang A L, Wang W L, et al. Influences of Co^{2+} in Seawater on Growth and Activities of AKP and ATPase of *Penaeus chinensis* Postlarvae [J]. Acta scientiarum naturalium universitatis Sunyatseni, 2000, 39(Suppl.):123-126.

[8] Liu C Q, Wang A L, Wang W L, et al. Influences of metal ions in seawater on activities of alkaline phosphatase(AKP) and ATPase in mysis and postlarvae of *Penaeus chinensis* [J]. Journal of fisheries of China,2001,25(4):298-303.

[9] Liu C Q, Wang A L, Wang W L, *et al.* Influences of Zn^{2+} and Mn^{2+} in Seawater on the Activity of Alkaline Phosphatase (AKP) in Postlarvae of Kuruma Prawn *Penaeus japonicus* [J]. Fisheries Science & Technology Information, 2002, 29(5):195-197.

[10] Yeh Su-Tuen, Liu Chun-Hung, Chen Jiann-Chu. Effect of copper sulfate on the immune response and susceptibility to *Vibrio alginolyticus* in the white shrimp *Litopenaeus vannamei* [J]. Fish & Shellfish Immunology,2004, 17:437-446.

[11] Ai C X. Effects of copper ion and zinc ion on humoural immune factors of *Scally serrata* [D].Postdoctoral Report of Xiamen University.2004.

[12] Wu Z W, Pan L Q, Zhang H X. Effects of heavy metal ions on SOD activity of *Litopenaeus vannamei* hepatopancreas, gill and blood [J]. Chinese journal of applied ecology, 2005,16(10): 1962-1966.

[13] Sun J J, Ding M L. Effects of ammonia-N on anti-disease ability of *Penaeus chinensis* [J]. Oceanologia et limnologia sinica,1999,30 (3):267-272.

[14] Chen J C, Cheng S Y, Chen C T, et al. Changes of oxyhemocyanin, protein and free aminoacid levels in the

hemolymph of *Penaeus japonicus* exposed to ambient ammonia [J].Comp Biochem Physiol,1994, 109A: 339-347.

[15] Chen J C, Nan F H. Effect of ambient ammonia on ammonia-N excretion and ATPase activity of *Penaeus chinensis* [J]. Aquat Toxic,1992,23:1-10.

[16] Cheng W, Chen JC. Effects of environmental factors on the immune responses of freshwater prawn *Macrobrachium rosenbergii* and other decapod crustaceans [J]. J. Fish. Soc. Taiwan 2002, 29, 1-19

[17] Liu Chun-Hung, Chen Jiann-Chu. Effect of ammonia on the immune response of white shrimp *Litopenaeus vannamei* and its susceptibility to *Vibrio alginolyticus* [J]. Fish & Shellfish Immunology ,2004,16 (4): 321-334.

[18] Cheng W, Chen J C, The virulence of Enterococcus to freshwater prawn *Macrobrachium rosenbergii* and its immune resistance under ammonia stress [J]. Fish Shellfish Immunol. 2002, 12, 97-109.

[19] Cheng W, Chen Su-Mei , Wang Feng-I, et al. Effects of temperature, pH, salinity and ammonia on the phagocytic activity and clearance efficiency of giant freshwater prawn *Macrobrachium rosenbergii* to *Lactococcus garvieae* [J]. Aquaculture, 2003,219 (1-2): 111-121.

[20] Le Moullac G, Haffner P. Environmental factors affecting immuneresponse in Crustacea. Aquaculture, 2000, 191: 121–31.

[21] Guan Y Q. Effects of some typical environmental factors on the immune responses and outbreaks of white spot syndrome in penaeid shrimp [D]. Ph D. dissertation of Chinese Academy of Sciences.2003.

[22] Wnag Y, Hu Y B, Jiang R C. Effects of ammonia-N and nitrite-N on immune enzymes of *Macrobrachium rosenbergii* [J]. Journal of Zhejiang University(Science Edition),2005,32(6):698-705.

[23] Jiang L X, Pan L Q, Xiao G Q. Effects of ammonia-N on immune parameters of white shrimp *Litopenaeus vannamei* [J].Journal of Fishery Sciences of China,,2004,11(6):537-541.

[24] Huang H Z, Li Y, Song X H, et al. NH^{+}_{4}-N stress on immune function of *Eriocheir sinensis* [J]. Oceanologia et limnologia sinica, 2006,37(3):198-205.

[25] Hong M L, Chen L Q, Sun X J, et al. Metabolic and immune responses in Chinese mitten-handed crab (*Eriocheir sinensis*) juveniles exposed to elevated ambient ammonia. Comparative Biochemistry and Physiology, 2007, 145C:363–369.

[26] Cheng S Y, Chen J C. Hemocyanin oxygen affinity, and the fractionation of oxyhemocyanin and deoxyhemocyanin for *Penaeus monodon* exposed to elevated nitrite [J]. Aquat. Toxicol. 1999,45, 35-46.

[27] Chen J C, Cheng S Y. Hemolymph oxygen content, oxyhemocyanin, protein levels and ammonia excretion in the shrimp *Penaeus monodon* exposed to ambient nitrite [J]. J. Comp. Physiol., 1995, 164 B:530-535.

[28] Wu Z H, Liu C B, Liu C Y, et al. Histopathological research on chronic poisoning of *Penaeus chinensis* by nitrite and ammonia [J]. Journal of central china normal university,1999,33(1):119-122.

[29] Li Z H, Xie S, Wang W L, et al. Toxicity of Nitrite-N and Sodium Polyphosphate to the Shrimp *Macrobrachium nipponense* [J]. Chinese Journal of Zoology, 2004, 39(3): 12-16.

[30] Tseng I-Ting, Chen Jiann-Chu. The immune response of white shrimp *Litopenaeus vannamei* and its susceptibility to *Vibrio alginolyticus* under nitrite stress [J]. Fish & Shellfish Immunology, 2004,17 (4):325-333.

[31] Wang W N, Wang A L, Zhang Y J, et al. Effects of nitrite on lethal and immune response of *Macrobrachium nipponense* [J]. Aquaculture,2004, 232 (1-4): 679-686.

[32] Lin L, Ding M L, Sun J J, et al. Organic pollution enhance susceptibilites of *Penaeus chinensis* to

pathogenicbacteria [J].ACTA Oceanologia sinica, 1998,20(1):90-93.

[33] Ding M L, Lin L, Li G Y, et al. Effects of organic pollution on *Penaeus chinensis* body's intraenvironment and extraenvironment [J].Oceanologia et limnologia sinica,1997,28(1):7-12.

[34] Munoz M, Cedeno R, Rodriguez J.,et al. Measurement of relative oxygen intermediate production in haemocytes the penaeid shrimp, *Penaeus vannamei* [J] Aquaculture, 2000,191:89-107.

[35] Smith V J, Swindlehurst R J, Johnston P A, et al. Disturbance of host defense capability in the common shrimp, *Crangon crangon* by exposure to harbour dredge spoils [J]. Aquatic Toxicology, 1995, 32:43-58

[36] Smith V J. & Johnston P A. Differential haemotoxic effect of PCB congeners in the common shrimp, *Crangon crangon* [J]. *C*omparative Biochemistry and Physiolog,1992, 101C: 641-649.

[37] Bai J, Li Y Q, Li G R. Pilot study on the effect of monocrotophos on activity of PO in haemolymph of *Penaeus chinensis* [J]. Marine science, 1998, 3:35-37.

[38] Bai J, Li G R, Tang X X, et al. Studies on the effect of monocrotophos on SOD activities in *Penaeus chinensis* [J]. Marine science bulletin, 1998, 17(4):41-45.

[39] Bai J, Li G R, Li Y Q, et al. Study on the effect of monocrotophos on activity of lysozyme and bacteria content in haemolymph of *Penaeus chinensis* [J]. Marine science, 1998, 6:1-2.

几种环境因子对虾蟹类非特异性免疫的影响

艾春香，王晓娟，李少菁，王桂忠，林琼武

（厦门大学海洋与环境学院 福建 厦门 361005）

摘要：综述了近 10 a 国内外有关重金属、氨态氮、亚硝酸盐、有机污染物等几种环境因子对虾蟹类非特异性免疫影响的研究成果，以期为通过改善养殖环境条件提高虾蟹类自身免疫抗病力提供理论依据。同时，为进一步深入开展该领域的研究工作积累资料。

关键词：虾蟹类；非特异性免疫；重金属；污染物

Contrast of Seismic Reflection Characteristics of Gas Hydrate Distribution between Northeast SCS Slope and Hengchun Ridge

SHANG Jihong[1,2,3], LI Jiabiao[1,3], ZHANG Jiabao[4]

1. *Institute of Oceanology, Chinese Academy of Sciences, Qingdao* 266071, *Shandong, China;*
2. *Graduate University of Chinese Academy of Sciences, Beijing 100083, China;*
3. *Key Lab of Submarine Geosciences, Second Institute of Oceanography, State Oceanic Administration; Hangzhou* 310012, *Zhejiang, China;*
4. *Zhejiang Ocean University, Zhoushan* 316000, *Zhejiang, China;*

Abstract: By analyzing and interpreting the newly acquired seismic profile supported by the national 973 Program and synthesizing the data with other geologic & geographic information, we draw conclusions as follows. a) Two seismic reflections located at the northeast South China Sea (SCS) slope and the Hengchun ridge are the Bottom Simulated Reflections (BSRs). Yet, the genesis and process of the gas hydrate in these two areas are different because of different regional tectonics and geological environments; b) The genesis of gas hydrate located at the northeast SCS slope area is related to the broadly existing fracture zones, slumping tectosomes, and the distinctive shielding environment of pressure masking field formed by them. But the genesis of the gas hydrate at the Hengchun ridge is associated with the thrust nappe structures and accretionary wedges formed along the Manila subduction zone and the related sub-floor fluid channel system built by them; c) Since the analogous geologic bodies are broadly distributed at slope areas around SCS and the temperature-press environment is very suitable to the formation and conservation of the gas hydrate, we suggest that much more of this resource should be stored in these areas.

Keywords: BSR; gas hydrate; slumping block; accretionary wedge; thrust nappe tectosome; diapir;

Introduction

As one of the biggest marginal basins in west Pacific, South China Sea is located at the juncture area of Eurasia plate and West Philippine Sea Pacific plate(Pacific plate), and it has characteristics of a passive continental margin since Cretaceous. There are many oil and gas basins distributed at northern SCS, such as Pearl River Mouth basin, Qiongdongnan basin, Yinggehai basin and Beibuwan basin which have rich oil and gas resources. The complicated tectonic movements in the region in its long evolutionary

Received on July 16, 2007

history such as expansion, rifting, deposition, benefit the enrichment of all sorts of minerals greatly. According to the regional geologic information, the study area came into a deposition stage after mid-Miocene and deposited a very thick stratum with the thickness up to a range from 1000 m to 5000 m [1]. There are plentiful organic matters in the sediment which act as a sufficient origin of gas hydrate. At the same time, northern SCS slope is very extensive where many marine beaches, ridges, seamounts, troughs, mud diapirs, submarine canyons, sea fans developed extensively. The extension structure in upper strata with lots of slumping faults which are actively and extensively distributed in the continental margin and the island slope area can do good to the formation of submarine fluid channel systems. The plenty of various geologic bodies and suitable water depth, temperature-pressure field are favorable to the conservation of submarine organic and the formation of hydro-carbonaceous gas too. The tectonic features of imbricate thrust nappes distributed along the east side of Manila trench are more complicated. Plentiful hydro-carbonaceous gases upwelled with heat flow through fluid migaration channels, which were formed by typical thrust fault groups, and then covered by upper mixed organic and slumping blocks in shallow sediment just a few miles away beneath the seafloor. This semimetal and tectonic pattern could be of great benefit to the elutriation and conservation of the gas hydrate.

Actually, since in 1998 Yao Bochu pointed out for the first time that there must have existed gas hydrate at northern SCS [2], the Guangzhou Marine Geological Survey have carried out a series of investigations of gas hydrate at the slope area of northern SCS from 1999. After processing and analyzing the collected information, experts were sure that there are really gas hydrates in our country's sea area as potential mineral resources [3-5]. And from then on, because of the mysteriousness and its potential economic prospect of the new submarine resource which can compare with the traditional energy storage such as oil and coal, an upsurge to explore and study gas hydrate was raised extensively by lots of researchers. But related studies on abroad took the lead all along. Japan, India, America, Germany had invested to carry out large scale developing plans as early as 1995. Korea, Russian, Canada, France, England, Norway, Belgium and Australia are investigating aggressively now or have worked out programs already [3, 6]. In this article, we analyzed the seismic reflection profile across northeast SCS slope and southern Taiwan sea area which was acquired by R/V "Tanbaohao" in August, 2001, and discussed the formation laws, distribution features of gas hydrate existing at the continental slope, continental rise in northern SCS and its east subduction zone preliminarily, and explored the inner relationship between the gas hydrate and regional typical tectosomes. The paper can be of help to deepen the gas hydrate researches in future.

1 Characteristics of BSRs in the Northeast SCS Slope and Hengchun Ridge

1.1 Formation Environment of Gas Hydrate

Locating at the collision belt between Pacific Plate and East Asia Continental margin, SCS has complicated submarine terrain and tectonic environment. The deep sea plain of SCS is a rhombic basin along the NE direction and the diagonal lengths are 1500 and 810 km respectively while the average

water depth is over 1000 m [7]. The transition line between sea-bottom plain and continental slope or island slope is apparent. The sea floor inclines from north to south with huge sedimentation layers on it. The water depth of north slope SCS is from 200 to 3 400 m and the bottom sea water temperature is from 0 ºC to 10 ºC. The slope area widens from east to west and a series of seamounts, knolls and canyons are arranged on it also. Generally, we know that the current morphostructure of SCS was formed at the end of mid- Miocene and a series of approximately horizontal sediments settled down after that. It has a large deposition rate and therefore can construct a favorable surface pressure shield in the upper Quaternary sediment against fluid and gases' escape. Lots of organic matter in shallow sediments coming mostly from continents or islands can benefit the formation of hydrocarbon gases too. In the northern SCS area, many tectonic events like multi-time expansion of crust have happened since Cenozoic and thus formed a complicated geomorphology. The continuous movements of deep crust can speed up the formation of decomposing or thermal cracking gases in deep sediments. Simultaneously, there are many slumping faults, landslides, seamounts, steep terraces developed in our study area, and they are especially rich in diapir tectosomes and extension fractures, so a convenient and prosperous fluid migration system was developed maturely which can extend in all directions. All these conditions are fit for the formation and stable storage of gas hydrate very much. Thus we conjecture that there should be abundant gas hydrate resources existing in the SCS area. Furthermore, as an index for the existence of gas hydrate, BSRs were found multi-times in the continental slope area of SCS, especially at continental slopes, island slopes and deep trough area by many researchers too [4, 8-12].

Hengchun Ridge is the southern extension of Taiwan Orogenic Belt, and also belongs to the accretionary wedge of Manila subduction belt. At its west flank, the SCS dives into Philippine Sea Plate along the Manila Trench. There are lots of sedimental fragments scrubbing off the diving crust and forming typical imbricate thrust nappes and accretionary wedges. Three apparent tectonic domains can be partitioned to the wedges from bottom to top: plenty of thrust faults and anticlines dipping to the west at down slope; mixed strata sequences with continuous strong deforming reflections caused by thrust and bottom erosions at up slope; reversed thrust actions against the accretionary wedges [9]. The buninoid blocks, mud volcanoes, fault belts and thrust nappe tectosomes developed along the subduction belt are the reflections on seafloor of regional complex tectonic actions such as slumping, fracture, fluid effusion, extrusion of shallow sediments, and also the performances of regional inhomogeneous lithologic characters, big alteration of structures, strong activities of submarine heat flow and complicated formation mechanism. The complex accretionary wedges at subduction zones are always the hot area in the study of gas hydrate because the fracture, extrusion, and slipping raised by the subducting activities can be of great benefits to the upward migration of deep fluid and crystallization and lixiviation of organic matter. Although there are less investigations to the sea area of southern Taiwan than to the SCS marginal area, analogous signs of hydrate existence have already been found by some experts in the region [13, 14].

1.2 Data Source, Processing and General Characteristics

Data are obtained from the National 973 Program: Key Problems of Formation and Evolution of

China Marginal Sea and Its Important Resources Item. The research group entrusted Guangzhou Marine Geological Survey (China) with the multi seismic profiles investigation in northeast SCS. The seismic lines stretch from the northeast corner of SCS continental shelf to the Gagua Ridge, which runs southeastwardly across north shelf, slope and submarine canyon of SCS and eastwardly covers Manila Trench, Hengchun Ridge, North Luzon Trough, Huadung Basin. So it is a wide study area with complex submarine geomorphology (as showed in Fig.1, the isobath interval is 1000 m, data obtained from Taiwan Oceanography Data Bank). The multi-channel seismic data were collected by MSX shipboard seismograph mounted on R/V "Tanbaohao", and the reflected seismic data were recorded by IBM3591 tape machine via SEG-D format. The seismic channel interval is 12.5 m and the shot interval is 50 m. The sampling interval is 2 ms while the near offset distance is 250 m.

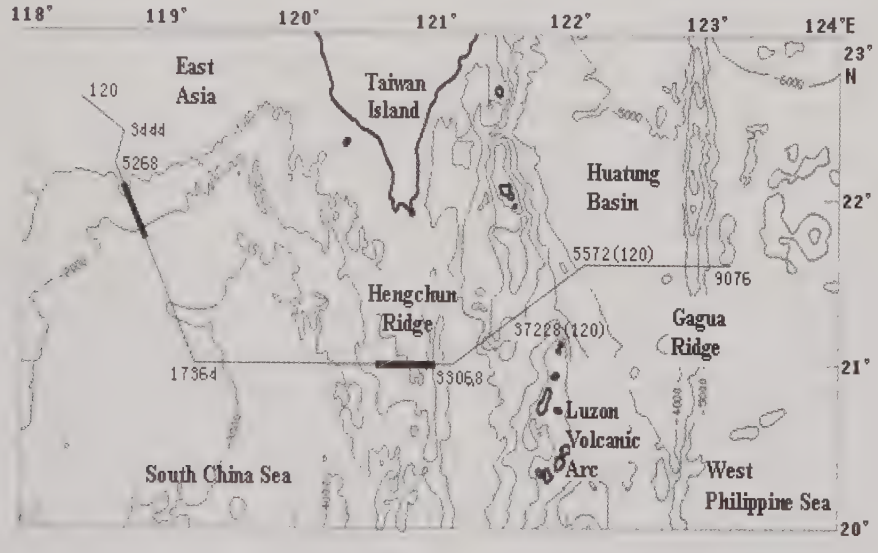

Fig.1 Locations of the 973 seismic survey lines and typical BSR sections on the regional bathymetric map.

(The thin fold lines show the position of survey lines, and two bold segments on the line are typical BSR positions, where the number marked at each corner of the fold lines is the track number of Common Depth Point (CDP).)

In order to improve the resolution and ensure the reliability of the data simultaneously, gain compensation and time-variation filtering were done subsequently after the routine processing were finished, such as observation system definition, data decoding, predictive deconvolution, velocity analysis, dynamic correction and migration to the whole profile. The worked result sketched out the shallow seafloor structure between northeastern SCS and Luzon volcano are in high resolution. In the result, in the slope area of north SCS, the original part of the line, the BSR characteristics and its surrounding tectonic environment are very similar to those which were obtained in the Xisha Trough [10]. Although there is no more detailed geophysical evidence, we are sure the refection is BSR in terms of the characteristics of geography, tectonic development status or from reflecting features. And, on the profile of the hengchun

ridge unit, south of Taiwan, there are obvious BSR features in shallow sediment which can be considered as the evidence of gas hydrate's existence. With the prodigious topographic relief and the imbricate thrust wedges formed in its west flank by subduction of SCS plate, Hengchun Ridge area has suitable environment for the formation of gas hydrate. And this is coincident with Song et al.'s view that the strong reflection layer has the characteristic of typical BSR in the Hengchun Ridge area [13, 14]

2 Relationship Between Gas Hydrate's Distribution and Regional Tectonic Environment

2.1 Slope Area of Northeast SCS

From the seismic data, 3 unconformable seismic interfaces can be distinguished in strata above Mid-Miocene in the area of SCS, which are interfaces between mid-Miocene and later-Miocene, later-Miocene and Pliocene, Pliocene and Quaternary [15]. But the strata are very obscure after migration to the profile on part of slope area because of large dip angle of terrain. The general structure showed on the profile appeared as rifting features represented by slumping normal fault groups. The normal faults are mainly in the northwest direction, also with some north and west ones. Most of these normal faults have grown maturely, which divided the seafloor into many zigzag fragmenting units. The faults have a big rupture depth, and some even stretch to the basement of the Cretaceous. They appeared with strong or weak seismic reflections, alternated with chaotic seismic reflections, irregular reflections, and showed as a "BSR Simulated Cap" [1] in shallow sediment. The confounded seismic reflection configurations exactly manifest the complex structure in the region such as fractures and fissures, slumping blocks, fast deposition blocks etc. From Fig.2 (a) we can see that, BSR in the slope area showed on profile is between CDP 6 800 and CDP 8 400, which is 0.25 s two-way time (TWT) beneath seafloor and on the top of slumping bodies. Its distribution is approximately parallel with the bottom's reflection, and some parts run across the strata slantly, while on the top of it is an amplitude blankness of the reflected wave, and beneath it is a chaotic reflection configuration. This strong reflection layer is not continuous with the reflections on both sides of it, and it is lying isolated on the top of the huge uplifting basement in the slope area. So we are sure that it is really a BSR.

Some researchers believe that gas hydrate's formation has a close relationship with strike-slip structures on the deep sea floor. It provides necessary conditions for gas hydrate's generation when the slumping process triggers fast deposition in some local area, which leads to a sectional pressure shield on the top of the sediment. Meanwhile, local slumping process can trigger the decomposition of the gas hydrates, leading to a further slump of the top deposition in upper slope areas. Thus a more complex deposition can be formed at the foot of the slope, which can provide a better environment for the hydrates' formation and conservation. Slumping body is always formed by fast deposition materials and has a high porosity, which can provide a conservation room for the formation of hydrates. Plenty of organic oddments existing in slumping blocks are buried quickly with no oxidation. When they are oxidized by lots of bacteria in the conservation room, methane is generated: At the same time, the slumping sedimentation with low sorting rate and low permeability is not suitable for the gas to give off, thus providing a good pressure

shield for the gas hydrate's formation Fig. 3(a).

From above we can see that the slumping body is one of the most important indications in the gas hydrate rich area. In SCS, slumping bodies mainly lie in the north slope and west margin areas, mostly in the Quaternary sediment, and their distribution trend is always controlled by faults. Sedimentation velocity in SCS varies greatly at different places and different periods, but in the Quaternary, sedimentation velocity puts up an obvious increasing trend generally in the whole SCS. Big sedimentation velocity is of benefit to the growth of abnormal sedimentation bodies such as slumping bodies and turbidite fans which can provide a capping function to the methane gas as a pressure field, and thus benefit to the formation of gas hydrate. In north SCS, slumps and fractures grow extensively, with a common water depth more than 500 m and a big sedimentation velocity in the Quaternary too, so it has a relatively proper temperature-pressure and tectonic environment for the formation of gas hydrate. And the clear BSR on the seismic profiles indicates a sky-high possibility of the existence of gas hydrate too.

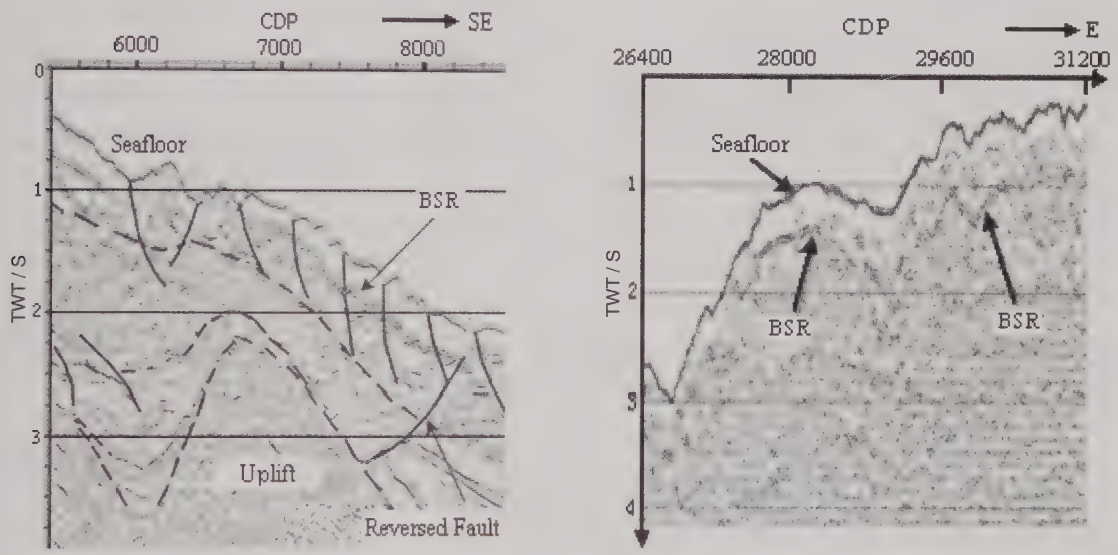

Fig.2 Detailed profiles of two sections showing apparent BSRs at northeast SCS and Hengchun Ridge

(a) Seismic profile located at the northern slope of SCS;

(b) Seismic profile located at the Hengchun Ridge, southern Taiwan;

2.2 Hengchun Ridge Section

On the seismic profile, BSR in the Hengchun Ridge appears in the range from CDP27, 200 to CDP30, 800, and the reflection characteristics are very clear as showed in (Fig. 2(b)). The strong reflection is 0.3 - 0.6 s(TWT) from seafloor and parallel with the seafloor reflection approximately while the reflection polarities are opposite to the seafloor reflection. In the mid section of the profile at the Hengchun

Ridge, there is a small depression where an oblique cross occurs in big angle between this strong reflection and other reflection layers. And there is also a clear amplitude blankness of reflection above it and strong amplitude reflections beneath it. These characteristics illuminate that the reflection layer is BSR. The profile segments were finely processed by Song et al., IGCAS in 2004 [13]. After the process of Stolt Migration in the F-K domain and Complex Trace Analysis of the migration profile, a more clear and continuous BSR image was obtained which sketched out the position of BSR transverse distribution and displayed strong amplitude of the reflected waves and various changes in the transverse direction. However, beneath BSR, other reflection interfaces can hardly be delineated out because of the most complex and chaotic interior reflections in the thrust nappe of accretionary wedges.

As the southern extension of Taiwan Orogen, Hengchun ridge is one of the most disputed focuses by geophysicists because of its geographic position and its tectonic evolutionary history. Taiwan Orogen Belt lies in the conjunction area of Eurasia Plate and Philippine Sea Plate, and it is also the connection point of Luzon Arc and Ryukyu Arc. The Orogen Belt is usually considered to be born from the collision between Eurasia Plate and Luzon Arc [16]. To the south of Taiwan Orogen beneath Hengchun ridge, a subduction system was formed by SCS plate's diving from its west flank to the east along the Manila Trench. Related clear epicenter depth profiles have proved that a Benioff Belt is lying eastwardly apparently under the subduction zone[17, 18].In the complex process of subduction, materials with rich organic matter on the upper ocean crust were scratched off and accumulated in the distortion front of the subduction. At the same time, the thickening sedimentation layers and their loads in the accretionary wedges region, together with the dehydrated and degassed organic materials, formed the typical imbricate thrust faults under extrusion circumstances, which can provide channels for the migration of deep pore water and methane gas upward through the thrust faults. Then the gas could change into gas hydrate in shallow strata in a stable and proper environment after a long time (Fig. 3(b)).

Data show that gas hydrate is widely distributed on the top of the subduction accretionary wedges and fore-arc-basin at the continental margin, especially in subduction accretionary wedges. Hengchun Ridge has exactly the proper tectonic environment as stated above, especially in its west flank. Along the ManilaTrench, the typical imbricate overthrust nappes, reversed accretionary wedges and other fractures provide favourable conditions for the formation and migration of the deep cracking gas and thermal liquid to the shallow sediment. Therefore, plenty of gas can be formed and conserved in these places. From our seismic profile, it can be seen that BSR is mainly distributed on the back of the anticline, ridge of back thrust accretionary wedges and near thrust faults. Thus we can be sure that the faults and subduction belts provide channels for the migration of the deep cracking gas, and then provide advantages for the formation and conservation of gas hydrate. There in it, the thrust nappe tectosomes are the most important and advantageous structures for the formation of gas hydrate acting as a fluid migration system.

Some institutes including Taiwan University have carried out seismic investigations using 6-channel or 12-channel seismometers in the southern Taiwan Island and northeast SCS [9, 14]. They acquired 8000km long survey lines and the total area covered was up to 27 000 km^2. Among them, BSRs, mud

diapirs, and mud volcanoes were found existing in an area of more than 20 000 km^2. The BSRs found were mainly in the accretionary wedges deposition area between Manila Trench and north Luzon Trough with the water depth between 800 m and 3 300 m. Therein, high quality BSRs were mainly distributed in the ridge area of the anticlines, near mud volcanoes and fault belts, several hundred meters beneath the seafloor in the southwest Taiwan Island and northeast Taixinan basin, with the water depth between I 500 m and 3 000 m. And the hydrate was deduced to have originated from the crystallization and precipitation of methane gases including free gases and dissolutive gases which migrated from deep sedimentation and accretionary wedges through typical thrust fault groups and fracture zones too. The origins of these hydrocarbon gases were related to the plentiful organic fragmental deposit which had come mainly from continental margin and Taiwan Orogen.

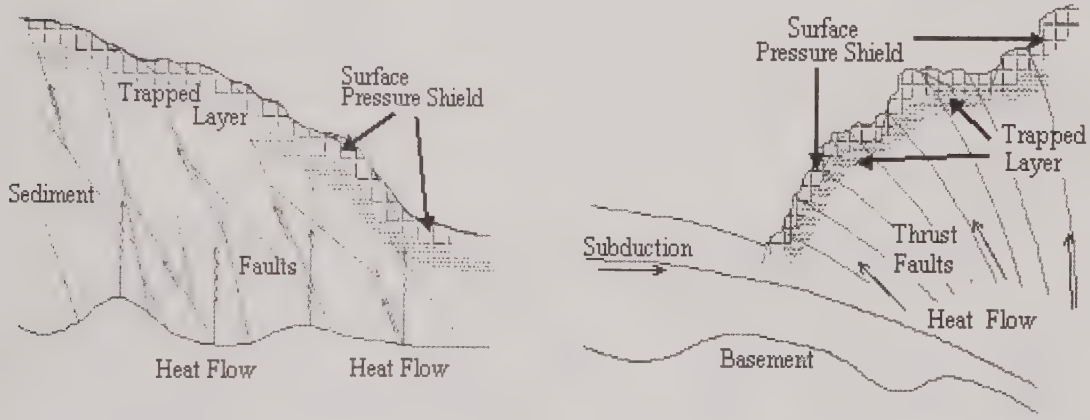

(a) (b)

Fig.3 Diagram of hydrate forming process in two sections respectively

(a) Northern slope area of SCS section;

(b) Hengchun ridge area at southern Taiwan section;

3 Conclusion

a) The shallow seismic reflections on profiles from CDP 6 800 to CDP 8 400 in the slope area of northeast SCS were characterized by the feature of extension fracture which was represented by typical slumping construction and a series of normal fault groups. The strong reflected layer in shallow sediments on seismic profiles containing blankness of amplitude is an obvious BSR. From this and other tectonic evidences we can reason out that there may be gas hydrate existing in the slope area. To the south of Taiwan, from CDP 27 200 to CDP 30 800 in the Hengchun Ridge section, especially at the back of accretion wedge of Manila Trench and on top of anticline structures, the thrust nappe structures and extruded fault zones developed extensively. And there are also blankness of amplitude and obvious BSR existing in shallow sediments on our profiles. This coincides with the results reached by Song Haibin et al.

too.

b) The geotectonic reasons of formation and process of gas hydrate are different between slope area and Hengchun Ridge section. In the slope area of northeast SCS, gas hydrate is related with the plenty of fractures and slumping blocks existing extensively, and it is mainly caused by the shielded pressure field formed by slumping and accumulation of shallow sediments, while in the Hengchun Ridge section, the origin of gas hydrate is related with the complex and convenient fluid migration system formed by nappe structures and accretionary wedges along the subduction belt.

c) Morphotectonics in SCS is complicated, and the analogous tectosomes as listed above are generally developed especially in the Manila Subduction Zone of northeast SCS and continental margin slope in northwest SCS where the water depth is more than 500 m l beneath the sea surface. So there should be a vast amount of gas hydrate in the expansive slope、continental rise area and the subduction zone in north SCS. Similar tectosomes were found in south SCS continental margin too. Although the evolutionary history of these structures is different from those in northeast SCS, there are still lots of organic matter in sediments and proper water pressure and temperature there. So it's a potential mineral exploration area with brilliant prospect.

d) We are sure that the factures, slumping blocks, accretionary wedges and diapir structures have a close relationship with the formation mechanism of gas hydrate, and all these tectosomes formed a favorable exterior tectonic environment for the formation and conservation of gas hydrate. So in the actual investigation, we can set out our survey with these target tectosomes, then look for the regional geophysical evidences such as BSR et al. and carry out detailed exploration contrapositively in the delineated region. By doing so, we can reduce much additional workload in the actual field exploration and indoor study.

Acknowledgements

This work was supported in part by the China National Key Basic Research Project——"Formation and Evolution of Chinese Marginal Seas and the Major Issues of Important Resources" (G2000046700).

References

[1] Sha Zhibin, Yang Muzhuang, Liang Jin, et al. The Characteristics of the Abnormal Physiognomys of Seabed related to Gas Hydrate in North Slope, South China Sea [J]. Wuhan: China University of Geosciences Press. 2003, 14:29-34.

[2] Yao Bochu. Preliminary Exploration of Gas Hydrate in the Northern Margin of the South China Sea [J]. Marine Geology & Quaternary Geology, 1998, 18(4):11-18.

[3] He Jiaxiong.The Evolving of Gas Hydrate and the Exploration Foreground in the North of South China Sea [J]. Offshore Oil, 2003, 23(1):57-64.

[4] Zhang Guangxue, Huang Yongyang, Chen Bangyan, et al. Prospect of Gas Hydrate Resources in the South China Sea [J]. Marine Geology & Quaternary Geology, 2002, 22(1): 75-81.

[5] Wu Bihao, Zhang Guangxue, Zhu Youhai, et al. Progress of the Gas Hydrate Investigation in China Offshore [J]. Earth Science Fronties, 2003, 10(1):177-189.

[6] Ma Zaitian, Geng Jianhua, Dong Jianhua, et al. Seismic Recognition Studies on Marine Gas Hydrate [J]. Marine Geology & Quaternary Geolog, 2002, 22(1):1-8.

[7] Yao Bochu. The Gas Hydrate in the South China Sea [J]. Journal of Tropical Oceanography, 2001, 20(2): 20-28

[8] Berner U, Faber E. Hydrocarbon Gases in Surface Sediments of the South China Sea [A]. JIN Xianglong, Kudrass H R, PautoT G. Marine Geology and Geolophysics of the South China Sea [C]. Beijing: China Ocean Press.1990, 199-211.

[9] Chi W C., Reed D L, Liu C S, et al. Distribution of the Bottom-Simulation Reflector in the Offshore Taiwan Collision Zone [J]. TAO. 1998, 9(4):779-794.

[10] Yang Muzhuang, Wu Nengyou, Wu Shiguo, et al. Special Geological Environment at Northern Slope of South China Sea and Distribution of BS [A]. Li Jiabiao, Gao Shu. Evolution and Resources Effects of China Marginal Basins [C]. Beijing: China Ocean Press. 2004, 176-181.

[11] Song Haibin, Geng Jianhua, Wang How-king, et al. A Preliminary Study of Gas Hydrates in Dongsha Region North of South China Sea [J]. Chinese Journal of Geophysics, 2001,44(5): 687-695.

[12] Lu Zhengquan, Qiang Zuji, Wu Bihao. Exploring Gas Hydrates by Satellite-Based thermal Infrared remote Sensing in the South China Sea [J]. Acta Geologica Sinica, 2002, 76(1):100-106.

[13] Song Haibin, Wu Nengyou, Wu Shiguo, et al. Processing to the national 973 Seismic Profiles in Northeast South China Sea and ITS BSR Characteristic [A]. Li Jiabiao, Gao Shu. Evolution and Resources Effects of China Marginal Basins [C]. Beijing: China Ocean Press. 2004, 182-185.

[14] Shyu Chuen-tien, Hsu Shu-kun, Liu Char-shin. Heatflows off Southwest Taiwan: Measurements over Mud Diapirs and Estimated from Bottom Simulating Reflectors [J]. Tao, 1998, 9(4):795-812

[15] Jin Qinhuan. Geology and Oil & Gas Resources in South China Sea [M]. Beijing: Geological Publishing House. 1989, 257-262.

[16] Fuh S C, Liu C S, Lundberg N, et al. Strike–slip Faults Offshore Outhern Taiwan: Implications for the oblique Arc-continent Collision Processes [J]. Tectonophysics, 1997, 274:25-40.

[17] Tsai Y B. Seismotectonics of Taiwan [J]. Tectonophysics, 1986, 125:17-35.

[18] Tang J C, Chemenda A I. Numerical Modeling of Arc-continent Collision: Application to Taiwan [J]. Tectonophysics, 2000, 325:23-42.

南海东北部陆坡与恒春海脊天然气水合物分布的地震反射对比

尚继宏[1,2,3]，李家彪[1,3]，章家保[4]

（1. 中国科学院海洋研究所，山东 青岛 266071；2. 中国科学院研究生院，北京 100083；3. 国家海洋局第二海洋研究所海底科学重点实验室，浙江 杭州 310012；4. 浙江海洋大学，浙江 舟山 316000）

摘 要：经过对“探宝号”调查船在2001年8月在南海东北部陆坡及台湾南部恒春海脊海域采集的多道地震剖面资料进行的地震反射波数据分析、研究和解释，结果表明：（1）南海东北部陆坡段区域和台湾南部恒春海脊海域地震剖面上均显示有被作为天然气水合物存在标志的BSR，但两区域构造成因、形式和相关地质环境的不同造成了此两处的天然气水合物成因及过程的不同。（2）南海东北部陆坡区域的水合物形成与该区广泛发育的断裂带、滑塌构造体及其所形成的压力场屏蔽环境有关，而台湾南部恒春海脊海域的天然气水合物的形成则与马尼拉海沟俯冲带相关的逆冲推覆构造、增生楔等及其所对应的海底流体疏导体系有关。（3）南海陆缘区域广泛发育有各种断裂带、滑塌构造体、泥底辟、俯冲带、增生楔等，且温压环境合适，是天然气水合物矿藏极有可能广泛分布的区域。

关键词：BSR；天然气水合物；滑塌体；泥底辟；叠瓦状逆冲推覆构造；增生楔

Analysis on the basement constitution of the southern Okinawa Trough

LIU Jianhua[1,2], GAO Jinyao[1,2], FANG Yinxia[1,2], WU Shuigen[1,2]

1. *Key Lab of Submarine Geosciences, SOA, Hangzhou* 310012, *Zhejiang, China*

2. *The Second Institute of Oceanography, SOA, Hangzhou* 310012, *Zhejiang, China*

Abstract: Based on the data of seismic reflection, seismic refraction and magnetism collected in the research area and geology obtained from adjacent areas, this paper deals with the issue of basement constitution of the southern part of the Okinawa Trough. In the shelf basin of the East China Sea, Taiwan folded belt and Ryukyu Islands folded belt which surround the trough, outcrop Later Paleozoic, Mesozoic and Eogene strata. In the southern trough, multichannel seismic reflection data indicate that the overlying strata are composed of Neogene and Quaternary deposits, and the acoustic basement consists of Eogent and even older strata. Seismic refraction profiles show that there are Eogene and Mesozoic velocity layers with longitudinal velocities of 4.7 - 5.3 km/s and 6.3 km/s respectively beneath the Quaternary-Miocene Layers. Qualitative analysis and forward and reversed calculation of magnetic data show that the magnetic basement is mainly formed by metamorphic rocks, the Yanshanian neutral-acid magmatic rocks and the Himalayan neutral-basic magmatic rocks being the next components, and the magnetic basement is mostly corresponding to the acoustic basement. Comprehensive analyses demonstrate that the basement of the southern Okinawa Trough is mainly formed by Eogene system and Mesozoic and Upper Paleozoic groups metamorphosed in varying degrees, and the basic magmatic rocks of Himalayan epoch have been formed in some parts of the basin.

Key words: Okinawa Trough basin, basement institution, magnetic basement

Introduction

Located at the eastern margin of the East China Sea (ECS), the Okinawa Trough is a back-arc basin with strong tectonic activities. The trough, as well as Ryukyu Island Arc and Ryukyu Trench, comprises a complete trench-arc-basin system of western Pacific margin. Its geological significance has given rise to extensive attention of the geoscientists both from China and abroad. They have carried out studies of multi-subjects on it for a long period of time [1-11]. The crustal property and origin mechanism are two major subjects among them [12-15].

The constitution of the trough is an important scientific subject which has close link with the subjects mentioned above. Since 1980's, the studies on the basement constitution of the Okinawa Trough have

Received on Sep 9, 2007

made certain progress. The views as follows have been put forward. The basement is composed of the Eogene system, Mesozoic group or even older strata [16]; The basement of basin, as well as the rising belt of the shelf margin of ECS and the folded belt of the Ryukyu Islands, is formed by the Upper Paleozoic group and Permian system[1]; the basement is mainly composed of Miocene series and Pliocene volcanic rocks[2]; or magnetic lineations exist in the floor of the southern Okinawa Trough [17].

Based on the data of geology collected in the adjacent areas and seismic reflection, seismic refraction and magnetism obtained from the studied area, the paper would make a discussion on the basement constitution of the southern Okinawa Trough by means of qualitative analysis and forward calculation and reversed calculation,.

The discussed area for this paper is located in the southern part of the Okinawa trough southwest of the Miyako depression, an area between 24° - 27°N and 122° - 127°E. This area is of the deepest water in the trough. The bathymetric contours are generally in NE trend, with a nearly E-W trend in the western margin. The water is deepening from about 150 m at the shelf margin of ECS and about 200 m at the island- shelf margin of the Yaeyame Islands and Miyako Islands to over 2000 m in the trough floor. There is a maximum water depth of 2294 m in the Yaeyama graben (Fig.1).

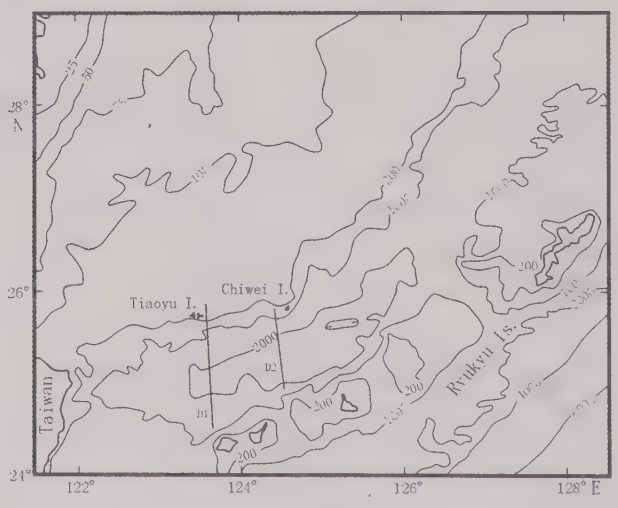

Fig.1 Bathymetric map of the southern Okinawa Trough (Isobaths are in meter)

Note: D1 and D2 are the reflection seismic profile number

1 Geological setting of the adjacent areas

The southern Okinawa Trough is bordered on the shelf basin of ECS, the Taiwan folded belt and the

1) Zhou Zhiwu, 1986. The Study is on tectonic characteristics and petroleum resources of the East China Sea.

2) Jiang Yongquan, 1989. The study is on basement property and tecdtonic regionalization of the East China Sea.

Ryukyu Islands folded belt to the northwest, west and southeast respectively.

The oldest stratum found in the adjacent areas of the southern trough so far is the Proterozoic metamorphic rocks encountered at the Lingfeng No. 1 well of Taibei Depression of the shelf basin of ECS. It consists of biotitic hornblende plagioclass, gneisses with the Rb-Sr age are of 1 680 Ma [7]. This stratum is corresponding to the Chencai Group and Jianou Group outcropping in the eastern Zhejiang and Fujian Provinces of China, which are composed of callys, quartzite, mable and gneiss and with the ages of Pre-Devonian and Pre-Sinian period respectively.

The Later Paleozoic strata are well developed in the adjacent areas of the southern Okinawa Trough. There is Danan'ao Group outcropping in the eastern flank of the Central Mountains of Taiwan folded belt [18]. As the oldest stratum in this belt, it is composed of a suite of kata-metamorphic rocks such as clays, quartzite, crystalline limestone, gneiss and marble. Their primary rocks are the geosynclinal-facies deposits. The fossils of fusulinacea and anthozoa preserved in the crystalline limestone suggest that its age is Permian. There are green schist, phyllite and Permian marble in the Ryukyu Islands, which are the oldest rocks in the islands and make up residual basement block of Hercynian-Indosinian epoch (a tectonic phase between Triassic and Earlier Jarassic in Chinese literature). They are mainly distributed along the margin of the islands closed to the trough, and are corresponding to the Danan'ao group in the Taiwan folded belt in the lithological characters. Seismic reflection data indicate that there is reflection sequence beneath the Mesozoic system in the eastern part of the shelf basin of ECS. To the west of the shelf basin of ECS, slightly metamorphosed Upper Paleozoic strata have been found in the eastern coastal zones of Zhejiang and Fujian Provinces, China. They can be separated into two parts. The lower one is composed of Upper Devenian-Lower Carboniferous fine-clastic sedimentary rocks with carbonatite bands. The upper one consists of Middle Carboniferous coarse-clastic rock, fine-clastic rock and carbonatite. Their thickness and lithological characters suggest that they belong to the deposits of geosynclinal facies. The above-mentioned facts show that Taiwan and Ryukyu Islands, together with southwest Japan and Philippines, belong to a eugeosynclIne, and form a part of Pacific-marginal geosycline system. The miogeosyncline of this geosyncline system may comprise the shelf of ECS and the coastal areas of Zhejiang and Fujian Provinces, China [19].

Since Mesozoic, the eastern margin of Asia has been largely affected by subduction of the Pacific plate. In the coastal areas of Zhejiang and Fujian Provinces of China and the west part of the ECS shelf, Later Jurassic-Earlier Cretaceous neutral-acid volcanic rocks and Yanshanian (a tectonic phase between Jarassic to Cretaceous in Chine literature) granites are well developed. The Upper Cretaceous marine-facies strata are developed in the southern part of the shelf basin of ECS. The drilling wells at Yunlin, Beigang and Penghu Islands of Taiwan show that there are marine-facies Mesozoic system in the wells, which are composed of altered sandstone, altered feldspar-sandstone and altered volcanic rocks containing fossils of Cretaceous ammonites and mollusk. There are complicated Mesozoic metamorphic rocks located outside the Paleozoic system in the Ryukyu Islands. They are marine-facies sediments formed along the continental margin after folding of Paleozoic geosyncline.

2 Covering strata and acoustic basement

Multichannel seismic reflection profiles show that the covering strata are thin in the slopes and thickening toward the axis in the southern Okinawa Trough. Correspondingly, the acoustic basement is deepening from the slopes to the axis. After interpretation and comparison, five seismic interfaces named T_0^1, T_1^0, T_1^1, T_2^0 and T_g respectively have been distinguished in the southern Okinawa Trough. Meanwhile, four seismic reflection sequences have been separated, with names of Sequence A, Sequence B, Sequence C and Sequence D (acoustic basement sequence). The sequence A can be further divided into three subsequences (Fig.2). The thickness of sequences and subsequences in the profile D1 and profile D2 have been calculated in terms of an average seismic velocity of ECS.

2.1 Sequence A

Located between sea bottom and seismic interface T_1^1, the sequence A is characterized by continuous and linear internal reflectors divergent towards the axis of trough, high amplitude and high apparent frequency. The thickness is increasing from the slopes to the axis. The former is 600 m in general, while the latter can reach as thick as 1800 m. It is supposed to be formed by the Quaternary deposits. Its interval velocity is about 1.6 - 2.0 km/s for Holocene and 2.23 - 2.4 km/s for Pleistocene [16, 20].

The sequence A can be further divided into three subsequences, i.e., subsequence A_1, subsequence A_2 and subsequence A_3, by the seismic interfaces T_0^1 and T_1^0 which are existed inside the sequence A.

"Offshore Miyako Island" key well was drilled in 1980, with a depth of 3 711 m (including water depth 286 m). Quaternary stratum of 234 m has been drilled. It consists of yellow gray medium-coarse sandstone and pebbly sandstone, which contain fossils of foraminifera and bivalve [21]. The sequence A seems to correspond to this stratum.

2.2 Sequence B

Lying between seismic interfaces T_1^1 and T_2^0, it is similar to sequence A in general features of internal reflection patterns, but is of slightly lower apparent frequency and amplitude and slightly undulate internal reflectors. The seismic interface T_1^1 represents a tectonic movement called the Okinawa Trough movement [7]. It is 500 m thick in the slopes and can be as thick as 2000 m in the axis. It has an interval velocity about 2.51- 3.13 km/s and is supposed to be composed of the Pliocene deposits.

"Offshore Miyako Island" key well Drilled 2360 m Pliocene stratum. It is composed of mudstone, siltite and sandstone, which contain planktonic foraminifera and calcareous nannofossil. The Sequence B is supposed to correspond to this stratum.

2.3 Sequence C

Located between seismic interfaces T_2^0 and T_g, it is quite different from the overlying sequences A

and B in general internal reflection patterns. With low apparent frequency and amplitude, its internal reflectors are discontinuous and are affected by a system of faults. The seismic interface T_2^0 represents a stronger tectonic movement called the Longjing movement [7]. It is about 500 m thick in the slope and reaches as thick as 1 500 m in the axis. With an interval velocity of 3.67- 4.59 km/s, it is supposed to be formed by the Miocene deposits.

"Offshore Miyako Island" key well drilled 831 m Miocene stratum. It is composed of sandstone, mudstone and shale, which contain planktonic foraminifera and calcareous nannofossil. The Sequence C is supposed to correspond to this stratum.

2.4 Acoustic basement sequence

The seismic interface T_g forms the top boundary of the acoustic basement. Its surface is undulate obviously, and affected by faults and intrusive masses. Beneath the seismic interface T_g can still be seen some internal reflectors with low apparent frequency, low amplitude and big inclination, which make the acoustic basement sequence in an angular unconformity with the overlying sequence. It has the interval velocities of 4.72 - 5.67 km/s and 6.16~6.71 km/s. The acoustic basement is supposed to be composed of Eogene and Pre-Eogene metamorphic rocks and sedimentary rocks. The buried depth of acoustic basement is increasing from the slopes to the axis of the trough in general. For example, it is 4 km deep in the northern slope closed to the shelf margin of ECS, and about 7 km deep in the axis in the profile D1.

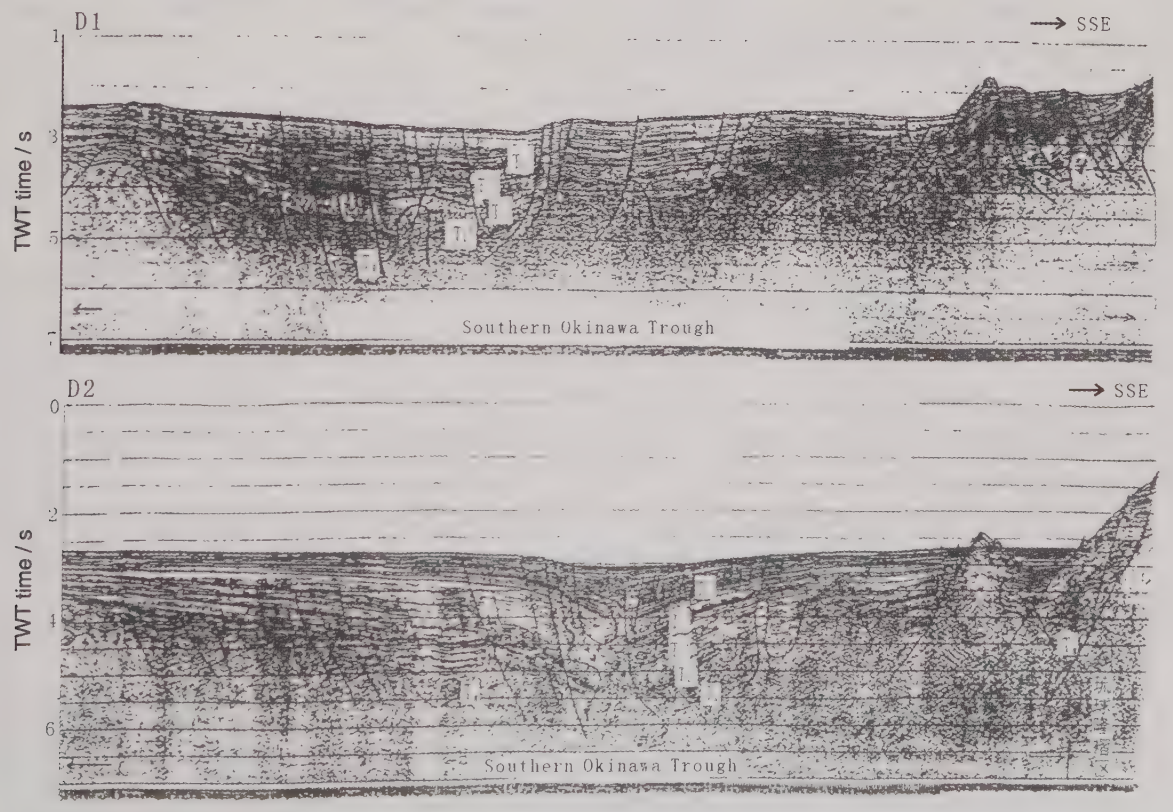

Fig.2 Multichannel seismic reflection profiles in the southern Okinawa Trough
(See Fig.1 for profile location)

3 Velocity layers

Refraction and reflection seismic surveys on the crustal structure have been conducted in the Okinawa Trough [17, 22-24]. Refraction seismic survey carried out near the southern Okinawa Trough has found the Eogene and Mesozoic velocity layers beneath the Miocene layer. In the refraction seismic profiles, five velocity layers as follows have been separated [22].

(1) Velocity layers I-II: Their longitudinal-wave velocity varies between 1.8 km/s and 3.2 km/s and the thickness is about 2 km. Both velocity and thickness of two layers are corresponding to the sequences A and B in the reflection seismic profiles. They are supposed to be the Pliocene and Quaternary deposits.

(2) Velocity Layer III: It is of longitudinal-wave velocity varying between 3.6 km/s and 4.4 km/s and is 3 km thick. Corresponding to seismic reflection sequence C, it may belong to the Miocene deposit.

(3) Velocity IV: With a Longitudinal-wave velocity varying between 4.7 km/s and 5.3 km/s, it is interpreted to be the Eogene deposit. The profiles show that a rather strong folding took place after the deposit of this layer, which resulted in the rising belt of the shelf margin of ECS and depression of the Okinawa Trough.

(4) Velocity layer V: With a longitudinal-wave velocity of 6.3 km/s, it is interpreted to be the Mesozoic deposit.

Refraction seismic data show that there are Eogene, Mesozoic and even older strata existed beneath the Later Cenozoic deposits in the Okinawa Trough.

4 Constitution and buried depth of the magnetic basement

4.1 Constitution of the magnetic basement

The magnetic anomalies in the southern Okinawa Trough are rather complicated and of following features in general (Fig.3).

(1) The southern trough is short of typical magnetic lineations resulted from basaltic basement of the Oceanic crust, although there are wavelike anomalies and positive-negative accompanied high-amplitude anomalies related to the basic magmatic rocks in some parts of the western slope and the southeastern margin of the trough floor.

(2) The magnetic basement is mainly composed of metamorphic rocks and magmatic rocks. The magnetic anomalies resulted from the latter are various and cover rather large areas, which demonstrates that magmatism is rather stronger in the trough during geological history.

4.1.1 Magnetic anomalies resulted from metamorphic rocks of the basement

They are gently changed positive and negative anomalies. This kind of anomalies is of following features: Most anomalies are positive; Their amplitude is medium varying between 50 nT and 80 nT, a few being bigger than 100 nT; And their wavelength is rather longer, some being as long as 60 km. They mostly appear in the trough floor.

4.1.2 Anomalies resulted from the magmatic rocks

4.1.2.1 High-amplitude positive-negative accompanied anomalies

This kind of anomalies has following features: Positive and negative anomalies are accompanied, the former usually being at southern side and the latter at northern side; the amplitude is rather higher, varying between 400 nT and 700 nT; The wavelength is rather short, being 20 - 30 km in general (Fig. 4). They mostly appear along the southeastern margin of the trough floor. This kind of anomalies is believed to be related to the basic magmatic rocks which intruded into basement or overlying strata or erupted out of the sea bottom along faults.

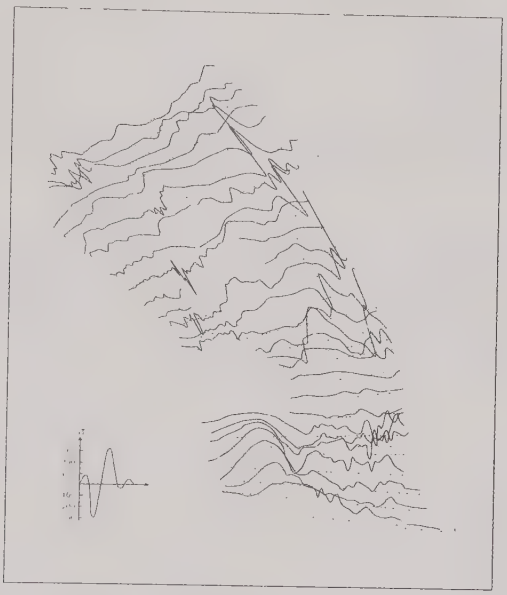

Fig.3 Magnetic anomaly (ΔT) profiles of the southern Okinawa Trough

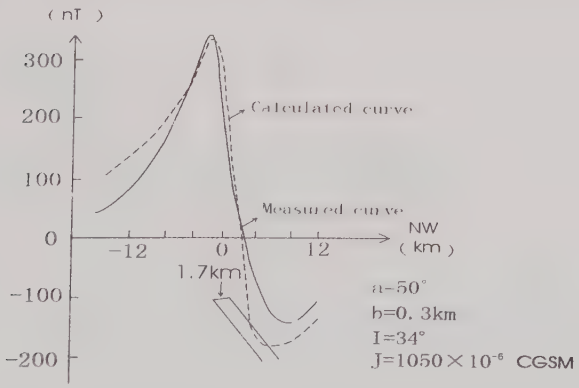

Fig.4 Positive-negative accompanied high-amplitude anomaly and its forward calculation curve

4.1.2.2 Wavelike anomalies

This kind of anomalies is of following characters: wavelike shape, short wavelength and low amplitude less than 200nT. They can be traced in nearby profiles, which makes them look like magnetic lineations. The anomalies are only found in the western slope of the trough. It is assumed that the anomalies are resulted from neutral or basic magmatic rocks intruding into the basement or overlying strata along faults.

4.1.2.3 Long-wavelength, high-amplitude positive anomalies

This kind of anomalies appears in the northwestern and northeastern margins of the trough, which is located at the transitional area between the continental shelf of ECS and the trough floor. They have high amplitude, the maximum being 350 nT, and long wavelength, and can be traced along nearby profiles. The forward calculation of an anomaly in the northwestern margin shows that it is resulted from a magnetic body with intensity of 495×10^{-6} CGSM and a buried depth of 10 km, which is supposed to be an intrusive mass of granite (Fig. 5).

There is a same kind of anomalies existing in the trough floor south of Tiaoyu Island. The slight difference is that the latter has narrower wavelength. They are interpreted being resulted from acid-neutral intrussive masses.

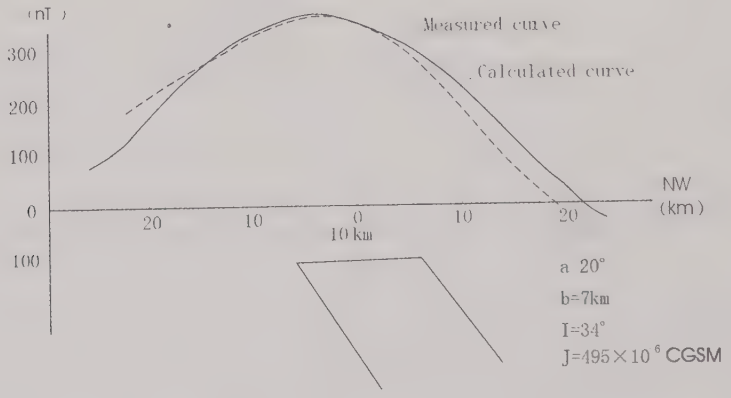

Fig.5 Long-wavelength, high-amplitude positive anomaly and its forward calculation curve

4.1.2.4 Low-amplitude undulate anomalies and high-frequency anomalies

These two kinds of anomalies are distributed in the shelf margin north of Chiwei Islet and Tiaoyu Island. The former has low amplitude less than 100 nT and sawtoothlike shape. It could be resulted from volcanic rocks with uneven and weak magnetic properties. The latter has short wavelength, high frequency and high amplitude varying between 200 nT and 300 nT in general. It is supposed to be resulted from basic volcanic rocks. The Miocene-Quaternary volcanic rocks and volcanic classic rocks outcropping

in the Chiwei Islet and Tiaoyu Island are the proof to support the above interpretation.

From above-mentioned analysis, it can be concluded that neutral-acid magmatism and neutral-basic magmatism are mainly occurred in Yanshanian epoch and Himalayan epoch (a tectonic phase between the Latest Cretaceous and Miocene in Chinese literature) respectively.

4.2 Buried depth of magnetic basement

The buried depth of magnetic basement of the southern Okinawa Trough is calculated on the basis of $\triangle Z_{\perp}$ anomaly which is transferred from magnetic anomaly ($\triangle T$) (Fig.6).

The main character for buried depth in the southern trough is that it increases from northwestern and southeastern slopes to the trough floor. It is about 3 - 4 km deep in shelf margin of ECS, and reaches 5~7 km deep in the trough floor. The value and variation tendency of buried depth for magnetic basements are nearly the same as those of the acoustic basement. It is suggested that the magnetic basement is corresponding to the acoustic basement and the Eogene strata have been metamorphosed more or less in addition to the Paleozoic and Mesozoic strata in the southern trough.

In some places such as the slope west of Tiaoyu Island, the buried depth of magnetic basement is deeper than that of the acoustic basement, where the former depth is as big as 9 km, and the latter is 4 km. The forward calculation has shown that the magnetic basement represents the top surface of intrusive granite body, which suggests that there are Eogene, Mesozoic and Paleozoic metamorphic strata existing between the magnetic basement and Later Cenozoic deposits.

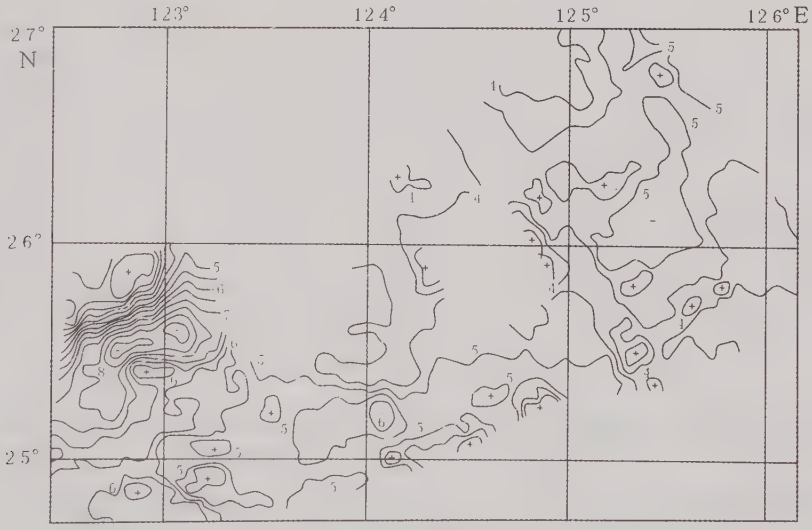

Fig.6 Buried depth of magnetic basement in the southern Okinawa Trough
(The Contour is in meter)

5 Conclusion

In addition to the Cenozoic strata, there are Pre-Devonian, Later Paleozoic and Mesozoic strata in

the shelf basin of ECS, Taiwan folded belt and Ryukyu Islands belt which surround the trough. Among them, Pre-Devoniain and Later Paleozoic strata have been metamorphized, and the Mesozoic and Eogene have been metamorphosed in varying degrees. The seismic reflection data indicate that the overlying strata are composed of Later Cenozoic deposits, and the acoustic basement consists of Pre-Miocene series. The seismic refraction data reveals that there are Eogene and Mesozoic velocity layers with longitudinal velocities of 4.7- 5.3 km/s and 6.3 km/s respectively. The magnetic data show that the trough floor is short of magnetic lineations resulted from oceanic basalt. The magnetic basement mainly consists of metamorphic rocks. Its buried depth coincides with that of the acoustic basement, which suggests that the Eogene series, together with Paleozoic and Mesozoic system has been metamorphized in varying degrees. In the northwestern margin of the trough, the buried depth of magnetic basement composed of granite body is much deeper than that of the acoustic basement, which means that there are Eogene strata existed beneath the Later Cenozoic system. All facts mentioned above demonstrate that the basement is composed of the Eogene series and Mesozoic and Upper Paleozoic system metamorphosed in varying degrees (Fig.7).

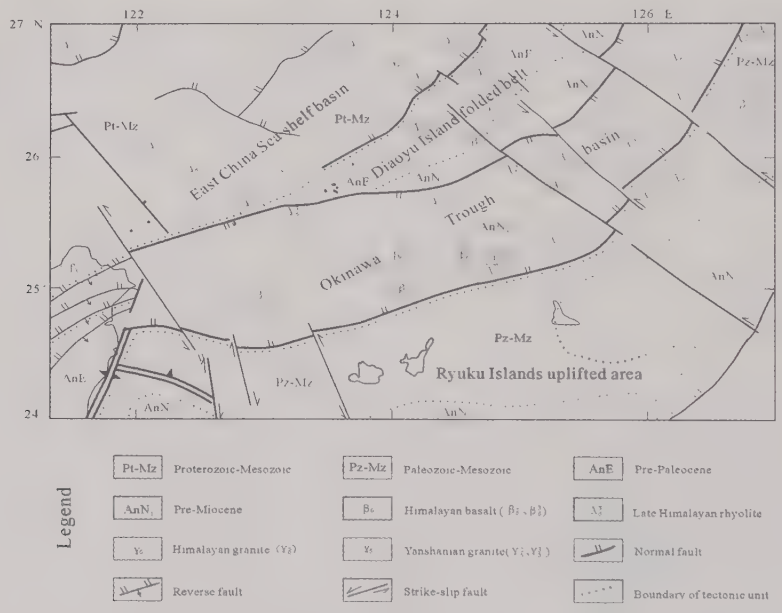

Fig.7 The Pre-Neogene basement structure of southern Okinawa Trough and adjacent areas

In geological history, magmatism is very strong in the trough. The neutral-acid magmatic rocks are mainly formed during Yashanian epoch, which are concentrated in the northwestern and northeastern margins. The neutral-basic magmatic rocks are mainly formed during Himalayan epoch, which are scattered in different places. The wavelike magnetic anomalies appeared in the western slope and positive-negative accompanied high-amplitude anomalies found in the southeastern margin of the floor are resulted from basic magmas, which shows that the basic magmas in certain quantity have been formed in some places of the trough.

Acknowledgments

This paper was supported by the National Key Basic Research Project of China under contract No. 2007CB411703 and contract No. 2007CB411702. The authors are greatly indebted to senior engineer Yang Wenda at Shanghai Offshore Petroleum Bureau and Professor Lin Changsong at Second Institute of Oceanography, SOA.

References

[1] Kaneko Y, Honkura Y. Electrical conductivity structure beneath the Okinawa Trough and the Ogasawara Arc [J]. Report of Hydrograhic Res., 1987, 22: 135-147.

[2] Kimura M, Uyeda S, Katao Y, et al. Active hydrothermal mounds in the Okinawa Trough back-arc basin, Japan [J]. *Tectonophysics*, 1988, 145: 319-324.

[3] Yamano M, Uyeda S, Foucher J P, et al. Heat flow anomaly in the middle Okinawa Trough [J]. Tectonophysics, 1989, 159: 307-318.

[4] Li Naisheng. The tectonic property of Okinawa Trough [J]. *Oceanologia et Limnologia Sinica,* 1990, 21 (6): 536-543.

[5] Kimura M, Furukawa M, Izawa E, et al. Report on DELP1988 cruises in the Okinawa Trough, part 7, Geologic investigation of the central rift in the middle to southern Okinawa Trough [M]. Bull. Eri. Unive. Tokyo, 1991, 66 (1): 179-210.

[6] Kinoshita M, Yamano M, Kasumi Y, et al. Report on DELP1988 cruises in the Okinawa Trough, part 8, Heat flow measurements [M]. Bull. Earthq. Res. Inst., 1991, 66: 211-228.

[7] Liu Guangding. Geological and geophysical features of China seas and adjacent regions [M]. Beijing: Science Press, 1992, 289-301.

[8] Liu Guangding. Atlas of geology and geophysics of China seas and adjacent regions [M]. Beijing: Science Press, 1993, 57-59.

[9] Furukawa M, Tokuyama H, Nishizawa S, et al. Report on DELP1988 cruises in the Okinawa Trough, part 2, Seismic reflection studies in the southwestern part of the Okinawa Trough. Bull. Earthq. Res. Inst., 1991, 66: 17-36.

[10] Zhou Zhuyi, Liao Zongting, Jin Xingchun, et al. Okinawa Trough—the highest stage of continental tension rifting in back-arc setting [J]. Marine Geology & Quaternary Geology, 2001, 21(10): 57-64.

[11] Li Xishuang, Liu Baohua, Wu Jinlong, et al. Seismic reflection facies and deposit systems in the west slope of the Okinawa Trough [J]. Oceanologia et Limnologia Sinica, 2003, 35(2): 120-129.

[12] Kimura M. Back-arc rifting in the Okinawa Trough [J]. Marine and Petroleum Geology, 1985, 2: 222-239.

[13] Letouzey J, Kimura M. Okinawa Trough genesis: Structure and evolution of back-arc basin developed in a continent [J]. Marine and Petroleum Geology, 1985, 2: 111-130.

[14] Sibuet J C, Letouzey S, Barbier F, et al. Back-arc extension in the Okinawa Trough [J]. J. Geo. Res., 1987, 92(B13):14041-14063.

[15] Sibuet J C, Deffontaines B, Hsu S K, et al. Okinawa Trough back arc basin: Early tetonic and magmatic evolution [J]. J. Geo. Res., 1998, 103(B12):30245-30267.

[16] Jin Xianglong, Yu Puzhi. Tectonic features and evolution of the Okinawa Trough [J]. Scientia Sinica (series B), 1987, (2): 196-203.

[17] Lee C-S, Shor G. G. Jr, Bibee L D, et al. Okinawa Trough: origin of a back-arc basin [J]. Marine Geology, 1980, 35(1- 3): 219-241.

[18] Zhang Wenyou. *Ocean and land geotectonics of China and adjacent regions* [M]. Beijing: Science Press, 1986, 375-383.

[19] Ren Jishun, Jiang Chunfa, Zhang Zhengkun, et al.. Geotectonics and evolution of China [M]. Beijing: Science Press, 1980, 61-62.

[20] Jin Xianglong, Zhuang Jiezao, Tang Baojue, et al. Characteristics of the seismic reflection pattern in the Okinawa Trough [J]. Oceanologia et Limnologia Sinica, 1985, 16 (6): 48-487.

[21] Tanya H. "Offshore Miyako Island" key well. Translations of submarine geology, 1985, (6): 29-34.

[22] Leyden R, Ewing M, Murauchi S. Sonobuoy refraction measurements in East China Sea [J]. Am. Assoc. Pet. Geol. Bull., 1973, 57：2396-2403.

[23] Jin Xianglong, Yu Puzhi, Lin Meihua, et al. Analyses on the crustal structure and property of the Okinawa Trough [J]. Oceanologia et Limnologia Sinica, 1983, 14 (2): 105-116.

[24] Hirata N, Kinoshita H, Katao H, et al. Report on DELP 1988 cruises in the Okinawa Trough, part 3, Crustal structure of the southern Okinawa Trough [M]. Bull. Earthq. Res. Inst., 1991, 66: 37-70.

冲绳海槽南段基底组成探讨

刘建华[1,2]，高金耀[1,2]，方银霞[1,2]，吴水根[1,2]

(1. 国家海洋局海底科学重点实验室，浙江 杭州 310012；2. 国家海洋局第二海洋研究所，浙江 杭州 310012)

摘要：本文根据反射地震、折射地震、磁力等资料，结合周边地质，探讨冲绳海槽南段基底组成。在海槽周边的东海陆架盆地、台湾褶皱带和琉球岛弧褶皱带，均出露不同程度变质的晚古生代、中生代和早第三纪地层。多道反射地震表明，海槽南段沉积盖层由上第三系和第四系组成，声学基底由下第三系及更老地层构成。邻近海槽的折射地震揭示，除第四系－中新统速度层之外，还存在纵波速度分别为 4.7 ～ 5.3 km/s 和 6.3 km/s 的下第三系和中生界速度层。磁异常分析和正反演拟合计算结果表明，海槽磁性基底主要由变质岩系构成，次为燕山期中酸性岩浆岩和喜山期中基性岩浆岩，磁性基底大部分相当声学基底。综合分析表明，海槽南段基底主要由不同程度变质的下第三系、中生界和上古生界构成；在海槽某些构造部位，已有喜山期基性岩浆岩形成。

关键词：冲绳海槽 基底组成 磁性基底

Seagrass Bed Ecosystem Service Valuation — A Case Research on Hepu Seagrass Bed in Guangxi Province

HAN Qiuying[1,2], HUANG Xiaoping[2], SHI Ping[1], ZHANG Jingping[2]

1. *Yantai Institute of Coastal Zone Research for Sustainable Development, Chinese Academy of Sciences, Yantai* 264003, *Shandong, China;*
2. *LED, South China Sea Institute of Oceanology, Chinese Academy of Sciences, Guangzhou* 510301, *Guangdong, China*

Abstract: Seagrass bed ecosystem is a coastal ecosystem with abundant biodiversity and high production. It is also an important system for the sustainable development of human society and economy. Based on the local research, statistical data and prevenient research results, the main services of Hepu seagrass ecosystem were analyzed in the paper, including fishing production, nutrient cycling, scientific research, protecting the coast from eroding, climate regulation, biodiversity, culture, bequest valuation, option valuation and existence valuation and so on. At the same time, we used ecological and economic methods for economic evaluation of seagrass in Hepu of Guangxi, including the market valuation method, contingent valuation method, carbon and tax method, benefit transfer method and expert survey method. The results showed that the total valuation of the Hepu seagrass ecosystem service was about 6.29×10^5 Yuan RMB/ha in 2005. Among these services, the indirect using valuation is the main aspect, which was 4.47×10^5Yuan RMB/ha in 2005, accounting for 70.97 % of the total valuation. The non-using valuation was 1.54×10^5 Yuan RMB/ha in 2005, accounting for 24.52 % of the total valuation. The direct using valuation is the least, which was only 2.84×10^4 Yuan RMB/ha in 2005, accounting for 4.51 % of the total valuation.

Keywords: Seagrass bed; ecosystem service; valuation; Hepu; South China

Introduction

Seagrass bed plays an important role in coastal ecosystem [1], providing significant habitat and food resources for other living marine resources, and having an effect on the circulation of carbon, nitrogen and phosphorus in the world [2-4]. Many natural and human-induced events created disturbances of seagrass in the world [5]. Developing evaluation of seagrass ecosystem has an effect on protecting seagrass ecosystem and strengthening the environment consciousness of people. There is no research on seagrass and few paper about study on the evaluation of seagrass compared with mangrove and coral reef. Watson researched the economic valuation of prawn produced by seagrass in the Cairns Bay [6]. Costanza evaluated the valuation of nutriment circulation and material production of seagrass [7].

Received on December 10, 2007

Evaluation on seagrass is in the initiatory phase in China. Li [8] and Huang [9] researched the valuation of seagrass in Li'an Port of Hainan Island and Hepu of Guangxi Province, but they only evaluated the valuation of fishing production, ecosystem nutrient cycling, protecting the coast from eroding of seagrass, and did not research the climate regulation and biodiversity valuation.

According to modern ecological economics, the ecological service valuation of seagrass includes direct using valuation, indirect using valuation and non-using valuation [10]. Direct using valuation mainly includes marine culture and tidal flat fishing valuation produced by seagrass. Indirect using valuation includes offshore fishing, protecting the coast from eroding, climate regulation, biodiversity, scientific research and ecosystem nutrient cycling and purifying seawater valuation, which aren't used in production and consumption directly. Non-using valuation includes bequest valuation, option valuation and existence valuation [11]. Based on local statistical data, prevenient research results and the characters of Hepu seagrass ecosystem in Guangxi Province, the main service valuation of Hepu seagrass ecosystem was analyzed in the paper, which would provide the scientific foundation for the sustainable use of Hepu seagrass ecosystem in Guangxi.

1 Study methods

1.1 Introduction of study area

Hepu seagrass bed about 540 ha (in 2002) was located in the marine area of Hepu County in Guangxi (Fig.1). There were *Halophila ovalis*, *Zostera japonica*, *Halophila beccarii* and *Halodule uninervis*, et al., and *Halophila ovalis* were the dominant species [9]. The average coverage ratios of *Halophila ovalis* in Xialongwei and Shabei seagrass bed were respectively 38.8 % and 41.5 % [8]. Hepu seagrass is located in the *Dugong dugon* National Nature Reserve of Hepu. *Halophila ovalis* is the food resource of *Dugong dugong*. In recent years, Hepu seagrass bed has been interrupted badly, including digging clamworms and shells, marine culture, as well as typhoon and storm tide, and the degradation trend was evident.

1.2 Evaluation methods

1.2.1 Market valuation method

Market valuation method evaluates the seagrass valuation according to the market price of the production produced by seagrass, which is used to evaluate the valuation of the marine culture and tidal flat fishing. Based on the statistical data from Statistics Bureau, Shatian Town and Shankou Town in Hepu County, fishing earning was 1.73×10^9 Yuan RMB in Hepu County in 2005, in which offshore fishing earning was 5.43×10^8 Yuan RMB, and the area of marine culture was 800 ha, and marine culture earning was 6.17×10^4 Yuan RMB /a·ha. And offshore fishing earning was 2.03×10^8 Yuan RMB in Shatian Town and Shankou Town.

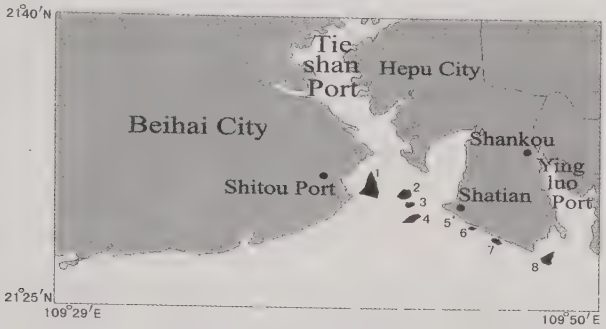

Fig.1 Distribution of seagrass in Hepu of Guangxi

1. Salt field seagrass bed in Beimu 2. Gaoshatou seagrass bed 3. Shabei seagrass bed
4. Xialongwei seagrass 5. Danshuikou seagrass bed 6. Ronggenshan seagrass bed
7. Shanliao seagrass bed 8. Yingluo port seagrass bed

1.2.2 Carbon and tax method

Seagrass can absorb CO_2 and release O_2. According to the photosynthesis equation of plants, synthesizing 1 g dry substance can absorb 1.629 g CO_2, and release 1.1914 g O_2 [12]. The economic valuation of seagrass absorbing CO_2 and releasing O_2 can be calculated on the basis of the overseas and domestic fee standard of releasing CO_2 and the cost making O_2 [13].

1.2.3 Benefit transfer method

Benefit transfer method is a method that cites the results of other interrelated projects, when a project is short of benefit numerical valuation, adequate funds, time and manpower [14]. This study mainly cited the study results from Costanza and the special report of Chinese seagrass. For example, Costanza gained that the ecosystem nutrient cycling valuation of seagrass in the world was 19 002 $/a·ha and the science research valuation of coastal zone in the world was 62 $/a·ha [7]. The special report of Chinese seagrass gave that the tidal flat fishing earning of seasgrass bed area in Hepu County was 9 733 Yuan RMB/a·ha [9].

1.2.4 Contingent valuation method

Contingent valuation method is a normal method that is used to conclude the willing-to-pay of the public to environment resources, and consequently gains the bequest valuation, option valuation and existence valuation of resources [15]. In this study, we sent out 500 questionnaires to the householders in the Hepu County, received 421 effective questionnaires and gained the willing-to-pay of every householder for protecting the limited seagrass resources. The average willing-to-pay (E (WTP)) can be calculated by mathematical expectation formula of discrete variables:

$$E(\mathrm{WTP}) = \sum_{i=1}^{n} A_i P_i$$

A_i—Bid account $10 \leq A_i \leq 1000$ Yuan RMB

P_i—Probability of visited person selecting the account $0 \leq P_i \leq 1$

n—Selected probability numbers $n=25$

1.2.5 Expert survey method

Expert survey method is a method that evaluates seagrass valuation using the knowledge, experience and analyses the ability of experts who are surveyed. In this study, we sent out 300 questionnaires to the experts studying seagrass and ecological economics, and received 128 effective questionnaires. The problems of the expert questionnaire mainly included the contribution ratio of seagrass to marine culture, tidal flat fishing and offshore fishing, percentage of seagrass reducing the cost repairing coast, and biodiversity valuation of seagrass of each ha. These parameters can be calculated by discrete variable:

$$C=\sum_{i=1}^{n} A_i P_i$$

P_i—Probability of visited person selecting the account $0 \leq P_i \leq 1$

n—Selected probability numbers $n=10$

In the expert questionnaire, the contribution ratio of seagrass to the marine culture ranged from 10 % to 90 %, the contribution ratio to the tidal flat fishing ranged from 10 % to 90 %, the percentage of reducing the cost for repairing coast ranged from 10 % to 90 %, the biodiversity valuation of seagrass ranged from 10 $/a·ha to 10000$/a·ha.

According to the former formula, the contribution ratios of seagrass to the marine culture, tidal flat fishing and offshore fishing were respectively 32.8 %, 84.3 % and 45.6 %. The percentage of seagrass of reducing the cost for repairing coast was 45.9 %. The biodiversity valuation of seagrass was 8000 $/a·ha in 2005. If 1 $ can be exchanged into 8 Yuan RMB, the biodiversity valuation of seagrass was 64 000 Yuan RMB/a·ha in 2005.

2 Results

2.1 Direct using valuation

2.1.1 Marine culture valuation

The calculated formula was $L_1=C_1W_1$, where,

L_1—the marine culture valuation produced by seagrass of each ha

C_1—the contribution ratio of seagrass to the marine culture

W_1—the marine culture valuation of each ha in marine area of seagrass

From the former formula, the marine culture valuation of seagrass in Hepu was 2.02×10^4 Yuan RMB/a·ha in 2005.

2.1.2 Tidal flat fishing valuation

The calculated formula was $L_2 = C_2 W_2$, where,

L_2—the tidal flat fishing valuation produced by seagrass every ha

C_2—the contribution ratio of seagrass to the tidal flat fishing

W_2—the tidal flat fishing earning of each ha in marine area of seagrass

The tidal flat earning in the seagrass area was 9733 Yuan RMB/a·ha in 2005 [9]. From the former formula, the tidal flat fishing valuation produced by seagrass in Hepu was 8.20×10^3 Yuan RMB/a·ha in 2005.

2.2 Indirect using valuation

2.2.1 Offshore fishing valuation

The calculated formula was $L_3 = C_3 W_3$, where,

L_3—the offshore fishing valuation produced by seagrass

C_3—the contribution ratio of seagrass to the offshore fishing

W_3—the catching fishing earning in Shatian Town and Shankou Town

The offshore fishing valuation produced by seagrass in Hepu was 9.26×10^7 Yuan RMB/a in 2005. The seagrass area in Hepu was 540 ha in 2005. So the offshore fishing valuation produced by seagrass was 1.71×10^5 Yuan RMB/a·ha in 2005.

2.2.2 Valuation protecting the coast from eroding

The calculated formula was $L_4 = C_4 W_4$, where,

L_4—the valuation protecting the coast from eroding produced by seagrass in Hepu

C_4—cost for repairing every year in seagrass area if there is no seagrass

W_4—the percentage of seagrass reducing cost repairing coast

$W_4 = W'_4/(1 - C_4)$

W'_4—actual repairing cost in the seagrass area every year

According to the questionnaire to the Hepu County government, there were 700 people to protect

the coast from eroding, and everyone gained the subsidy of 10000 Yuan RMB. The other cost for repairing was 2.20×10^6 Yuan RMB/a. The valuation protecting the coast from eroding produced by seagrass was 7.81×10^6 Yuan RMB /a in 2005. The seagrass area in Hepu in 2005 was 540 ha. So the valuation protecting the coast from eroding produced by seagrass was 1.45×10^4 Yuan RMB/a·ha in 2005.

2.2.3 Climate regulation valuation

The calculated formula was $L_5=f(x_{51})+f(x_{52})$, where,

$f(x_{51})$—the valuation of Hepu seagrass absorbing CO_2

$f(x_{52})$—the valuation of Hepu seagrass releasing O_2

The average dry mass of seagrass bed in Hepu was 25.5 g/m^2 [9], that is, 0.255 t/ha. We can gain seagrass in Hepu absorbing 0.415 t/ha CO_2, in which there was 0.113 t/ha C, and releasing 0.304t O_2. Based on the current international standard of carbon tax rate and Chinese situation, the mean between the forestation cost, which was 250 Yuan RMB/t, and international standard of carbon tax, which was 150 $/t, was used as carbon tax standard. It was 770 Yuan RMB/t [16]. The valuation of Hepu seagrass absorbing CO_2 was 87.01Yuan RMB/a·ha. The cost of making O_2 in industry was 400 Yuan RMB/a [17]. The valuation of Hepu seagrass releasing O_2 was 121.6 Yuan RMB/a·ha. The climate regulation valuation of Hepu seagrass was 208.61 Yuan RMB/a·ha in 2003. If the discount rate was 5 %, the climate regulation valuation of Hepu seagrass was 2.30×10^2 Yuan RMB/a·ha in 2005.

2.2.4 Biodiversity valuation

According to the former expert survey method, the biodiversity valuation of seagrass was 64000Yuan RMB/a·ha in 2005. On the basis of the standard of important species habitat function offered by international wetlands and their ecological benefit (Tab.1) [18], the area and rare species account number in seagrass bed in Hepu, the grade of the Hepu seagrass bed was confirmed and the controlling cost was gained. There were *Dugong dugon*、*Chelonia mydas* and *Hippocampus trimaculatus* in the rare species of Hepu seagrass bed. That made the habitat function of Hepu seagrass in the grade from 3 to 4 and the controlling cost was from 10×10^4 $ to 100×10^4 $. Based on area proportion, the controlling cost in Hepu seagrass was 5.4×10^5 $. If exchange rate was that 1 $ was changed into 8 Yuan RMB, the controlling cost in Hepu seagrass was 4.32×10^6 $. The biodiversity valuation can be 4.32×10^6 Yuan RMB/a, that is 8 000 Yuan RMB/a·ha.

The mean of two former methods was 3.6×10^4Yuan RMB/a·ha, which was the biodiversity valuation of Hepu seagrass.

2.2.5 Scientific research valuation

Scientific research valuation is usually evaluated according to the scientific research investment and the factual cost of scientific researchers [12]. Because the seagrass research in China was at the initiatory stage and scientific research cost is much less than actual scientific research valuation, we used the mean

of scientific research valuation of the world and China to evaluate the seagrass valuation in Hepu. Costanza thought that the scientific research valuation of global coastal zone ecosystem was 62 $/a·ha in 1997 [7]. If the exchange rate was that 1 $ was changed into 8 Yuan RMB and the discount rate was 5 %, the scientific research valuation of global coastal zone ecosystem was 732.79 $/a·ha in 2005. Chen concluded that the average scientific research valuation of Chinese ecosystem was 382 Yuan RMB/a·ha in 2000[19]. If the discount rate was 5 %, the scientific research valuation of Chinese ecosystem was 487.51 Yuan RMB/a·ha in 2005. We thought that the mean of the scientific research valuation of Chinese ecosystem and global coastal zone ecosystem, which was 6.10×10^2 Yuan/a·ha, was the scientific research valuation of Hepu seagrass in 2005.

Tab.1 The criteria and ecological benefits of the function providing habitats for the wildlife of wetlands

Level	Area	Numbers of rare species	Controlling cost /$\times 10^4$$
1	>100 000	>10	>10 000
2	>10 000	>8	>1 000
3	>1 000	>4	>100
4	>100	>2	>10
5	<100	<2	<10

2.2.6 Ecosystem nutrient cycling valuation

There has been no interrelated studies on the nutrient cycling process of seagrass ecosystem in Hepu. In this study, the result of Costanza(1997) was adopted, whose study gained the ecosystem nutrient cycling valuation was 19002 $/a·ha [7]. If the exchange rate was that 1 $ was changed into 8 Yuan RMB and the discount rate was 5 %, the ecosystem nutrient cycling valuation of Hepu seagrass was 2.24×10^5 Yuan RMB/a·ha in 2005.

2.2.7 Purifying seawater valuation

In this study, the total nitrogen (TN) and total phosphorus (TP) were calculated. The ratio of C:N:P in seagrass ecosystem was 474 : 24 : 1[20]. According to the former study, seagrass in Hepu absorbed 0.415 t/ha CO_2 in which there was 0.113t/ha C every year, so the mass of nitrogen in Hepu seagrass was 5.72×10^3 t/a·ha and the mass of phosphorus was 2.38×10^4 t/a·ha. The cost of wiping off pollution of TN was 2.66×10^4 Yuan RMB/t and the cost of wiping off pollution of TP was 55.86×10^4 Yuan RMB/t in 2003 [16]. The purifying seawater valuation of Hepu seagrass was 287Yuan RMB/a·ha in 2003. If the exchange rate was that 1 $ was changed into 8 Yuan RMB, the purifying seawater valuation of Hepu seagrass was 3.16×10^2 Yuan RMB/a·ha in 2005.

2.3 Non-using Valuation

According to the contingent valuation method, the willing-to-pay of every householder for protecting the limited seagrass resources was 143 Yuan RMB/a. Based on the result from developed countries, the willing-to-pay of non-household to scenic spots and the wild areas was from 9$ to 107$/a [21]. If the exchange rate was that 1 $ was changed into 8 Yuan RMB, the mean of the 3 former numbers was 357

Yuan RMB/a, which was thought as the willing-to-pay of every household to Hepu seagrass. On the basis of the statistical data from Statistics Bureau, there were 23 3266 households in Hepu County. The non-using valuation of Hepu seagrass was 8.33×10^7 Yuan RMB/a in 2005, which was 1.54×10^5 Yuan RMB/a·ha.

Based on the former evaluation on Hepu seagrass bed ecosystem service, the total valuation of seagrass bed ecosystem service in Hepu was 6.29×10^5 Yuan RMB/a·ha in 2005, in which direct using valuation was 2.84×10^4 Yuan RMB/a·ha, and indirect using valuation was 4.47×10^5 Yuan RMB/a·ha and non-using valuation was 1.54×10^5 Yuan RMB/a·ha (Tab.2).

Tab. 2 The valuation of Hepu seagrass bed

Valuation type	Service function	Evaluation method	Evaluation result/$\times 10^2$ Yuan RMB/a·ha
Direct using valuation	Marine culture	Market valuation method expert survey method	202
Indirect using valuation	Tidal flat fishing	Market valuation method	82
	Offshore fishing	Market valuation method expert survey method	1710
	Protecting the coast from eroding	Expert survey method	145
	Climate regulation	Carbon and tax method	2.30
	Biodiversity	Benefit transfer method and expert survey method	360
	Scientific Research	Benefit transfer method	6.10
	Ecosystem Nutrient Cycling Value	Market valuation method benefit transfer method	2240
	Purifying Seawater	Market valuation method	3.16
Non-using valuation	Bequest valuation, option valuation and existence valuation	Contingent valuation method benefit transfer method	1543
Total valuation	—	—	6293.56

Tab.3 The percentage of Hepu seagrass ecosystem valuation

Valuation type	Evaluation result /$\times 10^2$Yuan RMB/a·ha	Percentage of the total valuation
Direct using valuation	284	4.51 %
Iindirect using valuation	4466.56	70.97 %
Non-using valuation	1543	24.52 %
Total valuation	6293.56	100 %

3 Discussion

The ecosystem service valuation of Hepu seagrass bed was mainly indirect using valuation and non-using valuation, which accounted for 95.49 % of total economic valuation (Tab.3). Offshore fishing and ecosystem nutrient cycling valuation were especially biggish, which respectively accounted for 27.17 % and 35.59 %, this reflecting the significance of seagrass to the offshore fishing and ecosystem nutrient cycling. The direct using valuation only accounted for 4.51 % of total economic valuation of Hepu seagrass. The main threats of Hepu seagrass were digging clamworms and shells, and marine culture. For the sustainable use of Hepu seagrass, the fishery activities endangering seagrass bed in Hepu should be managed well.

In this study, the total valuation of seagrass bed ecosystem service in Hepu was 6.29×10^5Yuan RMB/a·ha in 2005, which was obviously higher than the result from other studies in China [9]. It was because that the climate regulation valuation, biodiversity valuation, purifying seawater valuation and scientific research valuation were evaluated, which were not evaluated in other studies in China [9].

From the former study, the total valuation of seagrass ecosystem service in Hepu was 6.29×10^5 Yuan RMB/a·ha in 2005. This showed that the seagrass ecosystem service function was very important, which didn't accord with the scientific research investment and recognition degree to seagrass in China. Chinese government should promote the protection and scientific research investment.

The research on the ecological benefit of seagrass in China was at the initiatory stage. The error of the statistical data and the difference of evaluation methods may bring the error of evaluation results. Because of few researchers on seagrass in China, the expert questionnaires were sent out to the overseas experts studying seagrass and ecological economics in this study. The research result, impacted by Chinese situation and people's conception, may have some errors. The study needs more discussion.

Acknowlegements

This project was supported by the Innovative Engineering Project of Chinese Academy of Sciences (Grant No.KSCZ2-SW-132), United Nations Environment Program/Global Environment Fund (UNEP/GEF) (Grant No. UNEP/GEF/SCS/Chi/MoU2c), Project of Science and Technology Development Plan in Shandong Province (Grant No. 2007GG2Q706019).

References

[1] Nagelkerken I, Velde G, Gorissen M W, et al. Importance of mangroves, seagrass beds and the shallow coral reef as a nursery for important coral reef fishes, using a visual census technique[J]. Estu. Coast. shelf sci., 2000, (51): 31-44.

[2] Den H C. The sea grasses of the world [M]. Amsterdam: North Holland Publication. 1970. 275.

[3] Edgar G J. Comparisons of species richness, size-structure and production of benthos in vegetated and unvegetated habits in Western Port, Victoria [J]. J. Exp. Mar. Bio. Eco., 1994, (176): 201-226.

[4] Fortes M D. Mangroves and seagrass beds of East Asia: habitat under stress [J]. Ambio, 1988, (17): 207-213.

[5] Frederick T S, Sandy W E. Natural and human-induced disturbance of seagrasses [J]. Environ. Cons., 1996, 23(1): 17-27.

[6] Watson R A, Coles R G, Lee W J. Stimulation estimates of annual yield and landed value for commercial penaeid prawns from a tropical seagrass habitat, Northern Queensland, Australia [J]. Jour. Mar. Freshwater Res., 1993, (44): 211-219.

[7] Costanza R, d'Arge R, de Groot R, et al. The value of the world's ecosystem services and natural capital [J]. Nature, 1997, (387): 253-260.

[8] Li Y H. Study on the ecological characters, service function and protection of Hepu seagrass bed in Guangxi [D].

South China Sea Institute of Oceanology, Chinese Academy of Sciences, 2004.

[9] Huang X P, Huang L M, Li YH, et al. the special report of Seagrass in China [R]. South China Sea Institute of Oceanology, Chinese Academy of Sciences, 2005.

[10] James S. The scsio-economic costs and benefits of coastal habitat rehabilitation and creation [J]. Mar. Pollu. Bul., 1999, (37): 373-382.

[11] Helena M. Compensation for landowners affected by mineral development: the Fijian experience [J]. Resour. Policy, 2000, (26): 115-125.

[12] Xin K, Xiao D N. Wetland ecosystem service valuation——a case researches on Panjin area. Acta Ecologica Sinica, 2002, 22(8): 1345-1349.

[13] Thomas P S. The use of biological criteria as a tool for water resource management [J]. Environ. Sci. Policy, 2000, (3): 43-49.

[14] Cui B S, Yang Z F. Benefit valuation of typical wetlands in Jilin Province [J]. Resour. Sci., 2001, 23(3): 55-61.

[15] Mitchell R, Carson R. Using surveys to value public goods: The contingent valuation method [M]. Washington D C: Resources for the future. 1989.

[16] Zhuang D C, Ou W X, Ding D S. Evaluation of lake recovery area eco-economy benefit in Dongting Lake wetland [J]. J. Nat. Resour., 2003, 18(5): 536-543.

[17] Pan W B, Tang T, Deng H B, et al. Lake ecosystem services and their ecological valuation——a case study of Baoan Lake in Hubei Province [J]. Chin. J. Appl. Ecol., 2002, 12(10): 1315-1318.

[18] Xiao D N, Hu Y M, Li X Z. Study on scape ecology of delta wetland around Bohai [M]. Beijing: Science Publishing Company. 2001. 368-389.

[19] Zhang Z X, Zhang X S. The valuation of ecosystem benefit in China [J]. Chin. Sci. Bul., 2000, 45(1): 17-22.

[20] Duarte C M. Seagrass nutrient content [J]. Mar. Eco. Pro. Ser., 1990, (67): 201-207.

[21] Adger W N, Brown K, Cervigni R, et al. Total economic value of forests in Mexico [J]. Ambio, 1995, 24(5): 285-295.

广西合浦海草床生态系统服务功能价值评估

韩秋影[1,2]，黄小平[2]，施平[1]，张景平[2]

（1. 中国科学院烟台海岸带可持续发展研究所，山东 烟台，264003；

2. 中国科学院南海海洋研究所热带海洋环境动力学重点实验室，广东 广州，510301）

摘 要： 海草床生态系统是生物多样性丰富和生产力高的近岸海洋生态系统，本文以广西合浦海草床为例，结合实地调查、已有的研究成果和当地统计资料，综合运用生态经济学、资源经济学等基本理论和方法，对该地区海草生态系统的服务功能进行了价值评估。结果表明 2005 年该地区海草生态系统的服务功能价值为 6.29×105 元/a•ha，其中间接利用价值最大，为 4.47×105 元/a•ha，占总经济价值的 70.97 %；其次为非利用价值，为 1.54×105 元/a•ha，占总经济价值的 24.52 %；最少的是直接利用价值为 2.84×104 元/a•ha，仅占总经济价值的 4.51 %。

关键词： 海草床；生态系统服务；价值评估；广西合浦

海 洋 通 报（英文版）

HAIYANG TONGBAO

2008 年 5 月　第 10 卷　第 1 期

目　次

HYCOM 模式对赤道及北太平洋海表温度的模拟……高　松 等 (14)

奥东后江湾冲流带滩面高频振动及动力作用分析…… 冯砚青 等 (27)

硫酸盐-甲烷界面与甲烷通量及下伏水合物赋存的关系 …… 方银霞 等 (37)

台州湾海域表层沉积物中多环芳烃的浓度水平、富集规律及来源 ……金彬明 等 (45)

海洋发光孤菌的生长和发光条件的研究 ……方宏达 等 (53)

几种环境因子对虾蟹类非特异性免疫的影响 ……艾春香 等 (63)

南海东北部陆坡与恒春海脊天然气水合物分布的地震反射特征对比 …… 尚继宏 等 (74)

冲绳海槽南段基底组成探讨 …… 刘建华 等 (86)

广西合浦海草床生态系统服务功能价值评估 …… 韩秋影 等 (96)

Marine Science Bulletin

Marine Science Bulletin publishes papers on marine science and technology including physical oceanography, chemical oceanography, marine biology, marine geology, environmental oceanography, estuarine & coastal sciences, marine technology, digital ocean, coastal zone management, ocean engineering, marine economics, etc., and aims to promote international academic exchange.

Editor-in-Chief: LIN Shaohua (林绍花)

Associate Editor-in-Chief: HE Guangshun (何广顺) YANG Ying (杨 鹰)

Executive Editor: HE Xuewu (何学武) QIU Wenjing (邱文静)
ZHANG Xiaoxian (张潇娴) WANG Zhankun (王占坤)

English proofed by: WANG Qi (王琦)

semi-annually (started in 1999, sam 19)
Publication date: May. 15th and Oct. 15th

Marine Science Bulletin **(Vol. 10, No. 1, May 2008)**

Responsible Institution:
State Oceanic Administration of China
Sponsored by:
National Marine Data and Information Service
Edited by:
Office of Marine Science Bulletin (English edition)
Printed by:
Printery of National Marine Date and Information Service

Published by:
Office of Marine Science Bulletin (English edition)
E-mail: msb@mail.nmdis.gov.cn
Tel: (022) 24011287
Address: 93 Liuwei Rd., Hedong District, Tianjin 300171, China

ISSN1000-9620
CN12-1271/N

Price: $ 30.00 / ￥18.00 Per year